

University of Windsor

## Scholarship at UWindor

---

Electronic Theses and Dissertations

Theses, Dissertations, and Major Papers

---

8-27-2019

# Novel System Identification Techniques For Battery Management System

Sheikh Arif Raihan  
*University of Windsor*

Follow this and additional works at: <https://scholar.uwindsor.ca/etd>

---

### Recommended Citation

Raihan, Sheikh Arif, "Novel System Identification Techniques For Battery Management System" (2019). *Electronic Theses and Dissertations*. 7834.  
<https://scholar.uwindsor.ca/etd/7834>

This online database contains the full-text of PhD dissertations and Masters' theses of University of Windsor students from 1954 forward. These documents are made available for personal study and research purposes only, in accordance with the Canadian Copyright Act and the Creative Commons license—CC BY-NC-ND (Attribution, Non-Commercial, No Derivative Works). Under this license, works must always be attributed to the copyright holder (original author), cannot be used for any commercial purposes, and may not be altered. Any other use would require the permission of the copyright holder. Students may inquire about withdrawing their dissertation and/or thesis from this database. For additional inquiries, please contact the repository administrator via email ([scholarship@uwindsor.ca](mailto:scholarship@uwindsor.ca)) or by telephone at 519-253-3000ext. 3208.

NOVEL SYSTEM IDENTIFICATION TECHNIQUES FOR BATTERY  
MANAGEMENT SYSTEM

by

Sheikh Arif Raihan

A Thesis

Submitted to the Faculty of Graduate Studies  
through the Department of Electrical and Computer Engineering  
in Partial Fulfilment of the Requirements for  
the Degree of Master of Applied Science at the  
University of Windsor

Windsor, Ontario, Canada

© 2019 Sheikh Arif Raihan

NOVEL SYSTEM IDENTIFICATION TECHNIQUES FOR BATTERY  
MANAGEMENT SYSTEM

by  
Sheikh Arif Raihan

APPROVED BY:

---

J. Ahamed  
Department of Mechanical, Automotive and Materials Engineering

---

N. Kar  
Department of Electrical and Computer Engineering

---

B. Balasingam, Advisor  
Department of Electrical and Computer Engineering

August 27, 2019

# Declaration of Co-Authorship / Previous Publication

## Co-Authorship

I hereby declare that this thesis incorporates material that is result of joint research, as follows: Chapters 2, 3, and 4 of this thesis were co-authored with professor Balasingam, who provided supervision and guidance during the research and writing process. In all cases, the key ideas, primary contributions, data analysis, interpretation, and writing were performed by the author.

I am aware of the University of Windsor Senate Policy on Authorship and I certify that I have properly acknowledged the contribution of other researchers to my thesis, and have obtained written permission from each of the co-author(s) to include the above material(s) in my thesis.

## Previous Publication

Thesis chapter	Publication title/full citation	Publication status
2	Raihan, Sheikh Arif & Balasingam, Balakumar. (2019). Recursive Least Square Estimation Approach to Real-Time Parameter Identification in Li-ion Batteries.	Accepted
3	Raihan, Sheikh Arif & Balasingam, Balakumar. (2019). A Novel Approach to Real-Time Parameter Identification in Li-ion Batteries.	Under review
4	Raihan, Sheikh Arif & Balasingam, Balakumar. (2019). Robust Battery Fuel Gauge: Algorithm and Evaluation.	Under review

I certify that I have obtained a written permission from the copyright owner(s) to include the above published material(s) in my thesis. I certify that the above material describes work completed during my registration as a graduate student at the University of Windsor.

## General

I declare that, to the best of my knowledge, my thesis does not infringe upon anyone's copyright nor violate any proprietary rights and that any ideas, techniques, quotations, or any other material from the work of other people included in my thesis, published or otherwise, are fully acknowledged in accordance with the standard referencing practices. Furthermore, to the extent that I have included copyrighted material that surpasses the bounds of fair dealing within the meaning of the Canada Copyright Act, I certify that I have obtained a written permission from the copyright owner(s) to include such material(s) in my thesis. I declare that this is a true copy of my thesis, including any final revisions, as approved by my thesis committee and the Graduate Studies office, and that this thesis has not been submitted for a higher

degree to any other University or Institution.

# Abstract

In this thesis, we presents a novel approach for system identification of a Li-ion batteries. First, we we present a robust approach to estimate the equivalent circuit model (ECM) parameters of a Li-ion battery that offers several advantages over existing ones. Particularly, (i) The proposed approach depends only on measured voltage across and current through the battery; (ii) We theoretically derive the estimation error in terms of the voltage and current measurement errors; (iii) The proposed approach is unaffected by the effect of hysteresis in batteries; (iv) The proposed approach is applicable in time-varying conditions; and (v) The new ECM identification approach can be implemented for different ECM approximations with little change in the algorithm. The proposed algorithm was tested on simulated as well as real world battery data and found to be accurate within 1% uncertainty. Finally, we discuss about the battery fuel gauge (BFG). We suggest an improved BFG of an existing one that estimate ECM parameter as well as the state of charge (SOC) in real time. Then we use the BFG evaluation scheme to validate the performance of an improved BFG and compare its performance with its predecessor. The comparison shows the performance improvement of the improved BFG in objective terms — using the BFG evaluation metrics. Therefore, this thesis further aims to highlight the importance of employing objective performance analysis to quantify the performance of different versions of BFG being proposed in the literature and demonstrate its use case using simulated as well as real world data.

# Acknowledgements

First of all, I would like to express my profound gratitude to my creator, the owner of the universe, Almighty Allah who has blessed me with my existence and the prosperous future in every aspects of my life.

Further, I would like to extend my earnest gratitude to my supervisor Dr. B. Balasingam, who offered me an opportunity to be a graduate student and conduct research under his guidance. He gave me all the support and confidence needed to complete this thesis. I would also like to thank him for spending limitless time in discussing about the research papers, projects and the thesis.

I would like to thank Dr. Shahrrava and Dr. Ahmadi for their constant support in the courses. I would also like to thank all the staff members of our department for their kind support. Especially, I thank Andria Ballo for her help and support. Further I thank the fellow graduate students for their cooperation during the research period.

I would like to express my heartfelt endearment to my love, Zara who has been my inspiration to the direction of my goal. I would like to thank MA for her endless care when it was needed and Baba for his beneficial suggestions. Also I thank Zayan for being supportive. And, finally, I would like to thank my parents for all the hardships they have gone through to raise me up and to support me in my education.



# Contents

<b>Declaration of Co-Authorship / Previous Publication</b>	<b>iii</b>
<b>Abstract</b>	<b>vi</b>
<b>List of Tables</b>	<b>xi</b>
<b>List of Figures</b>	<b>xii</b>
<b>1 Introduction</b>	<b>1</b>
1.1 Organization of the Thesis . . . . .	2
<b>2 Recursive Least Square Estimation Approach to Real-Time Parameter Identification in Li-ion Batteries</b>	<b>5</b>
2.1 Introduction . . . . .	5
2.2 Mathematical Derivation of a New Measurement Model . . . . .	8
2.2.1 Measurement Model Derivation for Battery ECM . . . . .	10
2.3 Summary of the Proposed Algorithm . . . . .	14
2.4 Results . . . . .	17
2.4.1 Objective Performance Analysis . . . . .	17
2.4.2 Performance Analysis using Different Temperatures . . . . .	19
2.5 Conclusion . . . . .	20
2.6 Bibliography . . . . .	23

<b>3</b>	<b>A Novel Approach to Real-Time Parameter Identification in Li-ion Batteries</b>	<b>27</b>
3.1	Introduction . . . . .	27
3.2	Mathematical Derivation of a New Measurement Model . . . . .	34
3.2.1	Measurement Model Derivation for Model 1 . . . . .	35
3.2.2	Measurement Model Derivation for Model 2 . . . . .	37
3.2.3	Measurement Model Derivation for Model 3 . . . . .	39
3.2.4	Measurement Model Derivation for Model 4 . . . . .	43
3.3	Summary of the Proposed Algorithm . . . . .	47
3.4	Theoretical Performance Analysis . . . . .	53
3.5	Results . . . . .	56
3.5.1	Objective Performance Analysis . . . . .	56
3.5.2	Model Mismatch Analysis . . . . .	58
3.5.3	Performance Analysis using Different Temperatures . . . . .	58
3.5.4	Performance Analysis Using Multiple Batteries . . . . .	59
3.6	Conclusion . . . . .	60
3.7	Bibliography . . . . .	69
<b>4</b>	<b>Robust Battery Fuel Gauge: Algorithm and Evaluation</b>	<b>75</b>
4.1	Introduction . . . . .	75
4.2	Details of the New Battery Fuel Gauge . . . . .	81
4.2.1	Battery Equivalent Circuit Model . . . . .	81
4.2.2	Battery OCV Model . . . . .	82
4.2.3	ECM Parameter Estimation . . . . .	83
4.2.4	State of Charge Tracking . . . . .	86
4.2.5	Block Diagram of the Robust BFG . . . . .	89
4.3	Details of the Validation Method . . . . .	90
4.3.1	Coulomb Counting (CC) Metric . . . . .	90

4.3.2	OCV Metric . . . . .	91
4.3.3	TTV Metric . . . . .	92
4.4	Results . . . . .	95
4.4.1	Performance Analysis of Proposed BFG using Simulated Profile	95
4.4.2	Performance Analysis of Proposed BFG using Real Load Profile	99
4.5	Conclusion . . . . .	103
4.6	Bibliography . . . . .	116
<b>5</b>	<b>Conclusion and Future Work</b>	<b>121</b>
	<b>Vita Auctoris</b>	<b>123</b>

# List of Tables

2.1	ECM Parameter Estimation Error (in %)	19
3.2	Estimation Error (in %) for Model 1	57
3.3	Estimation Error (in %) for Model 3	58
3.4	Estimation Error (in %) considering Model Mismatch	59
4.5	BFG evaluation by CC metric (%)	96
4.6	BFG evaluation by OCV metric	97
4.7	BFG evaluation by TTV metric (%)	98

# List of Figures

2.1	<b>Equivalent circuit models (ECM) of a battery.</b> Battery equivalent circuit model that is widely used in the literature to represent Li-ion batteries. In this chapter, we present a generalized approach to estimate the ECM parameter. . . . .	9
2.2	<b>Measured voltage and current profile.</b> Voltage across the battery terminals and current through the battery . . . . .	19
2.3	<b>Parameter Estimation for Battery Equivalent Circuit Model.</b> Mean square error of the estimated parameters are plotted for different values of measurement noise. . . . .	20
2.4	<b>Performance of the ECM identification algorithm at multiple temperatures.</b> Estimated values of the ECM parameters are plotted against batch number for data collected from the same battery cell used in Samsung Galaxy 4 smartphones (Samsung EB 575152) at eight different temperatures. . . . .	21
2.5	<b>Performance of the ECM identification algorithm on multiple batteries.</b> Estimated values of the ECM parameters are plotted against the temperature in which the battery was kept. Each entry in this plot is obtained by averaging the estimated values for the last 10 batches corresponding to Fig. 3.11. . . . .	22

3.6	<b>Equivalent circuit models (ECM) of a battery.</b> Four different ECMs that are widely used in the literature to represent Li-ion batteries. In this chapter, we present a generalized approach to estimate the parameters under each model assumption. . . . .	36
3.7	<b>Estimation of <math>R_0</math> in Model 1.</b> Voltage across the battery terminals and current through the battery is shown in (a); mean square error of estimation over 200 Monte-Carlo runs is shown in (b). . . . .	62
3.8	<b>Parameter Estimation for Model 3.</b> Mean square error of the estimated parameters are plotted for different values of measurement noise. . . . .	63
3.9	<b>Model mismatch analysis.</b> The result of estimating Model 1 parameters from data that was simulated using Model 3. Mean square error against batch number is shown for the estimated parameter. . .	64
3.10	<b>Model mismatch analysis.</b> The results of estimating Model 3 parameters from data that was simulated using Model 4. Mean square error against batch number is shown for each estimated Model 3 parameter. . . . .	65
3.11	<b>Performance of the ECM identification algorithm at multiple temperatures.</b> Estimated values of the Model 3 parameters are plotted against batch number for data collected from the same battery cell used in Samsung Galaxy 4 smartphones (Samsung EB 575152) at eight different temperatures. . . . .	66
3.12	<b>Performance of the ECM identification algorithm on multiple batteries.</b> Estimated values of the Model 3 parameters are plotted against the temperature in which the battery was kept. Each entry in this plot is obtained by averaging the estimated values for the last 10 batches corresponding to Figure 3.11. . . . .	67

3.13	<b>Performance of the ECM identification algorithm on multiple batteries.</b> Estimated values of the Model 3 parameters are shown against batch number. . . . .	68
4.14	<b>Equivalent circuit models (ECM) of a battery.</b> Battery equivalent circuit model that is widely used in the literature to represent Li-ion batteries. In this chapter, we use a RLS based approach to estimate the ECM parameter [1,3] with some improvements. . . . .	81
4.15	<b>Block diagram of the proposed BFG.</b> The proposed BFG is designed to estimate ECM parameters as well as the SOC in real time. . . . .	89
4.16	<b>Shut down voltage for TTV metric validation.</b> Shut down voltage, $v_{sd}$ for TTV metric is determined by subtracting voltage drop, $v_d$ and hysteresis, $h(k)$ from $v_{sd}$ from the OCV. . . . .	92
4.17	<b>BFG evaluation using simulated load profile.</b> Simulated voltage and current are shown in (a); Estimated SOC is presented in (b); finally the validation of the proposed BFG is illustrated in (c). . . . .	107
4.18	<b>Visualization of TTV error in minutes.</b> A close up visualization of TTV metric using simulated data . . . . .	108
4.19	<b>Real voltage and current data from multiple batteries.</b> The effectiveness of the proposed BFG algorithm is verified by implementing it in three different batteries which are LG LGIP, Nokia BP 4L and Samsung EB555157VA measured at different temperature as indicated in the plots. . . . .	109
4.20	<b>SOC estimation using proposed BFG.</b> The SOC is estimated online using the proposed BFG and compared with the widely-used Coulomb counting approach in order to verify the robustness. The Coulomb counting approach uses battery capacity that was estimated prior to the experiment. . . . .	110

4.21	<b>ECM parameter estimation using the real load profile.</b> ECM parameter estimation is performed using the battery model shown in Figure 4.14. The $R_0$ , $R_1$ and $C_1$ estimations is illustrated in (a), (b) and (c) respectively for multiple batteries. . . . .	111
4.22	<b>BFG evaluation based on CC metric using multiple batteries.</b> New CC metric is developed in order to validate the proposed algorithm to estimate SOC based on extended Kalman filter discussed in Section 4.2.4 . . . . .	112
4.23	<b>Predicted time to reach shut down voltage vs. actual TTV.</b> The real data from multiple batteries are used to calculate and compare the predicted time to reach certain shut down voltages. The zoomed version of Figure (a) is shown in Figure (b) illustrating the true TTV calculated using the data from LG LGIP at different temperature and the expected TTV. Figure (c) and (d) shows the results of predicted and actual TTV using the data from Nokia BP 4L and Samsung EB555157VA. . . . .	113
4.24	<b>Predicted time to reach shut down voltage vs. actual terminal voltage.</b> The real data from multiple batteries are used to calculate and compare the predicted time to reach certain shut down voltages. The zoomed version of Figure (a) is shown in Figure (b) illustrating the true TTV calculated using the data from LG LGIP at different temperature and the expected TTV. Figure (c) and (d) shows the results of predicted and actual TTV plotted against the voltage using the data from Nokia BP 4L and Samsung EB555157VA. . . . .	114
4.25	<b>BFG evaluation based on TTV metric</b> The proposed BFG is evaluated based on TTV errors (in minute) for each time index. . . . .	115



# Chapter 1

## Introduction

In this manuscript-style thesis, we explore the research and development of technology in the realm of battery management system (BMS) presented as a collection of his previously submitted and published works. Due to increasing concern on the environmental effects of fossil fuels, here is a need to develop renewable energy storage systems, such as, rechargeable batteries.. Lithium-ion batteries are widely used as an energy storage device because of their high energy density. It is necessary to ensure the safe operation of battery when it is connected to a systems or load. BMS is designed to monitor, control the states of battery such as terminal voltage, current, temperature and estimate state-of-charge (SOC), state-of-health (SOH), state-of-power (SOP), time-to-voltage (TTV). In order to obtain accurate estimation of the states of a battery, an appropriate modeling of battery is crucial which can be achieved by precise estimation of the parameters of a battery model. Indeed, the development of algorithm in order to estimate the battery equivalent circuit model and the online estimation of SOC is the main theme of this thesis.

Battery management system has three major components, namely optimal charging algorithm (OCA), cell balancing circuitry (CBC) and battery fuel gauge. Battery charging strategies, charging speed, charging efficiency, charging temperature rise and the battery cycle life are controlled by optimal charging algorithm. On the other hand,

the individual cell of a battery might have different capacity or different impedances and states of charge which in turn cause the imbalances among the cells in a battery pack. Cell balancing circuitry transfers the charge from one cell to another until the state of charge becomes equal among all the cells in a battery pack. Finally, battery fuel gauge (BFG) is designed to provide accurate estimation of the parameters of a battery equivalent circuit model, state of charge, state of available peak power, state of health and the capacity of a battery. The OCA and CBC components of BMS depend on BFG for their functioning.

This thesis is focused on BFG where we represent the Li-ion battery by means of equivalent circuit model (ECM) and develop algorithm in order to estimate the ECM parameters of battery. We develop four equivalent circuit model considering the dynamic loading conditions. Most of the existing approaches regarding ECM parameter identification rely on offline characteristics of a battery in order to estimate parameters online. Therefore, we focus on developing a new approach based on recursive least square method in order to estimate the battery ECM parameters in real time that only requires the measured voltage and current. We further propose a new battery fuel gauge to estimate battery SOC online in the later part of the thesis. ECM parameters identification and online SOC estimation will be explored in different chapters of the thesis, and as such we have dedicated this research toward future development of this algorithm for hardware implementation of a battery management system.

## **1.1 Organization of the Thesis**

We have elected to present this thesis structured according to the manuscript format rather than the traditional format. That is, the chapters to follow consist of manuscripts previously written and submitted by the author, with first authorship. Chapters 2, 3, and 4 (referred to herein as “manuscript chapters”) are included in

this thesis as written at the times of their submissions, in chronological order, with alterations to format and slight modifications to content in order to maintain a cohesive thesis structure. As prescribed by the manuscript format, abstracts have also been omitted. It is the belief of the author that by virtue of the chosen format their thought process, understanding of the research topic and its place in the modern world, and journey toward producing increasingly meaningful contributions, are far more accurately conveyed as a story told through a collection of chronological works.

While a traditional thesis commonly contains a general literature review and problem statement, the we have chosen to forego these sections in the traditional sense. The reader will find that each of the manuscript chapters provide their own introductions which serve the purpose of familiarizing the reader with both the context of the research and relevant literature. To include a general literature review and problem statement in this thesis would be to introduce unnecessary redundancy. It must be noted, however, that some amount of redundancy will persist throughout the manuscript chapters as a consequence of each being originally written as their own, standalone entities.

The remainder of this thesis is organized as follows: In Chapter 2, the first of the author's accepted work in IEEE Electrical Power and Energy Conference (EPEC 2019) is presented. In this chapter, a novel approach to real time parameter identification of a Li-ion battery is proposed. The method is based on recursive least square (RLS) method. An equivalent circuit model (ECM) of the Li-ion battery is introduced in this chapter. The proposed approach tends to estimate the ECM parameters of the battery which requires only measure voltage and currents whereas, the existing approaches rely on open circuit voltage (OCV)- state of charge (SOC) characteristics, hysteresis and temperature. Chapter2 is a shorter version of Chapter 3. In Chapter 2 we propose one equivalent circuit model which is denoted as 'model 3' in Chapter 3. In Chapter 3, we propose four equivalent circuit model of a Li-ion batteries considering the dynamic loading condition and estimate the ECM parameters

for each of these models based on RLS method. We perform our proposed algorithm in to individual model. The algorithm is tested using simulated data and further the robustness is verified by employing it into real data from multiple batteries recorded at different temperature. We analyze the model mismatch issue in order to realize the performance of the proposed approach in practical scenario.

Finally, Chapter 4 presents a robust battery fuel gauge (BFG) where the we developed a new approach to estimate SOC online. The ECM parameter identification algorithm from Chapter 3 is incorporated in Chapter 4 to estimate ECM parameter and the SOC simultaneously so that the algorithm can capture the change in parameters and the SOC in real time due to the temperature and aging. We compare the estimated SOC using the proposed approach with widely used SOC estimation technique called Coulomb counting (CC) to verify our performance. Although Coulomb counting is a popular approach, it has certain limitations such as it requires the initial condition of the SOC to begin estimation. Moreover, it requires the knowledge of true battery capacity. Therefore, the proposed BFG in Chapter 4 tends to focus on exterminating this limitations. The proposed BFG is further evaluated by introducing the three new validation technique: CC Metric, OCV Metric and TTV Metric. The results demonstrate the state-of-art performance of the proposed BFG.

# Chapter 2

## Recursive Least Square Estimation Approach to Real-Time Parameter Identification in Li-ion Batteries

### 2.1 Introduction

Rechargeable batteries play a major role as a fundamental part of the renewable energy storage systems, electric vehicles, equipment and power tools, consumer electronics, military and aerospace supplies due to their high power and high energy density. Safe, efficient and reliable operation of a battery is therefore becoming the prime objective for the upcoming era of energy storage. In this regards, battery management system (BMS) has become an integral part of the rechargeable battery systems that are used for energy storage. An efficient way to identify battery's performance could increase the safety, efficiency and reliability of battery pack in a system.

Important modules of a BMS [6] are the battery fuel gauge (BFG), cell balancing circuitry (CBC), and optimal charging algorithm (OCA). Online estimation of available peak power, state-of-charge, state-of-health of the battery is required in practical

scenario. Further, ECM parameters change according to the variation of temperature, aging, cell balancing, change of state-of-charge (SOC), state-of-health (SOH) and load. Therefore, real time ECM parameter identification is critical in battery management systems.

Modeling the Li-ion batteries in the form of an electrical equivalent circuit models (ECM) is a widely accepted approach in BMS [13,15]. In an overly simplified form the ECM approximation, a Li-ion battery reduces to a resistive element that is in series to the electromotive force (EMF) element of the battery [14,15]. More realistic extended ECMs include several RC elements as well as a hysteresis voltage in the ECM. The parameters of the ECM needs to be known in order to estimate the SOC as well as remaining power both of which are crucial for battery management [2,17]. For example, the knowledge of SOC and remaining power is crucial for an electric vehicle (EV) while it is on the road. Indeed, estimating the battery ECM parameters is an essential element in all applications where rechargeable batteries are used.

Many different approaches to estimate battery model parameter can be found in the existing literature. One of these used extended kalman filter method and state space model for the online parameter identification [20]. However, the convergence of the error for the estimating capacitance in that approach is not as good as for the estimation of other parameters. In [8], [18], [9], equivalent circuit model based parameter identification was presented where the hysteresis was not included in the model which may affect the performance. The offline approach for initialization is required in [1] for real-time parameter estimation. Another approach for real-time parameter estimation in [21] requires the knowledge of SOC in order to identify both the fast dynamics (resistance, charge transfer) and the slow dynamics (diffusion effect). Online battery model parameter estimation is critical as the parameters change according to the variation of temperature, aging, cell balancing, change of SOC, SOH and load and it can affect the available peak power [22]. Besides, offline parameter identification methods do not consider dynamic inputs. These observations justify

the need to develop more accurate approaches for real-time identification of ECM parameters in Li-ion batteries.

In this chapter, a robust approach is presented for real-time, linear estimation of dynamic equivalent circuit parameters for batteries. There are several existing works that developed parameter estimation algorithms for similar battery equivalent circuit models [4, 10, 11, 16, 18, 19]. In these existing works, the ECM parameter estimation is (either directly or indirectly) tied to the SOC estimation algorithm as well. Such dependence on SOC increases the complexity of the ECM identification algorithm; further, errors in SOC estimation, e.g., due to incorrect knowledge of the battery capacity, might affect the parameter estimates. Furthermore, SOC estimation algorithms depend on the OCV-SOC parameters [12] of the battery and any errors in the OCV-SOC characterization might affect the performance of these ECM identification algorithms as well. Hence, the primary objective of this chapter is to develop an approach to estimate the ECM model parameters in real-time without depending on other elements of a battery management system, such as OCV-SOC model parameters, SOC estimation algorithms and hysteresis modeling. Consequently, the developed approach in this chapter resulted in other benefits as well. The contributions of this chapter are summarized as follows:

- (i) *An online ECM parameter estimation method that depends only on measured voltage and current:* The proposed approach requires only the measured voltage across the battery terminals and current through the battery. Unlike prior approaches that require SOC, OCV-SOC parameters, temperature, and hysteresis modeling [7], the proposed approach is simplistic in terms of measurement and modeling requirements.
- (ii) *Effect of hysteresis in ECM identification is nullified:* Unlike previous approaches [4], the measurement model for the proposed approach takes the difference of adjacent voltage and current measurements, hence (considering that

adjacent samples are milliseconds apart), nullifying the effect of hysteresis in ECM parameter estimation.

- (iii) *Applicability in time-varying conditions:* The proposed ECM identification approach is built around the recursive least square (RLS) filter. As such, it is able to track time-varying parameters, e.g. it can track change in parameters due to temperature, SOC changes and aging.

The remainder of this chapter is organized as follows: In Section 3.2, we present the mathematical derivation of the new measurement model that is based only on the measured voltage across the battery and current through the battery. In Section 3.3, we summarize our proposed algorithm for ECM parameter estimation using the above-mentioned measurement model. In Section 4.4, we present objective evaluation of the proposed algorithm using a simulated battery model and by computing the mean square error (MSE); then the ECM identification algorithm is applied on data collected from real battery cell at different temperature controlled settings. The chapter is concluded in Section 3.6.

## 2.2 Mathematical Derivation of a New Measurement Model

Fig. 4.14 shows the battery equivalent circuit model where  $v(k)$  represents the measured voltage across the battery terminals and  $i(k)$  represents the current through the battery.  $h(k)$  represents the hysteresis voltage and  $R_1$  and  $C_1$  represents the resistive and the capacitive elements (RC circuit)

In [4], the knowledge of the OCV-SOC curve and the SOC of the battery,  $s(k)$ , was used to compute the OCV( $V_0(s(k))$ ) of the battery. Using this, the voltage-drop can



be computed as,

$$V_D(k) = V(k) - V_0(s(k)) \quad (2.1)$$

Based on the above voltage drop  $V_D(k)$ , an approach to estimate the battery ECM parameters ( $R_0, R_1, C_1, R_2, C_2$ ) was present in [4].

In this chapter, we develop an approach to estimate the ECM parameters without requiring the knowledge of  $V_D(k)$  i.e., without requiring the knowledge of  $\text{SOC}(s(k))$  and the OCV-SOC model parameters that are widely used in the literature to approximate battery.

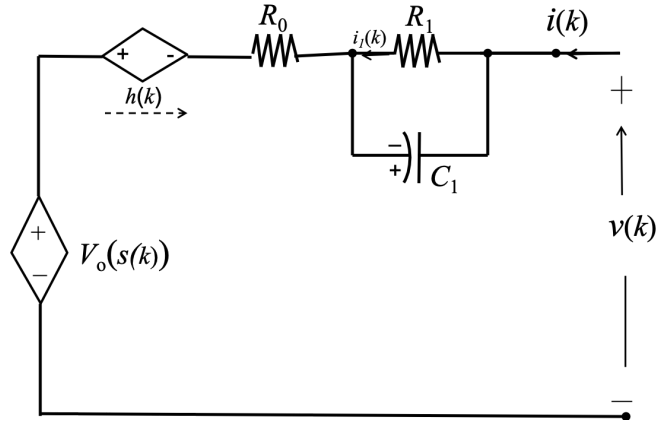


Figure 2.1: **Equivalent circuit models (ECM) of a battery.** Battery equivalent circuit model that is widely used in the literature to represent Li-ion batteries. In this chapter, we present a generalized approach to estimate the ECM parameter.

## 2.2.1 Measurement Model Derivation for Battery ECM

Based on the notations used in Fig. 4.14 the voltage across the battery terminals at time  $k$  and  $k + 1$  can be written as

$$v(k) = V_0(k) + i(k)R_0 + i_1(k)R_1 + h(k) \quad (2.2)$$

$$\begin{aligned} v(k+1) &= V_0(k+1) + i(k+1)R_0 + i_1(k+1)R_1 \\ &\quad + h(k+1) \end{aligned} \quad (2.3)$$

Subtracting (3.62) from (3.63), with the same assumptions that  $V_0(k+1) = V_0(k)$  and  $h(k+1) = h(k)$ ,

$$\begin{aligned} v(k+1) - v(k) &= [i(k+1) - i(k)]R_0 \\ &\quad + [i_1(k+1) - i_1(k)]R_1 \end{aligned} \quad (2.4)$$

Here,

$$i_1(k+1) = \alpha_1 i_1(k) + (1 - \alpha_1)i(k) \quad (2.5)$$

$$(2.6)$$

Taking Z-transform on the above, we can write

$$zI_1(z) = \alpha_1 I_1(z) + (1 - \alpha_1)I(z) \quad (2.7)$$

$$I_1(z) = \frac{1 - \alpha_1}{z - \alpha_1} I(z) \quad (2.8)$$

where

$$\alpha_1 = e^{-\frac{\Delta}{R_1 C_1}} \quad (2.9)$$

Applying Z-transform in (3.64) results in

$$\begin{aligned}
zV(z) - V(z) &= [zI(z) - I(z)]R_0 \\
&\quad + \left[ \frac{z(1 - \alpha_1)}{z - \alpha_1} - \frac{1 - \alpha_1}{z - \alpha_1} \right] I(z)R_1 \\
(z - 1)V(z) &= (z - 1)I(z)R_0 \\
&\quad + \frac{(z - 1)(1 - \alpha_1)}{z - \alpha_1} I(z)R_1 \\
(z - \alpha_1)V(z) &= (z - \alpha_1)I(z)R_0 + (1 - \alpha_1)I(z)R_1 \\
v(k + 1) - \alpha_1 v(k) &= [i(k + 1) - \alpha_1 i(k)]R_0 \\
&\quad + (1 - \alpha_1)i(k)R_1 \\
v(k + 1) &= \alpha_1 v(k) + [i(k + 1) - \alpha_1 i(k)]R_0 \\
&\quad + (1 - \alpha_1)i(k)R_1 \tag{2.10}
\end{aligned}$$

$$\begin{aligned}
v(k) &= \alpha_1 v(k - 1) + [i(k) - \alpha_1 i(k - 1)]R_0 \\
&\quad + (1 - \alpha_1)i(k - 1)R_1 \tag{2.11}
\end{aligned}$$

Subtracting (2.11) from (3.70),

$$\begin{aligned}
\tilde{v}(k) &= \alpha_1 \tilde{v}(k - 1) + [\tilde{i}(k) - \alpha_1 \tilde{i}(k - 1)]R_0 \\
&\quad + (1 - \alpha_1)\tilde{i}(k - 1)R_1 \tag{2.12}
\end{aligned}$$

where,  $\tilde{v}(k)$  and  $\tilde{i}(k)$  are the difference of terminal voltage and difference of the current the resistance for two consecutive time steps.

It is assumed that the sampling time is short enough (typically 0.1 seconds) such that the difference in OCV is negligible, i.e.,

$$V_0(k + 1) - V_0(k) = 0 \tag{2.13}$$

As the sampling time is short enough (typically 0.1 seconds), the difference in hysteresis between two consecutive time steps becomes negligible, hence, the effect of

hysteresis is nullified.

$$h(k+1) - h(k) = 0 \quad (2.14)$$

Now, let us consider the case where the quantities  $v(k)$  and  $i(k)$  are measured as follows

$$z_v(k) = v(k) + n_v(k) \quad (2.15)$$

$$z_i(k) = i(k) + n_i(k) \quad (2.16)$$

where  $n_v(k)$  and  $n_i(k)$  are the voltage and current measurement noise. Let us assume the measurement noise to be independently and identically distributed (i.i.d.) zero-mean Gaussian with standard deviations  $\sigma_v$  and  $\sigma_i$ , respectively.

Substituting (3.44) and (3.45) into (2.12),

$$\begin{aligned} \tilde{v}(k) &= \alpha_1 \tilde{v}(k-1) + \tilde{i}(k)R_0 - \tilde{i}(k-1)\tilde{R}_1 \\ \tilde{z}_v(k) - \tilde{n}_v(k) &= \alpha_1 [\tilde{z}_v(k-1) - \tilde{n}_v(k-1)] + [\tilde{z}_i(k) - \tilde{n}_i(k)]R_0 \\ &\quad - [\tilde{z}_i(k-1) - \tilde{n}_i(k-1)]\tilde{R}_1 \\ \tilde{z}_v(k) &= \alpha_1 \tilde{z}_v(k-1) + \tilde{z}_i(k)R_0 - \tilde{z}_i(k-1)\tilde{R}_1 \\ &\quad + \tilde{n}(k) \end{aligned} \quad (2.17)$$

where,

$$\tilde{n}(k) = \tilde{n}_v(k) - \alpha_1 \tilde{n}_v(k-1) - R_0 \tilde{n}_i(k) + \tilde{R}_1 \tilde{n}_i(k-1) \quad (2.18)$$

The above can be written in matrix format as follows

$$\tilde{z}_v(k) = \begin{bmatrix} \tilde{z}_v(k-1) & \tilde{z}_i(k) & -\tilde{z}_i(k-1) \end{bmatrix} \begin{bmatrix} \alpha_1 \\ R_0 \\ \tilde{R}_1 \end{bmatrix} + \tilde{n}(k) \quad (2.19)$$

where,

$$\tilde{R}_1 = \alpha_1 R_0 - (1 - \alpha_1) R_1 \quad (2.20)$$

The noise  $\tilde{n}(k)$  is correlative and it can be defined as

$$\sigma_n^2(l) = E \{ \tilde{n}(k) \tilde{n}(k-l) \} \quad (2.21)$$

which can be simplified for different possible scenarios as follows:

$$l = 0$$

$$\begin{aligned} \sigma_n^2(0) &= E \{ \tilde{n}(k) \tilde{n}(k) \} \\ &= E \{ \tilde{n}_v^2(k) + \alpha_1^2 \tilde{n}_v^2(k-1) + R_0^2 \tilde{n}_i^2(k) \\ &\quad + \tilde{R}_1^2 \tilde{n}_i^2(k-1) \} \\ &= 2\sigma_v^2 + 2\alpha_1^2 \sigma_v^2 + 2R_0^2 \sigma_i^2 + 2\tilde{R}_1^2 \sigma_i^2 \\ &= 2(1 + \alpha_1^2) \sigma_v^2 + 2(R_0^2 + \tilde{R}_1^2) \sigma_i^2 \end{aligned} \quad (2.22)$$

$$l = 1$$

$$\begin{aligned}
\sigma_n^2(1) &= E \{ \tilde{n}(k) \tilde{n}(k-1) \} \\
&= E \left\{ \left( -\alpha_1 \tilde{n}_v(k-1) + \tilde{R}_1 \tilde{n}_i(k-1) \right) \right. \\
&\quad \left. \left( \tilde{n}_v(k-1) - R_0 \tilde{n}_i(k-1) \right) \right\} \\
&= E \left\{ -\alpha_1 \tilde{n}_v^2(k-1) - R_0 \tilde{R}_1 \tilde{n}_i^2(k-1) \right\} \\
&= -2\alpha_1 \sigma_v^2 - 2R_0 \tilde{R}_1 \sigma_i^2
\end{aligned} \tag{2.23}$$

$$l \geq 2$$

$$\sigma_n^2(l) = E \{ \tilde{n}(k) \tilde{n}(k-l) \} = 0 \tag{2.24}$$

## 2.3 Summary of the Proposed Algorithm

Based on the derivations in Section 3.2, the voltage drop across the circuit components of each of the four equivalent circuit models can be written in the following form:

$$\tilde{v}(k) = \tilde{\mathbf{a}}(k)^T \mathbf{b} + \tilde{n}(k) \tag{2.25}$$

where

$$\tilde{\mathbf{a}}(k)^T = \left[ \tilde{v}_D(k-1) \quad \tilde{z}_i(k) \quad -\tilde{z}_i(k-1) \right] \tag{2.26}$$

$$\mathbf{b} = \left[ \alpha_1 \quad R_0 \quad \tilde{R}_1 \right]^T \tag{2.27}$$

where

$$\tilde{R}_1 = \alpha_1 R_0 - (1 - \alpha_1) R_1 \tag{2.28}$$



square method can be used to update the parameter estimated:

$$\hat{\mathbf{b}}_{\kappa+1} = \hat{\mathbf{b}}_{\kappa} + \mathbf{W}_{\kappa+1} \left( \tilde{\mathbf{v}}_{\kappa+1} - \tilde{\mathbf{A}}_{\kappa+1} \hat{\mathbf{b}}_{\kappa} \right) \quad (2.33)$$

where

$$\mathbf{W}_{\kappa+1} = \mathbf{P}_{\kappa+1} \tilde{\mathbf{A}}_{\kappa+1}^T \mathbf{S}_{\kappa+1}^{-1} \quad (2.34)$$

and

$$\begin{aligned} \mathbf{P}_{\kappa+1}^{-1} &= \mathbf{P}_{\kappa}^{-1} + \tilde{\mathbf{A}}_{\kappa+1}^T \Sigma^{-1} \tilde{\mathbf{A}}_{\kappa+1} \\ \mathbf{S}_{\kappa+1} &= \tilde{\mathbf{A}}_{\kappa+1} \mathbf{P}_{\kappa+1}^{-1} \tilde{\mathbf{A}}_{\kappa+1}^T + \Sigma \end{aligned} \quad (2.35)$$

Given the past parameter estimate for the previous batch,  $\hat{\mathbf{b}}_{\kappa}$ , its estimation error covariance  $\mathbf{P}_{\kappa}^{-1}$  (in inverse form), new set of measurements from the current batch  $\tilde{\mathbf{v}}_{\kappa+1}$  and the corresponding model  $\tilde{\mathbf{A}}_{\kappa+1}$ , the Algorithm 3 can be used to obtain the updated estimate  $\hat{\mathbf{b}}_{\kappa+1}$  and the updated estimation error covariance  $\mathbf{P}_{\kappa+1}^{-1}$ . It must be noted that dimension of  $\tilde{\mathbf{b}}_{\kappa}$  and  $\tilde{\mathbf{A}}_{\kappa}$  vary based on the assumed model.

**Remark 1 (Initialization)** *For the very first iteration of Algorithm 3 there is no prior knowledge of  $\hat{\mathbf{b}}_{\kappa}$ , i.e., when  $\kappa = 1$  there is no  $\hat{\mathbf{b}}_0$ . For this case, we will use a least square estimation without assuming any prior information about noise. This will reduce the covariance matrix to be an identity matrix, i.e.,*

$$\Sigma = \mathbf{I}_{L_b} \quad (2.36)$$

where  $\mathbf{I}_{L_b}$  is an  $L_b \times L_b$  identity matrix. As a result, for the first batch, the parameter



estimation is carried out using the least square (LS) algorithm as follows

$$\begin{aligned}\hat{\mathbf{b}}_1 &= \left( \tilde{\mathbf{A}}_1^T \tilde{\mathbf{A}}_1 \right)^{-1} \tilde{\mathbf{A}}_1^T \tilde{\mathbf{v}}_1 \\ \mathbf{P}_1 &= \left( \tilde{\mathbf{A}}_1^T \tilde{\mathbf{A}}_1 \right)^{-1}\end{aligned}\tag{2.37}$$

**Remark 2 (Battery parameter recovery)** *At every iteration of Algorithm 3, the parameter  $\hat{\mathbf{b}}_\kappa$  has three elements that can be indicated by  $\hat{\mathbf{b}}_\kappa(1)$ ,  $\hat{\mathbf{b}}_\kappa(2)$  and  $\hat{\mathbf{b}}_\kappa(3)$ . The parameters of the ECM can be recovered as follows:*

$$\begin{aligned}R_0 &= \hat{\mathbf{b}}_\kappa(2) \\ R_1 &= \frac{\left[ \hat{\mathbf{b}}_\kappa(1)\hat{\mathbf{b}}_\kappa(2) - \hat{\mathbf{b}}_\kappa(3) \right]}{1 - \hat{\mathbf{b}}_\kappa(1)} \\ C_1 &= -\frac{\Delta}{R_1 \ln(\hat{\mathbf{b}}_\kappa(1))}\end{aligned}\tag{2.38}$$

where,  $\Delta$  is the sampling time.

## 2.4 Results

In this section, we present the results of the proposed algorithm through various computer experiments. First, in subsection 3.5.1, a simulated battery model is used to objectively quantify the performance of the ECM identification algorithm. Then, in subsection 2.4.2, the proposed ECM identification algorithm is tested using data collected from five different battery cells at eight different temperatures.

### 2.4.1 Objective Performance Analysis

For the analysis in this subsection, typical battery usage data was simulated using the observation model shown in Fig. 4.14. First, the current through the battery is simulated to emulate typical battery usage data in a smartphone [3, 5]. Then the

voltage across the battery terminal is computed according to the model assumption. For example, the measured voltage is computed according to (3.62) — after accounting for the voltage and current measurement noise. This requires one to compute the SOC of the battery so that  $V_o(s(k))$  can be computed. For this purpose, we used the characteristics of a typical smart phone battery for the OCV-SOC parameter and  $C_{\text{batt}} = 1.5 \text{ Ah}$  for battery capacity. The exact equations and in-depth details for such battery data simulation is presented in [4]; in this chapter, we adopt the approach in [4] to simulate battery data for model shown in Fig. 4.14. The true value of the ECM parameters are set at  $R_0 = 0.2246 \Omega$ ,  $R_1 = 1 \Omega$  and  $C_1 = 50 \text{ F}$ . The analysis is repeated for three different values of the measurement errors:  $(\sigma_v = 1\mu\text{V}, \sigma_i = 1\mu\text{V})$ ,  $(\sigma_v = 10\mu\text{V}, \sigma_i = 10\mu\text{V})$ , and  $(\sigma_v = 100\mu\text{V}, \sigma_i = 100\mu\text{V})$ . Hence, with only the value of  $\sigma_v$  is indicated when discussing the results. Fig. 3.7 shows the resulting voltage across the battery terminals and current through the battery Model.

The Algorithm 3 is used on the voltage and current data to estimate the battery ECM parameters and their performance is analyzed against true values that are used to simulate the data. Throughout this chapter, the batch number at the ECM estimation algorithm is kept at  $L_b = 200$ . At a sampling time of  $\Delta = 0.1$  seconds, this amounts to 20 seconds of data in each batch. For comparison, the time constant of the RC circuit in the simulation is  $R_1 \times C_1 = 1 \times 50 = 50$  seconds.

The average estimation error for parameter identification is obtained by computing 200 *Monte-Carlo* runs and shown in Fig. 3.8 for three different values of measurement noise,  $\sigma_v = 1\mu\text{V}, 10\mu\text{V}$  and  $100\mu\text{V}$ . The conclusion is that the estimation error is 0.892% for  $R_0$ , 1.1033% for  $R_1$  and 0.2708% for  $C_1$  assuming  $\sigma_v = 1\mu\text{V}$  which implies that the ECM parameter estimation performance is close to optimal. As expected, the average estimation error slightly increases with the noise. This is further illustrated in Table 3.3 which summarizes the average estimation error over all the blocks and 200 Monte Carlo runs for different values of measurement noise. It shows the expected behavior that the estimation error increases with the noise.

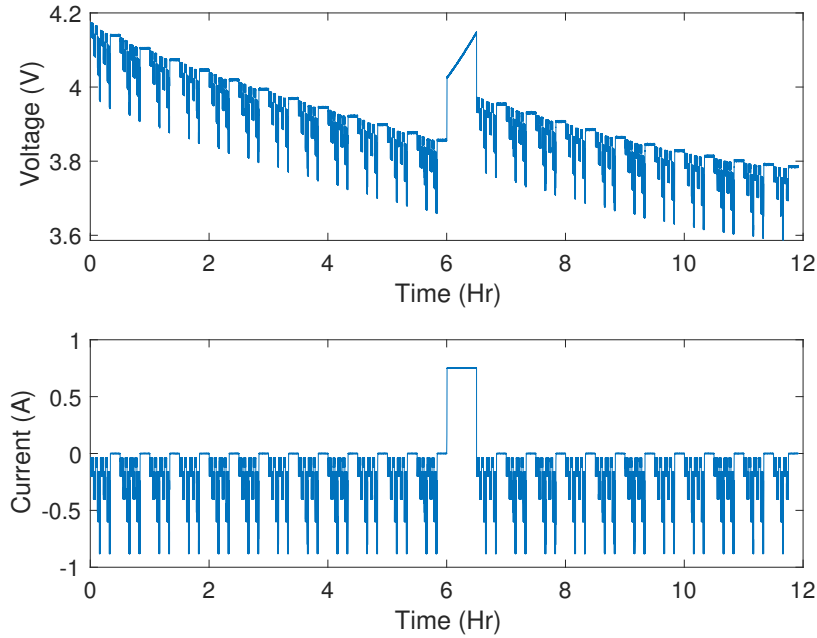


Figure 2.2: **Measured voltage and current profile.** Voltage across the battery terminals and current through the battery

Table 2.1: ECM Parameter Estimation Error (in %)

Parameter	$\sigma_v = 1\mu\text{V}$	$\sigma_v = 10\mu\text{V}$	$\sigma_v = 100\mu\text{V}$
R0	0.8922	0.8920	0.8967
R1	1.1033	1.3160	12.2375
C1	0.2708	0.2367	1.6002

## 2.4.2 Performance Analysis using Different Temperatures

In this subsection, we demonstrate the performance of the proposed approach for battery parameter estimation using data collected from a Samsung EB575152 battery cell at eight different temperatures ranging from  $-25^\circ\text{C}$  to  $45^\circ\text{C}$  at equal intervals. At each temperature, the cell is fully charged and kept at the specified temperature. Then a discharging-charging-discharging current, similar to the one shown in Fig. 3.7 is applied to the battery and the voltage across the battery terminals is recorded. These voltage-current data is then used by the ECM parameter estimation Algorithm 3.

Fig. 3.11 shows the estimated parameters against batch number and Fig. 3.12

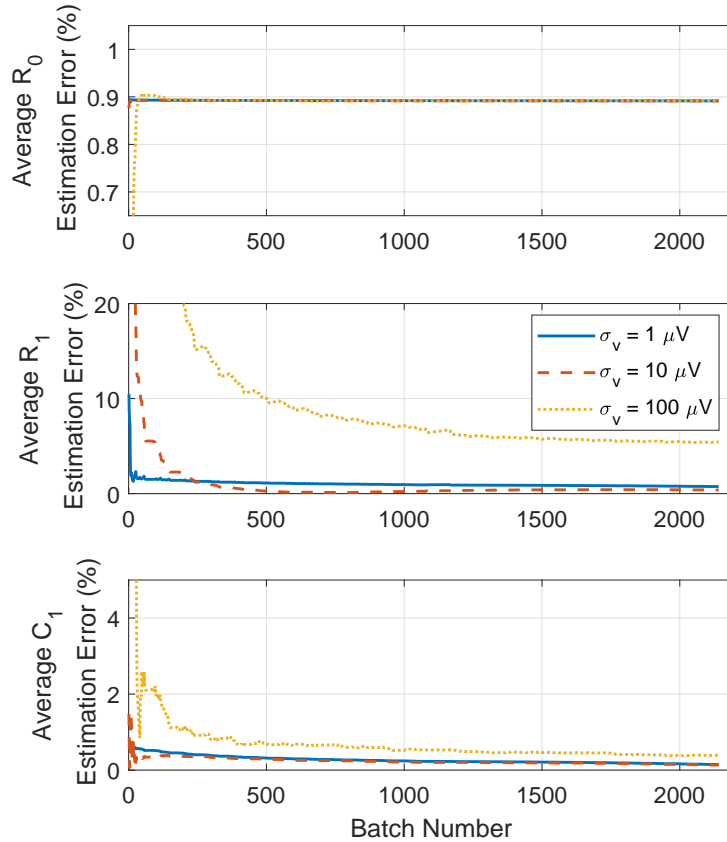


Figure 2.3: **Parameter Estimation for Battery Equivalent Circuit Model.** Mean square error of the estimated parameters are plotted for different values of measurement noise.

shows the steady-state estimated parameters against temperature. It is interesting to note that these estimated values, especially  $R_0$ , follows previously known pattern [12] regarding battery behaviour against temperature changes.

## 2.5 Conclusion

This chapter presents a novel approach for parameter identification of a Lithium ion battery equivalent circuit model (ECM) based on the recursive least square (RLS) filter. The proposed approach only requires measured voltage across the battery

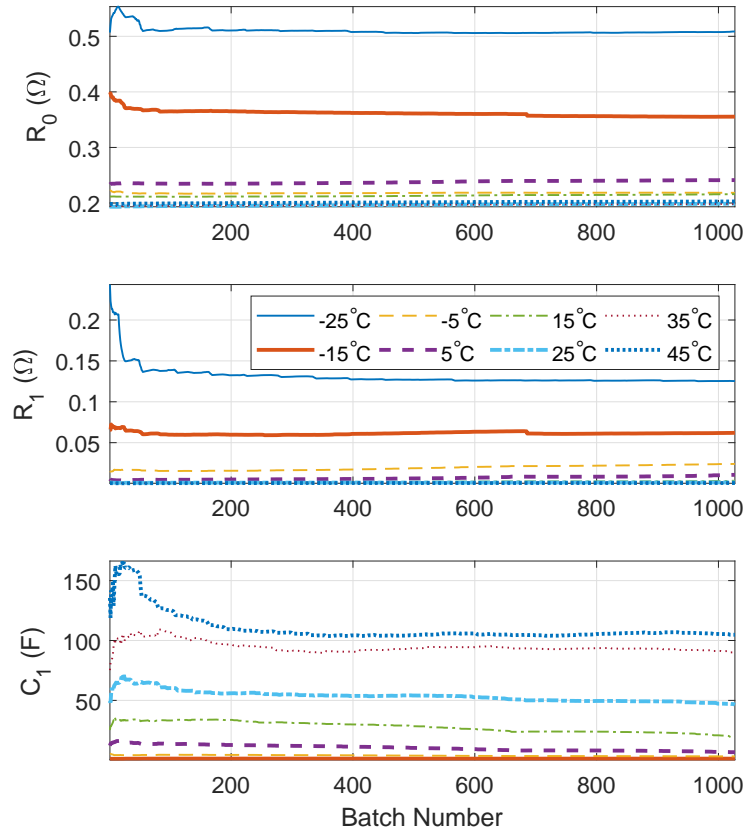


Figure 2.4: **Performance of the ECM identification algorithm at multiple temperatures.** Estimated values of the ECM parameters are plotted against batch number for data collected from the same battery cell used in Samsung Galaxy 4 smartphones (Samsung EB 575152) at eight different temperatures.

terminals and current through the battery. Estimation error due to the noise in measured voltage and current is derived based on the standard deviation of these measurement noises.

The MSE increases with model complexity, however, it remained 1% for battery equivalent circuit model under the assumption of the practical values of measurement noise. ECM parameters were estimated from the same battery cell at eight different temperatures; estimated parameters conformed to previously understood behaviour against temperature.

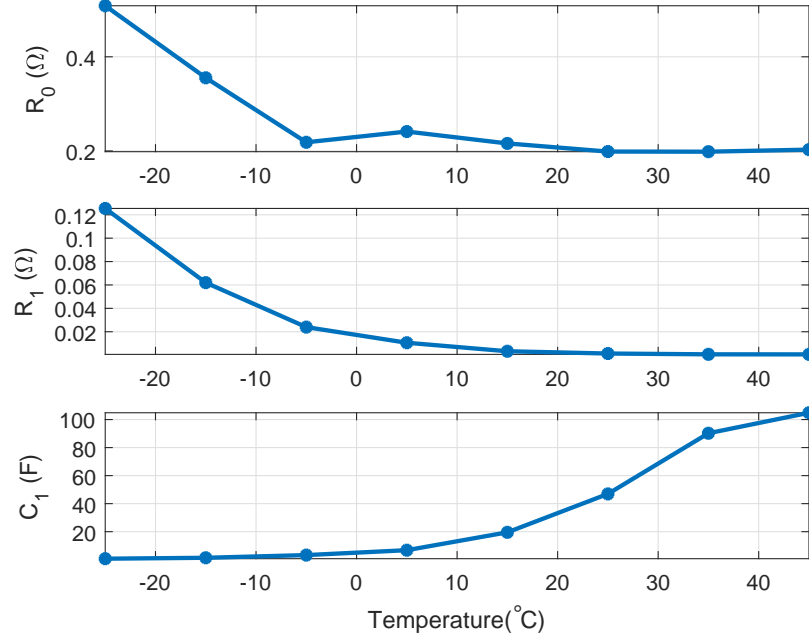


Figure 2.5: **Performance of the ECM identification algorithm on multiple batteries.** Estimated values of the ECM parameters are plotted against the temperature in which the battery was kept. Each entry in this plot is obtained by averaging the estimated values for the last 10 batches corresponding to Fig. 3.11.

---

**Algorithm 1**  $[\hat{\mathbf{b}}_{\kappa+1}, \mathbf{P}_{\kappa+1}^{-1}] = \text{BattECMID}[\hat{\mathbf{b}}_{\kappa}, \mathbf{P}_{\kappa}^{-1}, \tilde{\mathbf{v}}_{\kappa+1}, \tilde{\mathbf{A}}_{\kappa+1}]$

---

- 1: Construct the noise covariance matrix:  $\Sigma_{\kappa}$  using (4.138)

$$\begin{aligned}\sigma_n^2(0) &= 2(1 + \hat{\mathbf{b}}_{\kappa}^2(1))\sigma_v^2 + 2(\hat{\mathbf{b}}_{\kappa}^2(2) + \hat{\mathbf{b}}_{\kappa}^2(3))\sigma_i^2 \\ \sigma_n^2(1) &= -2\alpha_1\sigma_v^2 - 2\hat{\mathbf{b}}_{\kappa}(2)\hat{\mathbf{b}}_{\kappa}(3)\sigma_i^2\end{aligned}$$

- 2: Update Error Cov:  $\mathbf{P}_{\kappa+1}^{-1} = \mathbf{P}_{\kappa}^{-1} + \tilde{\mathbf{A}}_{\kappa+1}^T \Sigma^{-1} \tilde{\mathbf{A}}_{\kappa+1}$
  - 3: Update Residual Cov:  $\mathbf{S}_{\kappa+1} = \tilde{\mathbf{A}}_{\kappa+1} \mathbf{P}_{\kappa+1}^{-1} \tilde{\mathbf{A}}_{\kappa+1}^T + \Sigma$
  - 4: Update gain:  $\mathbf{W}_{\kappa+1} = \mathbf{P}_{\kappa+1} \tilde{\mathbf{A}}_{\kappa+1}^T \mathbf{S}_{\kappa+1}^{-1}$
  - 5: Update Parameter:  $\hat{\mathbf{b}}_{\kappa+1} = \hat{\mathbf{b}}_{\kappa} + \mathbf{W}_{\kappa+1}(\tilde{\mathbf{v}}_{\kappa+1} - \tilde{\mathbf{A}}_{\kappa+1} \hat{\mathbf{b}}_{\kappa})$
-

## 2.6 Bibliography

- [1] W. Allafi, K. Uddin, C. Zhang, R. M. R. A. Sha, and J. Marco. On-line scheme for parameter estimation of nonlinear lithium ion battery equivalent circuit models using the simplified refined instrumental variable method for a modified wiener continuous-time model. *Applied Energy*, 204:497–508, 2017. pages 6, 29
  
- [2] R. D. Anderson, Y. Zhao, X. Wang, X. G. Yang, and Y. Li. Real time battery power capability estimation. In *American Control Conference*, pages 592–597, 2012. pages 6, 28
  
- [3] G. Avvari, B. Pattipati, B. Balasingam, K. Pattipati, and Y. Bar-Shalom. Experimental set-up and procedures to test and validate battery fuel gauge algorithms. *Applied energy*, 160:404–418, 2015. pages xiv, 17, 56, 77, 81, 90, 91, 92, 95, 96, 97, 98, 101, 102, 103, 104
  
- [4] B. Balasingam, G. Avvari, B. Pattipati, K. Pattipati, and Y. Bar-Shalom. A robust approach to battery fuel gauging, part I: Real time model identification. *Journal of Power Sources*, 272:1142–1153, 2014. pages 7, 8, 9, 18, 29, 30, 31, 35, 39, 56, 77, 83
  
- [5] B. Balasingam, G. Avvari, K. Pattipati, and Y. Bar-Shalom. Performance analysis results of a battery fuel gauge algorithm at multiple temperatures. *Journal of Power Sources*, 273:742–753, 2015. pages xiv, 17, 56, 77, 81, 90, 91, 92, 104
  
- [6] B. Balasingam and K. Pattipati. Elements of a robust battery-management system: From fast characterization to universality and more. *IEEE Electrification Magazine*, 6(3):34–37, 2018. pages 5, 27

- [7] A. Farmann, W. Waag, and D. U. Sauer. Adaptive approach for on-board impedance parameters and voltage estimation of lithium-ion batteries in electric vehicles. *Journal of Power Sources*, 299:176–188, 2015. pages 7, 29, 30, 83
- [8] T. Feng, L. Yang, X. Zhao, H. Zhang, and J. Qiang. Online identification of lithium-ion battery parameters based on an improved equivalent-circuit model and its implementation on battery state-of-power prediction. *Journal of Power Sources*, 281:192–203, 2015. pages 6, 29
- [9] C. Fleischer, W. Waag, H.-M. Heyn, and D. U. Sauer. On-line adaptive battery impedance parameter and state estimation considering physical principles in reduced order equivalent circuit battery models: Part 1. requirements, critical review of methods and modeling. *Journal of Power Sources*, 260:276–291, 2014. pages 6, 29
- [10] J. Gomez, R. Nelson, E. E. Kalu, M. H. Weatherspoon, and J. P. Zheng. Equivalent circuit model parameters of a high-power Li-ion battery: Thermal and state of charge effects. *Journal of Power Sources*, 196(10):4826–4831, 2011. pages 7, 30
- [11] S. Jiang. A parameter identification method for a battery equivalent circuit model. Technical report, SAE Technical Paper, 2011. pages 7, 30
- [12] B. Pattipati, B. Balasingam, G. Avvari, K. R. Pattipati, and Y. Bar-Shalom. Open circuit voltage characterization of lithium-ion batteries. *Journal of Power Sources*, 269:317–333, 2014. pages 7, 20, 30, 59, 82
- [13] G. L. Plett. Extended Kalman filtering for battery management systems of LiPB-based HEV battery packs: Part 1. background. *Journal of Power sources*, 134(2):252–261, 2004. pages 6, 27, 76, 81



- [14] G. L. Plett. *Battery Management Systems, Volume I: Battery Modeling*. Artech House Publishers, 2015. pages 6, 28
- [15] G. L. Plett. *Battery Management Systems, Volume II: Equivalent-Circuit Methods*. Artech House Publishers, 2015. pages 6, 27, 28, 81
- [16] A. Seaman, T.-S. Dao, and J. McPhee. A survey of mathematics-based equivalent-circuit and electrochemical battery models for hybrid and electric vehicle simulation. *Journal of Power Sources*, 256:410–423, 2014. pages 7, 28, 30
- [17] W. Waag, C. Fleischer, and D. U. Sauer. Adaptive on-line prediction of the available power of lithium-ion batteries. *Journal of Power Sources*, 242:548–559, 2013. pages 6, 28
- [18] W. Waag, C. Fleischer, and D. U. Sauer. On-line estimation of lithium-ion battery impedance parameters using a novel varied-parameters approach. *Journal of Power Sources*, 237:260–269, 2013. pages 6, 7, 29, 30
- [19] W. Waag, C. Fleischer, and D. U. Sauer. Critical review of the methods for monitoring of lithium-ion batteries in electric and hybrid vehicles. *Journal of Power Sources*, 258:321–339, 2014. pages 7, 28, 30
- [20] T. Wang, L. Pei, R. Lu, C. Zhu, and G. Wu. Online parameter identification for lithium-ion cell in battery management system. In *Vehicle Power and Propulsion Conference*, pages 1–6, 2014. pages 6, 28
- [21] C. Zhang, W. Allafi, Q. Dinh, P. Ascencio, and J. Marco. Online estimation of battery equivalent circuit model parameters and state of charge using decoupled least squares technique. *Energy*, 142:678–688, 2018. pages 6, 29
- [22] X. Zhang, M. Xu, S. Habibi, F. Yan, and R. Ahmed. Offline parameter identification and state-of-charge estimation for healthy and aged electric vehicle

batteries based on the combined model. *World Academy of Science, Engineering and Technology, International Journal of Electrical, Computer, Energetic, Electronic and Communication Engineering*, 10(11):1384–1389, 2016. pages 6,

29

# Chapter 3

## A Novel Approach to Real-Time Parameter Identification in Li-ion Batteries

### 3.1 Introduction

Rechargeable batteries are an excellent form of energy storage. Particularly, Lithium based batteries have been widely adopted in electric vehicles, portable electronic equipment, household appliances, power tools, aerospace equipment and renewable energy storage systems, to name a few. A battery management system (BMS) [7], consisting of a battery fuel gauge, cell balancing circuitry, and optimal charging algorithm, is essential for the safe, reliable and efficient operation of a battery pack. The BMS uses three non-invasive measurements from the battery, voltage, current and temperature, to estimate the state of charge (SOC) and state of health (SOH); these estimates are used in BMS functions, such as the generation of optimal charging waveforms, cell balancing, and to activate safety protectors.

Modeling the Li-ion batteries in the form of an electrical equivalent circuit models (ECM) is a widely accepted approach in BMS [24, 28]. In an overly simplified form

the ECM approximation, a Li-ion battery reduces to a resistive element that is in series to the electromotive force (EMF) element of the battery [27,28]. More realistic extended ECMs include several RC elements as well as a hysteresis voltage in the ECM. The parameters of the ECM needs to be known in order to estimate the SOC as well as remaining power both of which are crucial for battery management [2,32]. For example, the knowledge of SOC and remaining power is crucial for an electric vehicle (EV) while it is on the road. Indeed, estimating the battery ECM parameters is an essential element in all applications where rechargeable batteries are used.

Battery ECM identification methods fall into two important categories: frequency domain methods and time domain methods. Frequency domain approaches employ electrochemical impedance spectroscopy (EIS) [29,31,34] where specified control signal at different frequency is applied to the battery and its response is measured for EIS analysis. As such, the EIS approach is considered an offline approach to ECM parameter identification. Further, considering the fact that specialized excitation pulses are applied, the accuracy of the EIS approaches are very high.

Time domain approach to ECM identification does not require a special excitation to be applied on the battery. As such, time domain ECM identification methods are suitable for online ECM parameter estimation by a BMS. Due to this, significant work was done in the past with the aim of developing ECM identification techniques through time-domain based algorithms. The extended Kalman filter (EKF) based approaches [21,25,35,38] propose to model and estimate the ECM parameters in a state-space model (SSM) along with other battery states, such as the SOC, battery capacity and hysteresis. The EKF approach suffers from the fact that it approximates the SSM to be linear and Gaussian whereas in reality the dynamics in a battery are hardly linear or Gaussian. Other approaches to estimate ECM parameters include auto regressive exogenous (ARX) models [39], least squares methods [18,19], and genetic algorithms [16]. There is little work in the present literature about performance bounds of ECM parameter estimation methods [37].

Battery model parameters can be identified by using either online or offline approaches. In [3], [9], [22], [41], the parameters were estimated offline following EIS and pulse discharging method. However, those approaches do not inspect the dynamic inputs and fail to operate under dynamic loading condition. Additionally, more model parameters were required in [3] as it induced more RC circuits in the model which in turns resulted in increased complexity to identify the parameters. Online battery model parameter estimation provides with the up-to-date knowledge of the available power in real time. Online estimation of available peak power (i.e. state of energy) of the battery is critical in some applications such as driving, portable equipment and medical devices [10], [11], [12], [30], [36]. However, the battery model parameters change according to the variation of temperature, aging, cell balancing, change of SOC, SOH and load and it can affect the available peak power [42]. For such dynamic scenario, offline parameter estimation approaches are not suitable.

Several approaches can be found in the literature regarding real time parameter identification. Equivalent circuit model based battery parameter identification was proposed in [14], [33], [15]. However, these approaches did not include hysteresis in the model which may affect the performance. There is one approach in [26], where author incorporated hysteresis by means of “zero state hysteresis” and “one state hysteresis” model. However, the method did not demonstrate the performance analysis regarding estimation of model parameter. The approach proposed in [1] for real-time parameter estimation requires an offline approach for initialization. Another approach for real-time parameter estimation in [40], which is based on decoupled weighted recursive least square, requires the knowledge of SOC in order to identify both the fast dynamics (resistance, charge transfer) and the slow dynamics (diffusion effect). In [13], impedance is modeled as a function of SOC and [12] requires the knowledge of SOC as well and does not consider measurement noise covariance analysis which was shown to be critical in [5]. In summary, ECM parameter estimation remains an important, ongoing problem for battery management systems.

In this chapter, a robust approach is presented for real-time, linear estimation of dynamic equivalent circuit parameters for batteries. There are several existing works that developed parameter estimation algorithms for similar battery equivalent circuit models [5, 17, 20, 29, 33, 34]. In these existing works, the ECM parameter estimation is (either directly or indirectly) tied to the SOC estimation algorithm as well. Such dependence on SOC increases the complexity of the ECM identification algorithm; further, errors in SOC estimation, e.g., due to incorrect knowledge of the battery capacity, might affect the parameter estimates. Furthermore, SOC estimation algorithms depend on the OCV-SOC parameters [23] of the battery and any errors in the OCV-SOC characterization might affect the performance of these ECM identification algorithms as well. Hence, the primary objective of this chapter is to develop an approach to estimate the ECM model parameters in real-time without depending on other elements of a battery management system, such as OCV-SOC model parameters, SOC estimation algorithms and hysteresis modeling. Consequently, the developed approach in this chapter resulted in other benefits as well. The contributions of this chapter are summarized as follows:

- (i) *An online ECM parameter estimation method that depends only on measured voltage and current:* The proposed approach requires only the measured voltage across the battery terminals and current through the battery. Unlike prior approaches that require SOC, OCV-SOC parameters, temperature, and hysteresis modeling [13], the proposed approach is simplistic in terms of measurement and modeling requirements.
- (ii) *Theoretical derivation of estimation error:* For the first time, the ECM parameter estimation error is derived in terms of the voltage/current measurement error standard deviations. In this chapter, we show the exact error bound when estimating battery resistance.

- (iii) *Effect of hysteresis in ECM identification is nullified:* Unlike previous approaches [5], the measurement model for the proposed approach takes the difference of adjacent voltage and current measurements, hence (considering that adjacent samples are milliseconds apart), nullifying the effect of hysteresis in ECM parameter estimation.
  
- (iv) *Applicability in time-varying conditions:* The proposed ECM identification approach is built around the recursive least square (RLS) filter. As such, it is able to track time-varying parameters, e.g. it can track change in parameters due to temperature, SOC changes and aging.
  
- (v) *Applicability to different ECM approximations of a real battery:* In this chapter, we show the derivation of ECM parameter estimation for four different ECM model approximations that were widely used in the literature.

The remainder of this chapter is organized as follows: In Section 3.2, we present the mathematical derivation of the new measurement model that is based only on the measured voltage across the battery and current through the battery. In Section 3.3, we summarize our proposed algorithm for ECM parameter estimation using the above-mentioned measurement model. Section 3.4 presents a theoretical performance analysis of the proposed ECM parameter estimation approach. In Section 4.4, we present objective evaluation of the proposed algorithm using several means; first using a simulated battery model and by computing the mean square error (MSE); then the ECM identification algorithm is applied on data collected from real battery cell at different temperature controlled settings; finally, the the ECM identification algorithm is applied to data collected from different commercial battery cells and the results are analyzed. The chapter is concluded in Section 3.6.

## List of Notations I

$\tilde{\mathbf{a}}(k)^T$  . observation model (see (4.134))

$\tilde{\mathbf{A}}_\kappa$  . . . .  $\kappa^{\text{th}}$  batch of observation model (3.108)

$\mathbf{b}$  . . . . . observation model parameter (4.135)

$\mathbf{b}_\kappa$  . . . . .  $\kappa^{\text{th}}$  batch of observation model parameter (3.108)

$C_1$  . . . . battery internal capacitance (Figure 4.14)

$C_2$  . . . . battery internal capacitance (Figure 4.14)

$h(k)$  . . . hysteresis at time  $k$  (3.55)

$i(k)$  . . . true current through the battery at time  $k$  (3.45)

$i_1(k)$  . . current through  $R_1$  (3.81)

$i_2(k)$  . . current through  $R_2$  (3.81)

$I(z)$  . . .  $z$ -transform of current (3.69)

$\tilde{i}(k)$  . . . difference of current between two consecutive time steps (3.54)

$\tilde{n}_1(k)$  . . measurement noise for ECM 1 (3.46)

$\tilde{n}_2(k)$  . . measurement noise for ECM 2 (3.56)

$\tilde{n}_3(k)$  . . measurement noise for ECM 3 (3.75)

$\tilde{n}_4(k)$  . . measurement noise for ECM 4 (3.93)

$n_v(k)$  . . voltage measurement error at time  $k$  (3.44)

$n_i(k)$  . . current measurement error at time  $k$  (3.45)



$\tilde{n}_v(k)$  .. difference of voltage measurement error between two consecutive time steps  
(3.58)

$\tilde{n}_i(k)$  .. difference of current measurement error between two consecutive time steps  
(3.59)

$\tilde{n}(k)$  ... difference of measurement noise between two consecutive time steps (4.135)

$\tilde{\mathbf{n}}_\kappa$  .....  $\kappa^{\text{th}}$  batch of noise covariance matrix (3.108)

$\mathbf{P}_\kappa$  ..... error covariance (3.124)

$\mathbf{P}_{\kappa+1}^{-1}$  .. inverse of error covariance (4.142)

$R_0$  ..... battery internal series resistance in Figure 4.14

$R_1$  ..... battery internal resistance in Figure 4.14

$R_2$  ..... battery internal resistance in Figure 4.14

$\mathbf{S}_{\kappa+1}$  .. updated residual covariance (4.142)

$v_D(k)$  . Voltage drops across model impedance at time  $k$  (3.39)

$v(k)$  ... true voltage across the battery terminal at time  $k$  (3.44)

$V_0(k)$  .. open circuit voltage (3.43)

$V(z)$  ..  $z$ -transform of measured terminal voltage (3.69)

$\tilde{v}(k)$  ... difference of measured voltage between two consecutive measurements (3.54)

$\tilde{\mathbf{v}}_\kappa$  .....  $\kappa^{\text{th}}$  batch of measured voltage (3.108)

$\mathbf{W}_{\kappa+1}$  . updated gain (4.141)

$z_v(k)$  .. measured voltage across the battery terminal at time  $k$  (3.44)

$z_i(k)$  .. measured current through the battery at time  $k$  (3.45)

$\tilde{z}_v(k)$  .. difference of measured battery terminal voltage between two consecutive time steps (3.46)

$\tilde{z}_i(k)$  .. difference of measured current through the battery between two consecutive time steps (3.46)

$\Delta$  ..... sampling time (3.122)

$\sigma_n$  ..... standard deviation of observation noise (3.61)

$\sigma_v$  ..... standard deviation of voltage noise (3.61)

$\sigma_i$  ..... standard deviation of current noise (3.61)

$\sigma_{n_3}^2(0)$  . 1<sup>st</sup> diagonal elements of error covariance matrix for model 3 (3.78)

$\sigma_{n_3}^2(1)$  . first off-diagonal elements of error covariance matrix for model 3 (3.79)

$\sigma_{n_4}^2(0)$  . diagonal elements of error covariance matrix for model 4 (3.97)

$\sigma_{n_4}^2(1)$  . first off-diagonal elements of error covariance matrix for model 4 (3.98)

$\sigma_{n_4}^2(2)$  . second off-diagonal elements of error covariance matrix for model 4 (3.99)

$\Sigma$  ..... noise covariance matrix (3.109)

## 3.2 Mathematical Derivation of a New Measurement Model

Figure 4.14 shows four different ECM types that are widely used in the literature to represent Li-ion batteries. In all four models,  $v(k)$  represents the measured voltage across the battery terminals and  $i(k)$  represents the current through the battery. In models 2 to 4,  $h(k)$  represents the hysteresis voltage. In model 3 and 4,  $R_1$  and  $C_1$  represents the resistive and the capacitive elements (RC circuit) and similarly in

model 4  $R_2$  and  $C_2$  represents a second resistive and capacitive elements.

In [5], the knowledge of the OCV-SOC curve and the SOC of the battery,  $s(k)$ , was used to compute the OCV( $V_0(s(k))$ ) of the battery. Using this, the voltage-drop can be computed as,

$$V_D(k) = V(k) - V_0(s(k)) \quad (3.39)$$

Based on the above voltage drop  $V_D(k)$ , an approach to estimate the battery ECM parameters ( $R_0, R_1, C_1, R_2, C_2$ ) was present in [5].

In this chapter, we develop an approach to estimate the ECM parameters without requiring the knowledge of  $V_D(k)$  i.e., without requiring the knowledge of SOC( $s(k)$ ) and the OCV-SOC model parameters that are widely used in the literature to approximate battery.

### 3.2.1 Measurement Model Derivation for Model 1

Based on the notations used in Figure 4.14(a) the voltage across the battery terminals at time  $k$  and  $k + 1$  can be written as

$$v(k) = V_0(k) + i(k)R_0 \quad (3.40)$$

$$v(k + 1) = V_0(k + 1) + i(k + 1)R_0 \quad (3.41)$$

From equation (3.40) and (3.41),

$$\begin{aligned} v(k + 1) - v(k) &= [i(k + 1) - i(k)]R_0 \\ \tilde{v}(k) &= \tilde{i}(k)R_0 \end{aligned} \quad (3.42)$$

where,  $\tilde{v}(k)$  and  $\tilde{i}(k)$  are the difference of terminal voltage and difference of the current the resistance for two consecutive time steps.

Further, it is assumed that the sampling time is short enough (typically 0.1 seconds)

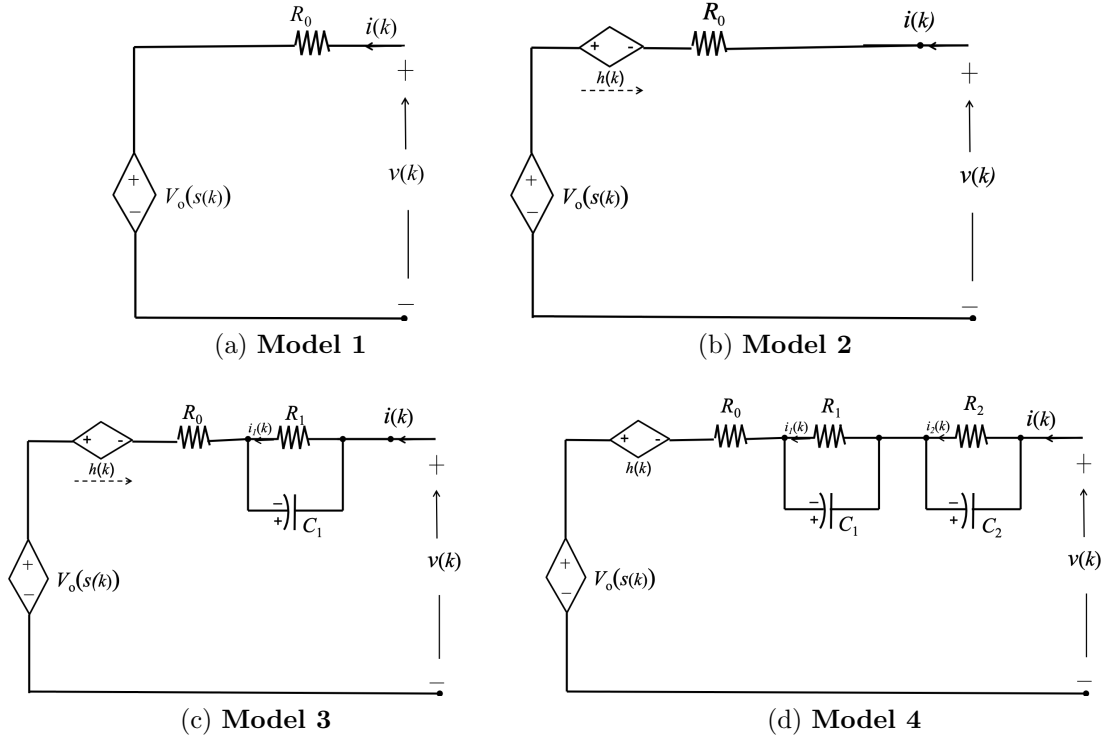


Figure 3.6: **Equivalent circuit models (ECM) of a battery.** Four different ECMs that are widely used in the literature to represent Li-ion batteries. In this chapter, we present a generalized approach to estimate the parameters under each model assumption.

such that the difference in OCV is negligible, i.e.,

$$V_0(k+1) - V_0(k) = 0 \quad (3.43)$$

Now, let us consider the case where the quantities  $v(k)$  and  $i(k)$  are measured as follows

$$z_v(k) = v(k) + n_v(k) \quad (3.44)$$

$$z_i(k) = i(k) + n_i(k) \quad (3.45)$$

where  $n_v(k)$  and  $n_i(k)$  are the voltage and current measurement noise. Let us assume

the measurement noise to be independently and identically distributed (i.i.d.) zero-mean Gaussian with standard deviations  $\sigma_v$  and  $\sigma_i$ , respectively.

By substituting (3.44) and (3.45) in (3.42), we get

$$\begin{aligned}\tilde{z}_v(k) - \tilde{n}_v(k) &= [\tilde{z}_i(k) - \tilde{n}_i(k)]R_0 \\ \tilde{z}_v(k) &= \tilde{z}_i(k)R_0 + \tilde{n}_1(k)\end{aligned}\tag{3.46}$$

where

$$\tilde{n}_1(k) = \tilde{n}_v(k) - \tilde{n}_i(k)R_0\tag{3.47}$$

$$\tilde{n}_v(k) = n_v(k+1) - n_v(k)\tag{3.48}$$

$$\tilde{n}_i(k) = n_i(k+1) - n_i(k)\tag{3.49}$$

and the noise  $\tilde{n}(k)$  is zero mean and variance

$$\begin{aligned}\sigma_n^2 &= E\{\tilde{n}_1(k)^2\} \\ &= E\{[n_1(k+1) - n_1(k)]^2\} \\ &= E\{n_1(k+1)^2\} + E\{n_1(k)^2\} \\ &= (\sigma_v^2 + R_0^2\sigma_i^2) + (\sigma_v^2 + R_0^2\sigma_i^2) \\ &= 2(\sigma_v^2 + R_0^2\sigma_i^2)\end{aligned}\tag{3.50}$$

### 3.2.2 Measurement Model Derivation for Model 2

Based on the notations used in Figure 4.14(b) the voltage across the battery terminals at time  $k$  and  $k+1$  can be written as

$$v(k) = V_0(k) + i(k)R_0 + h(k)\tag{3.52}$$

$$v(k+1) = V_0(k+1) + i(k+1)R_0 + h(k+1)\tag{3.53}$$

From equation (3.52) and (3.53),

$$\begin{aligned} v(k+1) - v(k) &= [i(k+1) - i(k)]R_0 \\ \tilde{v}(k) &= \tilde{i}(k)R_0 \end{aligned} \quad (3.54)$$

where,  $\tilde{v}(k)$  and  $\tilde{i}(k)$  are the difference of terminal voltage and difference of the current through the resistance for two consecutive time steps.

As the sampling time is short enough (typically 0.1 seconds), the difference in hysteresis between two consecutive time steps becomes negligible, hence, the effect of hysteresis is nullified.

$$h(k+1) - h(k) = 0 \quad (3.55)$$

Assuming that the voltage and current measurement noises are zero, and considering a batch of  $L_b$  measurements, the following vector observation model can be written:

By substituting (3.44) and (3.45) in (3.54), we get

$$\begin{aligned} \tilde{z}_v(k) - \tilde{n}_v(k) &= [\tilde{z}_i(k) - \tilde{n}_i(k)]R_0 \\ \tilde{z}_v(k) &= \tilde{z}_i(k)R_0 + \tilde{n}_2(k) \end{aligned} \quad (3.56)$$

where

$$\tilde{n}_2(k) = \tilde{n}_v(k) - \tilde{n}_i(k)R_0 \quad (3.57)$$

$$\tilde{n}_v(k) = n_v(k+1) - n_v(k) \quad (3.58)$$

$$\tilde{n}_i(k) = n_i(k+1) - n_i(k) \quad (3.59)$$

and the noise  $\tilde{n}_2(k)$  is zero mean and variance

$$\begin{aligned}
\sigma_n^2 &= E\{\tilde{n}_2(k)^2\} & (3.60) \\
&= E\{[n_2(k+1) - n_2(k)]^2\} \\
&= E\{n_2(k+1)^2\} + E\{n_2(k)^2\} \\
&= (\sigma_v^2 + R_0^2\sigma_i^2) + (\sigma_v^2 + R_0^2\sigma_i^2) \\
&= 2(\sigma_v^2 + R_0^2\sigma_i^2) & (3.61)
\end{aligned}$$

**Remark 3** *As the hysteresis effect is nullified, Model 2 reduces to the same observation model as that of Model 1. This was not the case in [5]. In the remainder of this chapter we will use Model 1 for performance analysis.*

### 3.2.3 Measurement Model Derivation for Model 3

Based on the notations used in Figure 4.14(c) the voltage across the battery terminals at time  $k$  and  $k+1$  can be written as

$$v(k) = V_0(k) + i(k)R_0 + i_1(k)R_1 + h(k) \quad (3.62)$$

$$\begin{aligned}
v(k+1) &= V_0(k+1) + i(k+1)R_0 + i_1(k+1)R_1 \\
&\quad + h(k+1) & (3.63)
\end{aligned}$$

Subtracting equation (3.62) from (3.63), with the same assumptions that  $V_0(k+1) = V_0(k)$  and  $h(k+1) = h(k)$ ,

$$\begin{aligned}
v(k+1) - v(k) &= [i(k+1) - i(k)]R_0 \\
&\quad + [i_1(k+1) - i_1(k)]R_1 & (3.64)
\end{aligned}$$

Here,

$$i_1(k+1) = \alpha_1 i_1(k) + (1 - \alpha_1) i(k) \quad (3.65)$$

Taking Z-transform on the above, we can write

$$zI_1(z) = \alpha_1 I_1(z) + (1 - \alpha_1) I(z) \quad (3.66)$$

$$I_1(z) = \frac{1 - \alpha_1}{z - \alpha_1} I(z) \quad (3.67)$$

where

$$\alpha_1 = e^{-\frac{\Delta}{R_1 C_1}} \quad (3.68)$$

Applying Z-transform in (3.64) results in

$$\begin{aligned} zV(z) - V(z) &= [zI(z) - I(z)]R_0 \\ &+ \left[ \frac{z(1 - \alpha_1)}{z - \alpha_1} - \frac{1 - \alpha_1}{z - \alpha_1} \right] I(z)R_1 \end{aligned} \quad (3.69)$$

$$\begin{aligned} (z - 1)V(z) &= (z - 1)I(z)R_0 \\ &+ \frac{(z - 1)(1 - \alpha_1)}{z - \alpha_1} I(z)R_1 \end{aligned}$$

$$(z - \alpha_1)V(z) = (z - \alpha_1)I(z)R_0 + (1 - \alpha_1)I(z)R_1$$

$$\begin{aligned} v(k+1) - \alpha_1 v(k) &= [i(k+1) - \alpha_1 i(k)]R_0 \\ &+ (1 - \alpha_1) i(k)R_1 \end{aligned}$$

$$\begin{aligned} v(k+1) &= \alpha_1 v(k) + [i(k+1) - \alpha_1 i(k)]R_0 \\ &+ (1 - \alpha_1) i(k)R_1 \end{aligned} \quad (3.70)$$

$$\begin{aligned} v(k) &= \alpha_1 v(k-1) + [i(k) - \alpha_1 i(k-1)]R_0 \\ &+ (1 - \alpha_1) i(k-1)R_1 \end{aligned} \quad (3.71)$$



Subtracting equation (3.71) from (3.70),

$$\begin{aligned}\tilde{v}(k) &= \alpha_1 \tilde{v}(k-1) + [\tilde{i}(k) - \alpha_1 \tilde{i}(k-1)]R_0 \\ &\quad + (1 - \alpha_1)\tilde{i}(k-1)R_1\end{aligned}\tag{3.72}$$

Substituting equation (3.44) and (3.45) into the equation (3.72),

$$\begin{aligned}\tilde{v}(k) &= \alpha_1 \tilde{v}(k-1) + \tilde{i}(k)R_0 - \tilde{i}(k-1)\tilde{R}_1 \\ \tilde{z}_v(k) - \tilde{n}_v(k) &= \alpha_1[\tilde{z}_v(k-1) - \tilde{n}_v(k-1)] + [\tilde{z}_i(k) - \tilde{n}_i(k)]R_0 \\ &\quad - [\tilde{z}_i(k-1) - \tilde{n}_i(k-1)]\tilde{R}_1 \\ \tilde{z}_v(k) &= \alpha_1 \tilde{z}_v(k-1) + \tilde{z}_i(k)R_0 - \tilde{z}_i(k-1)\tilde{R}_1 \\ &\quad + \tilde{n}_3(k)\end{aligned}\tag{3.73}$$

where,

$$\tilde{n}_3(k) = \tilde{n}_v(k) - \alpha_1 \tilde{n}_v(k-1) - R_0 \tilde{n}_i(k) + \tilde{R}_1 \tilde{n}_i(k-1)\tag{3.74}$$

The above can be written in matrix format as follows

$$\tilde{z}_v(k) = \begin{bmatrix} \tilde{z}_v(k-1) & \tilde{z}_i(k) & -\tilde{z}_i(k-1) \end{bmatrix} \begin{bmatrix} \alpha_1 \\ R_0 \\ \tilde{R}_1 \end{bmatrix} + \tilde{n}_3(k)\tag{3.75}$$

where,

$$\tilde{R}_1 = \alpha_1 R_0 - (1 - \alpha_1)R_1\tag{3.76}$$

The noise  $\tilde{n}_3(k)$  is correlative and it can be defined as

$$\sigma_{n_3}^2(l) = E \{ \tilde{n}_3(k) \tilde{n}_3(k-l) \} \quad (3.77)$$

which can be simplified for different possible scenarios as follows:

$$l = 0$$

$$\begin{aligned} \sigma_{n_3}^2(0) &= E \{ \tilde{n}_3(k) \tilde{n}_3(k) \} \\ &= E \{ \tilde{n}_v^2(k) + \alpha_1^2 \tilde{n}_v^2(k-1) + R_0^2 \tilde{n}_i^2(k) \\ &\quad + \tilde{R}_1^2 \tilde{n}_i^2(k-1) \} \\ &= 2\sigma_v^2 + 2\alpha_1^2 \sigma_v^2 + 2R_0^2 \sigma_i^2 + 2\tilde{R}_1^2 \sigma_i^2 \\ &= 2(1 + \alpha_1^2) \sigma_v^2 + 2(R_0^2 + \tilde{R}_1^2) \sigma_i^2 \end{aligned} \quad (3.78)$$

$$l = 1$$

$$\begin{aligned} \sigma_{n_3}^2(1) &= E \{ \tilde{n}_3(k) \tilde{n}_3(k-1) \} \\ &= E \left\{ \left( -\alpha_1 \tilde{n}_v(k-1) + \tilde{R}_1 \tilde{n}_i(k-1) \right) \right. \\ &\quad \left. (\tilde{n}_v(k-1) - R_0 \tilde{n}_i(k-1)) \right\} \\ &= E \left\{ -\alpha_1 \tilde{n}_v^2(k-1) - R_0 \tilde{R}_1 \tilde{n}_i^2(k-1) \right\} \\ &= -2\alpha_1 \sigma_v^2 - 2R_0 \tilde{R}_1 \sigma_i^2 \end{aligned} \quad (3.79)$$

$$l \geq 2$$

$$\sigma_{n_3}^2(l) = E \{ \tilde{n}_3(k) \tilde{n}_3(k-l) \} = 0 \quad (3.80)$$

### 3.2.4 Measurement Model Derivation for Model 4

Based on the notations used in Figure 4.14(d) the voltage across the battery terminals at time  $k$  and  $k + 1$  can be written as

$$v(k) = V_0(k) + i(k)R_0 + i_1(k)R_1 + i_2(k)R_2 + h(k) \quad (3.81)$$

$$\begin{aligned} v(k+1) &= V_0(k+1) + i(k+1)R_0 + i_1(k+1)R_1 \\ &\quad + i_2(k+1)R_2 + h(k+1) \end{aligned} \quad (3.82)$$

Substituting equation (3.81) from equation (3.82),

$$\begin{aligned} v(k+1) - v(k) &= [i(k+1) - i(k)]R_0 + [i_1(k+1) - i_1(k)]R_1 \\ &\quad + [i_2(k+1) - i_2(k)]R_2 \end{aligned} \quad (3.83)$$

Here,

$$i_1(k+1) = \alpha_1 i_1(k) + (1 - \alpha_1) i(k) \quad (3.84)$$

$$\Rightarrow zI_1(z) = \alpha_1 I_1(z) + (1 - \alpha_1) I(z) \quad (3.85)$$

$$\Rightarrow I_1(z) = \frac{1 - \alpha_1}{z - \alpha_1} I(z) \quad (3.86)$$

$$i_2(k+1) = \alpha_2 i_2(k) + (1 - \alpha_2) i(k) \quad (3.87)$$

$$\Rightarrow zI_2(z) = \alpha_2 I_2(z) + (1 - \alpha_2) I(z) \quad (3.88)$$

$$\Rightarrow I_2(z) = \frac{1 - \alpha_2}{z - \alpha_2} I(z) \quad (3.89)$$

where,

$$\begin{aligned} \alpha_1 &= e^{-\frac{\Delta}{R_1 C_1}} \\ \alpha_2 &= e^{-\frac{\Delta}{R_2 C_2}} \end{aligned} \quad (3.90)$$

From equation (3.83)

$$\begin{aligned}
zV(z) - V(z) &= [zI(z) - I(z)]R_0 + \left[\frac{z(1-\alpha_1)}{z-\alpha_1} - \frac{1-\alpha_1}{z-\alpha_1}\right]I(z)R_1 \\
&\quad + \left[\frac{z(1-\alpha_2)}{z-\alpha_2} - \frac{1-\alpha_2}{z-\alpha_2}\right]I(z)R_2 \\
(z-1)V(z) &= (z-1)I(z)R_0 + \frac{(z-1)(1-\alpha_1)}{z-\alpha_1}I(z)R_1 \\
&\quad + \frac{(z-1)(1-\alpha_2)}{z-\alpha_2}I(z)R_2 \\
V(z) &= I(z)R_0 + \frac{(1-\alpha_1)}{z-\alpha_1}I(z)R_1 + \frac{(1-\alpha_2)}{z-\alpha_2}I(z)R_2 \\
z^2V(z) &= [(\alpha_1 + \alpha_2)z + \alpha_1\alpha_2]V(z) \\
&\quad + [z^2 - (\alpha_1 + \alpha_2)z + \alpha_1\alpha_2]I(z)R_0 \\
&\quad + [z - \alpha_2 - \alpha_1z + \alpha_1\alpha_2]I(z)R_1 \\
&\quad + [z - \alpha_1 - \alpha_2z + \alpha_1\alpha_2]I(z)R_2 \\
\tilde{v}(k+2) &= (\alpha_1 + \alpha_2)\tilde{v}(k+1) + \alpha_1\alpha_2\tilde{v}(k) + \tilde{i}(k+2)R_0 \\
&\quad - (\alpha_1 + \alpha_2)R_0\tilde{i}(k+1) + \alpha_1\alpha_2R_0\tilde{i}(k) \\
&\quad + R_1\tilde{i}(k+1) - \alpha_2R_1\tilde{i}(k) - \alpha_1R_1\tilde{i}(k+1) \\
&\quad + \alpha_1\alpha_2R_1\tilde{i}(k) + R_2\tilde{i}(k+1) - \alpha_1R_2\tilde{i}(k) \\
&\quad - \alpha_2R_2\tilde{i}(k+1) + \alpha_1\alpha_2R_2\tilde{i}(k) \\
\tilde{v}(k+2) &= \alpha\tilde{v}(k+1) - \beta\tilde{v}(k) + R_0\tilde{i}(k+2) - \check{R}_1\tilde{i}(k+1) \\
&\quad + \check{R}_2\tilde{i}(k) \\
\tilde{v}(k) &= \alpha\tilde{v}(k-1) - \beta\tilde{v}(k-2) + R_0\tilde{i}(k) - \check{R}_1\tilde{i}(k-1) \\
&\quad + \check{R}_2\tilde{i}(k-2)
\end{aligned} \tag{3.91}$$

Substituting equation (3.44) and (3.45) into the equation (3.91),

$$\begin{aligned}
\tilde{z}_v(k) - \tilde{n}_v(k) &= \alpha[\tilde{z}_v(k-1) - \tilde{n}_v(k-1)] \\
&\quad - \beta[\tilde{z}_v(k-2) - \tilde{n}_v(k-2)] + R_0[\tilde{z}_i(k) \\
&\quad - \tilde{n}_i(k)] - \check{R}_1[\tilde{z}_i(k-1) - \tilde{n}_i(k-1)] \\
&\quad + \check{R}_2[\tilde{z}_i(k-2) - \tilde{n}_i(k-2)] \\
\tilde{z}_v(k) &= \alpha\tilde{z}_v(k-1) - \beta\tilde{z}_v(k-2) + R_0\tilde{z}_i(k) \\
&\quad - \check{R}_1\tilde{z}_i(k-1) + \check{R}_2\tilde{z}_i(k-2) + \tilde{n}_4(k)
\end{aligned} \tag{3.92}$$

which can be written in the following vector form

$$\tilde{z}_v(k) = \begin{bmatrix} \tilde{z}_v(k-1) & -\tilde{z}_v(k-2) \\ \tilde{z}_i(k) & -\tilde{z}_i(k-1) & \tilde{z}_i(k-2) \end{bmatrix} \begin{bmatrix} \alpha \\ \beta \\ R_0 \\ \check{R}_1 \\ \check{R}_2 \end{bmatrix} + \tilde{n}_4(k) \tag{3.93}$$

where the elements of  $\mathbf{b}$  are given by

$$\begin{aligned}
\alpha &= \alpha_1 + \alpha_2 \\
\beta &= \alpha_1\alpha_2 \\
\check{R}_1 &= (\alpha_1 + \alpha_2)R_0 - (1 - \alpha_1)R_1 - (1 - \alpha_2)R_2 \\
\check{R}_2 &= \alpha_1\alpha_2R_0 - \alpha_2(1 - \alpha_1)R_1 - \alpha_1(1 - \alpha_2)R_2
\end{aligned} \tag{3.94}$$

where,

$$\begin{aligned}
\tilde{n}_4(k) &= \tilde{n}_v(k) - \alpha\tilde{n}_v(k-1) + \beta\tilde{n}_v(k-2) - R_0\tilde{n}_i(k) \\
&\quad + \check{R}_1\tilde{n}_i(k-1) - \check{R}_2\tilde{n}_i(k-2)
\end{aligned} \tag{3.95}$$

The noise  $\tilde{n}(k)$  is correlative and it can be defined as

$$\sigma_{n_4}^2(l) = E \{ \tilde{n}_4(k) \tilde{n}_4(k-l) \} \quad (3.96)$$

which can be simplified for different possible scenarios as follows:

$$l = 0$$

$$\begin{aligned} \sigma_{n_4}^2(0) &= E \{ \tilde{n}_4(k) \tilde{n}_4(k) \} \\ &= E \{ \tilde{n}_v^2(k) + \alpha^2 \tilde{n}_v^2(k-1) + \beta^2 \tilde{n}_v^2(k-2) \\ &\quad + R_0^2 \tilde{n}_i^2(k) + \check{R}_1^2 \tilde{n}_i^2(k-1) + \check{R}_2^2 \tilde{n}_i^2(k-2) \} \\ &= 2 \left[ (1 + \alpha^2 + \beta^2) \sigma_v^2 + (R_0^2 + \check{R}_1^2 + \check{R}_2^2) \sigma_i^2 \right] \end{aligned} \quad (3.97)$$

$$l = 1$$

$$\begin{aligned} \sigma_{n_4}^2(1) &= E \{ \tilde{n}_4(k) \tilde{n}_4(k-1) \} \\ &= E \{ [-\alpha \tilde{n}_v(k-1) + \beta \tilde{n}_v(k-2) \\ &\quad + \check{R}_1 \tilde{n}_i(k-1) - \check{R}_2 \tilde{n}_i(k-2)] \\ &\quad [\tilde{n}_v(k-1) - \alpha \tilde{n}_v(k-2) \\ &\quad - R_0 \tilde{n}_i(k-1) + \check{R}_1 \tilde{n}_i(k-2)] \} \\ &= E \{ -\alpha \tilde{n}_v^2(k-1) - \alpha \beta \tilde{n}_v^2(k-2) \\ &\quad - R_0 \check{R}_1 \tilde{n}_i^2(k-1) - \check{R}_1 \check{R}_2 \tilde{n}_i^2(k-2) \} \\ &= 2 \left[ -\alpha(1 + \beta) \sigma_v^2 - \check{R}_1 (R_0 + \check{R}_2) \sigma_i^2 \right] \end{aligned} \quad (3.98)$$

$$l = 2$$

$$\begin{aligned}
\sigma_{n_4}^2(2) &= E \{ \tilde{n}_4(k) \tilde{n}_4(k-2) \} \\
&= E \{ [\beta \tilde{n}_v(k-2) - \check{R}_2 \tilde{n}_i(k-2)] \\
&\quad [\tilde{n}_v(k-2) - R_0 \tilde{n}_i(k-2)] \} \\
&= E \{ \beta \tilde{n}_v^2(k-2) + \check{R}_2 R_0 \tilde{n}_i^2(k-2) \} \\
&= 2 [\beta \sigma_v^2 + \check{R}_2 R_0 \sigma_i^2] \tag{3.99}
\end{aligned}$$

$$l \geq 3$$

$$\sigma_{n_4}^2(l) = E \{ \tilde{n}_4(k) \tilde{n}_4(k-l) \} = 0 \tag{3.100}$$

In this section, we defined a novel observation model and its noise characteristics to four different types of ECM approximations shown in Figure 4.14. In the next section, we will use these observation models to derive a parameter estimation algorithm for each case.

### 3.3 Summary of the Proposed Algorithm

Based on the derivations in Section 3.2, the voltage drop across the circuit components of each of the four equivalent circuit models can be written in the following form:

$$\tilde{v}(k) = \tilde{\mathbf{a}}(k)^T \mathbf{b} + \tilde{n}(k) \tag{3.101}$$

where

$$\tilde{\mathbf{a}}(k)^T = \begin{cases} \tilde{\mathbf{a}}_1^T(k) \triangleq \tilde{z}_i(k) & \text{Model 1} \\ \tilde{\mathbf{a}}_2^T(k) \triangleq \tilde{z}_i(k) & \text{Model 2} \\ \tilde{\mathbf{a}}_3^T(k) \triangleq [\tilde{v}_D(k-1) \quad \tilde{z}_i(k) \quad -\tilde{z}_i(k-1)] & \text{Model 3} \\ \tilde{\mathbf{a}}_4^T(k) \triangleq [\tilde{v}_D(k-1) \quad -\tilde{v}_D(k-2) \quad \tilde{z}_i(k) \\ \quad -\tilde{z}_i(k-1) \quad \tilde{z}_i(k-2)] & \text{Model 4} \end{cases} \quad (3.102)$$

$$\mathbf{b} = \begin{cases} \mathbf{b}_1 \triangleq R_0 & \text{Model 1} \\ \mathbf{b}_2 \triangleq R_0 & \text{Model 2} \\ \mathbf{b}_3 \triangleq [\alpha_1 \quad R_0 \quad \tilde{R}_1]^T & \text{Model 3} \\ \mathbf{b}_4 \triangleq [\alpha \quad \beta \quad R_0 \quad \check{R}_1 \quad \check{R}_2]^T & \text{Model 4} \end{cases} \quad (3.103)$$

$$\tilde{n}(k) = \begin{cases} \tilde{n}_1(k) & \text{Model 1} \\ \tilde{n}_2(k) & \text{Model 2} \\ \tilde{n}_3(k) & \text{Model 3} \\ \tilde{n}_4(k) & \text{Model 4} \end{cases} \quad (3.104)$$

for model 3

$$\begin{aligned} \tilde{R}_1 &= \alpha_1 R_0 - (1 - \alpha_1) R_1 \\ \tilde{H} &= h(k) - \alpha_1 h(k-1) \end{aligned} \quad (3.105)$$



and, for model 4

$$\begin{aligned}
\alpha &= \alpha_1 + \alpha_2 \\
\beta &= \alpha_1 \alpha_2 \\
\check{R}_1 &= (\alpha_1 + \alpha_2)R_0 - (1 - \alpha_1)R_1 - (1 - \alpha_2)R_2 \\
\check{R}_2 &= \alpha_1 \alpha_2 R_0 - \alpha_2(1 - \alpha_1)R_1 - \alpha_1(1 - \alpha_2)R_2
\end{aligned} \tag{3.106}$$

By stacking one observation  $\tilde{v}(k)$  below another, the observation model (4.133) can be written in matrix form as follows

$$\tilde{\mathbf{v}}_\kappa = \tilde{\mathbf{A}}_\kappa \mathbf{b}_\kappa + \tilde{\mathbf{n}}_\kappa \tag{3.107}$$

where  $\kappa$  is the batch number,

$$\begin{aligned}
\tilde{\mathbf{v}}_\kappa &= [\tilde{v}(\kappa L_b - L_b + 1), \tilde{v}(\kappa L_b - L_b + 1), \dots, \tilde{v}(\kappa L_b)]^T \\
\tilde{\mathbf{a}}_\kappa &= [\tilde{\mathbf{a}}(\kappa L_b - L_b + 1), \tilde{\mathbf{a}}(\kappa L_b - L_b + 1), \dots, \tilde{\mathbf{a}}(\kappa L_b)]^T \\
\tilde{\mathbf{n}}_\kappa &= [\tilde{\mathbf{n}}(\kappa L_b - L_b + 1), \tilde{\mathbf{n}}(\kappa L_b - L_b + 1), \dots, \tilde{\mathbf{n}}(\kappa L_b)]^T
\end{aligned} \tag{3.108}$$

and  $L_b$  is the batch length.

The noise  $\tilde{\mathbf{n}}_\kappa$  is zero mean with covariance matrices for each of the four cases given by

$$\Sigma = \begin{cases} \Sigma_1 & \text{Model 1} \\ \Sigma_2 & \text{Model 2} \\ \Sigma_3 & \text{Model 3} \\ \Sigma_4 & \text{Model 4} \end{cases} \tag{3.109}$$

where

$$\Sigma_1 = \begin{bmatrix} \sigma_{n_1}^2 & & & \\ & \sigma_{n_1}^2 & & \\ & & \ddots & \\ & & & \sigma_{n_1}^2 \end{bmatrix} \quad (3.110)$$

$$\Sigma_2 = \begin{bmatrix} \sigma_{n_2}^2 & & & \\ & \sigma_{n_2}^2 & & \\ & & \ddots & \\ & & & \sigma_{n_2}^2 \end{bmatrix} \quad (3.111)$$

$$\Sigma_3 = \begin{bmatrix} \sigma_{n_3}^2(0) & \sigma_{n_3}^2(1) & & & \\ \sigma_{n_3}^2(1) & \sigma_{n_3}^2(0) & \sigma_{n_3}^2(1) & & \\ & \ddots & \ddots & \ddots & \\ & & \sigma_{n_3}^2(1) & \sigma_{n_3}^2(0) & \sigma_{n_3}^2(1) \\ & & & \sigma_{n_3}^2(1) & \sigma_{n_3}^2(0) \end{bmatrix} \quad (3.112)$$

$$\Sigma_4 = \begin{bmatrix} \sigma_{n_4}^2(0) & \sigma_{n_4}^2(1) & \sigma_{n_4}^2(2) & & & \\ \sigma_{n_4}^2(1) & \sigma_{n_4}^2(0) & \sigma_{n_4}^2(1) & \sigma_{n_4}^2(2) & & \\ \sigma_{n_4}^2(2) & \sigma_{n_4}^2(1) & \sigma_{n_4}^2(0) & \sigma_{n_4}^2(1) & \sigma_{n_4}^2(2) & \\ & \ddots & \ddots & \ddots & \ddots & \ddots \\ & \sigma_{n_4}^2(2) & \sigma_{n_4}^2(1) & \sigma_{n_4}^2(0) & \sigma_{n_4}^2(1) & \sigma_{n_4}^2(2) \\ & & \sigma_{n_4}^2(2) & \sigma_{n_4}^2(1) & \sigma_{n_4}^2(0) & \sigma_{n_4}^2(1) \\ & & & \sigma_{n_4}^2(2) & \sigma_{n_4}^2(1) & \sigma_{n_4}^2(0) \end{bmatrix} \quad (3.113)$$

The individual terms of the noise variance  $\sigma_{n_1}^2 = \sigma_{n_2}^2 = \sigma_n^2$  are defined in (3.61) and the expressions for  $\sigma_{n_3}^2(0), \sigma_{n_3}^2(1), \sigma_{n_4}^2(0), \sigma_{n_4}^2(1)$  and  $\sigma_{n_4}^2(2)$  are derived in (3.78), (3.79), (3.97), (3.98) and (3.99) respectively.

Now, given the  $\kappa^{\text{th}}$  batch of observation  $\tilde{\mathbf{v}}_\kappa$  along with the model  $\tilde{\mathbf{A}}_\kappa$ , the parameter

$\mathbf{b}$  can be estimated through the least squares (LS) method as follows:

$$\hat{\mathbf{b}}_\kappa = \left( \tilde{\mathbf{A}}_\kappa^T \Sigma^{-1} \tilde{\mathbf{A}}_\kappa \right)^{-1} \tilde{\mathbf{A}}_\kappa^T \Sigma^{-1} \tilde{\mathbf{v}}_\kappa \quad (3.114)$$

When the next batch of observation  $\tilde{\mathbf{v}}_\kappa$  becomes available, the recursive least square method can be used to update the parameter estimated:

$$\hat{\mathbf{b}}_{\kappa+1} = \hat{\mathbf{b}}_\kappa + \mathbf{W}_{\kappa+1} \left( \tilde{\mathbf{v}}_{\kappa+1} - \tilde{\mathbf{A}}_{\kappa+1} \hat{\mathbf{b}}_\kappa \right) \quad (3.115)$$

where

$$\mathbf{W}_{\kappa+1} = \mathbf{P}_{\kappa+1} \tilde{\mathbf{A}}_{\kappa+1}^T \mathbf{S}_{\kappa+1}^{-1} \quad (3.116)$$

and

$$\begin{aligned} \mathbf{P}_{\kappa+1}^{-1} &= \mathbf{P}_\kappa^{-1} + \tilde{\mathbf{A}}_{\kappa+1}^T \Sigma^{-1} \tilde{\mathbf{A}}_{\kappa+1} \\ \mathbf{S}_{\kappa+1} &= \tilde{\mathbf{A}}_{\kappa+1} \mathbf{P}_{\kappa+1}^{-1} \tilde{\mathbf{A}}_{\kappa+1}^T + \Sigma \end{aligned} \quad (3.117)$$

Given the past parameter estimate for the previous batch,  $\hat{\mathbf{b}}_\kappa$ , its estimation error covariance  $\mathbf{P}_\kappa^{-1}$  (in inverse form), new set of measurements from the current batch  $\tilde{\mathbf{v}}_{\kappa+1}$  and the corresponding model  $\tilde{\mathbf{A}}_{\kappa+1}$ , the Algorithm 3 can be used to obtain the updated estimate  $\hat{\mathbf{b}}_{\kappa+1}$  and the updated estimation error covariance  $\mathbf{P}_{\kappa+1}^{-1}$ . It must be noted that dimension of  $\tilde{\mathbf{b}}_\kappa$  and  $\tilde{\mathbf{A}}_\kappa$  vary based on the assumed model.

**Remark 4 (Initialization)** *For the very first iteration of Algorithm 3 there is no prior knowledge of  $\hat{\mathbf{b}}_\kappa$ , i.e., when  $\kappa = 1$  there is no  $\hat{\mathbf{b}}_0$ . For this case, we will use a least square estimation without assuming any prior information about noise. This will reduce the covariance matrix to be an identity matrix, i.e.,*

$$\Sigma = \mathbf{I}_{L_b} \quad (3.118)$$

where  $\mathbf{I}_{L_b}$  is an  $L_b \times L_b$  identity matrix. As a result, for the first batch, the parameter estimation is carried out using the least square (LS) algorithm as follows

$$\begin{aligned}\hat{\mathbf{b}}_1 &= \left( \tilde{\mathbf{A}}_1^T \tilde{\mathbf{A}}_1 \right)^{-1} \tilde{\mathbf{A}}_1^T \tilde{\mathbf{v}}_1 \\ \mathbf{P}_1 &= \left( \tilde{\mathbf{A}}_1^T \tilde{\mathbf{A}}_1 \right)^{-1}\end{aligned}\tag{3.119}$$

**Remark 5 (Battery parameter recovery)** At every iteration of Algorithm 3, given  $\hat{\mathbf{b}}_\kappa$ , the ECM parameters are computed as follows: **Model 1 & 2:**

Here, the parameter  $\hat{\mathbf{b}}_\kappa$  has just one element which is the estimate of  $R_0$ , i.e.,

$$R_0 = \hat{\mathbf{b}}_\kappa\tag{3.120}$$

**Model 3:**

Here, the parameter  $\hat{\mathbf{b}}_\kappa$  has three elements that can be indicated by  $\hat{\mathbf{b}}_\kappa(1)$ ,  $\hat{\mathbf{b}}_\kappa(2)$  and  $\hat{\mathbf{b}}_\kappa(3)$ . The parameters of the ECM model 3 can be recovered as follows:

$$\begin{aligned}R_0 &= \hat{\mathbf{b}}_\kappa(2) \\ R_1 &= \frac{\left[ \hat{\mathbf{b}}_\kappa(1)\hat{\mathbf{b}}_\kappa(2) - \hat{\mathbf{b}}_\kappa(3) \right]}{1 - \hat{\mathbf{b}}_\kappa(1)} \\ C_1 &= -\frac{\Delta}{R_1 \ln(\hat{\mathbf{b}}_\kappa(1))}\end{aligned}\tag{3.121}$$

where,  $\Delta$  is the sampling time.

**Model 4:**

Here, the parameter  $\hat{\mathbf{b}}_\kappa$  has five elements indicated by  $\hat{\mathbf{b}}_\kappa(1) \dots \hat{\mathbf{b}}_\kappa(5)$ . The parameters

of the ECM model 4 can be recovered as follows:

$$\begin{aligned}
R_0 &= \hat{\mathbf{b}}_\kappa(3) \\
R_1 &= \frac{(\alpha_2 \hat{\mathbf{b}}_\kappa(1) - \hat{\mathbf{b}}_\kappa(2)) \hat{\mathbf{b}}_\kappa(3) - \alpha_2 \hat{\mathbf{b}}_\kappa(4) + \hat{\mathbf{b}}_\kappa(5)}{(\alpha_2 - \alpha_1)(1 - \alpha_2)} \\
C_1 &= -\frac{\Delta}{R_1 \ln(\hat{\mathbf{b}}_\kappa(3))} \\
R_2 &= \frac{(\alpha_1 \hat{\mathbf{b}}_\kappa(1) - \hat{\mathbf{b}}_\kappa(2)) \hat{\mathbf{b}}_\kappa(3) - \alpha_1 \hat{\mathbf{b}}_\kappa(4) + \hat{\mathbf{b}}_\kappa(5)}{(\alpha_1 - \alpha_2)(1 - \alpha_1)} \\
C_2 &= -\frac{\Delta}{R_2 \ln(\hat{\mathbf{b}}_\kappa(3))}
\end{aligned} \tag{3.122}$$

where

$$\begin{aligned}
\alpha_1 &= \frac{\left(-\hat{\mathbf{b}}_\kappa(1) + \sqrt{\hat{\mathbf{b}}_\kappa^2(1) - 4\hat{\mathbf{b}}_\kappa(2)}\right)}{2} \\
\alpha_2 &= \frac{\left(-\hat{\mathbf{b}}_\kappa(1) - \sqrt{\hat{\mathbf{b}}_\kappa^2(1) - 4\hat{\mathbf{b}}_\kappa(2)}\right)}{2}
\end{aligned} \tag{3.123}$$

### 3.4 Theoretical Performance Analysis

In this section, we derive error bounds for the model identification strategies presented in Section 3.2.

The error covariance matrix  $\mathbf{P}_\kappa$  corresponding to the above LS estimation of  $\tilde{\mathbf{b}}_\kappa$  is given by the following equation [8]

$$\mathbf{P}_\kappa = \left( \tilde{\mathbf{A}}_\kappa^T \Sigma^{-1} \tilde{\mathbf{A}}_\kappa \right)^{-1} \tag{3.124}$$

where the model parameter  $\mathbf{A}_\kappa$  is defined in (4.134) which is also re-written below

$$\tilde{\mathbf{A}}_\kappa = [\tilde{z}_i(\kappa L_b - L_b + 1), \dots, \tilde{z}_i(\kappa L_b)]^T \tag{3.125}$$

Next, we will simplify and analyze the above covariance matrix.

For Model 1 the parameter to be estimated is  $\mathbf{b} = R_0$ ; the inverse of the noise covariance,  $\Sigma^{-1}$ , simplifies to

$$\Sigma^{-1} = \begin{bmatrix} \sigma_n^{-2} & & & \\ & \sigma_n^{-2} & & \\ & & \ddots & \\ & & & \sigma_n^{-2} \end{bmatrix} = \frac{1}{\sigma_n^2} \mathbf{I} \quad (3.126)$$

where  $\mathbf{I}$  is an  $L_b \times L_b$  identity matrix. Substituting (3.126) and (3.125) into (3.124), the noise covariance for model 1 becomes,

$$\begin{aligned} \mathbf{P}_\kappa &= \left( \sigma_n^{-2} \tilde{\mathbf{A}}_\kappa^T \tilde{\mathbf{A}}_\kappa \right)^{-1} \\ &= \left( \sigma_n^{-2} (\tilde{z}_i^2(1), \dots, \tilde{z}_i^2(L_b)) \right)^{-1} \\ &= \sigma_n^2 \left( \sum_{k=1}^{L_b} \tilde{z}_i^2(k) \right)^{-1} \end{aligned} \quad (3.127)$$

where, without loss of generality, we assumed the first batch, i.e.,  $\kappa = 1$ .

From (3.127), one can conclude the following about the estimation error:

1. *Measurement error effect:* The estimation error is proportional to  $\sigma_n^2 = 2(\sigma_v^2 + R_0^2 \sigma_i^2)$ .
2. *Number of sample effect:* The more the number of samples  $L_b$  the lower the estimation error.
3. *Sampling time effect:* Let us recall that each sample  $\tilde{z}_i(k)$  is defined by

$$\tilde{z}_i(k) = z_i(k+1) - z_i(k) \quad (3.128)$$

based on which, the following can be written

$$\sum_{k=1}^{L_b} \tilde{z}_i(k) = z_i(L_b + 1) - z_i(1) \quad (3.129)$$

Further, the following inequality is always true

$$(x_1 + x_2 + \dots x_N)^2 > (x_1^2 + x_2^2 + \dots x_N^2) \quad (3.130)$$

as long as the signs of all  $x_k$ ,  $k = 1, \dots, N$ , are the same. From this, we can write that

$$(z_i(L_b + 1) - z_i(1))^2 > \sum_{k=1}^{L_b} \tilde{z}_i^2(k) \quad (3.131)$$

The observation (3.131) tells us that the estimation error can be reduced by increasing the time between two adjacent samples — as long as the direction of current through the battery remains unchanged (either charging or discharging). However, the further the two samples are apart, the more the assumption in (3.43) is violated. Further, the performance might be affected by measurement noise. In this chapter, we do not analyze the performance due to downsampling — an elaborate performance analysis for best hardware implementation is left out as a future work.

**Remark 6** *The noise covariance matrix contains only the diagonal elements thus implying the white noise. According to the Cramer Rao Lower Bound(CRLB), the diagonal elements of the covariance matrix is equal to the inverse of Fisher Information Matrix,  $J^{-1} = \sigma_n^2 \left( \tilde{\mathbf{A}}_\kappa^T \tilde{\mathbf{A}}_\kappa \right)^{-1}$ . Therefore, the proposed approach for model 1 satisfy the Cramer Rao Lower Bound(CRLB) which makes the estimator Minimum Variance Unbiased Estimator.*

The only parameter being estimated under the Model 2 assumption is  $R_0$  where the observation model is identical to that of Model 1. As such, the discussion regarding the estimation error variance is the same that for Model 1.

For Model 3 and 4, analytical simplification similar to (3.127) is impossible. However, the above three effects, *measurement error effect*, *number of samples effect*, and

*sampling time effect*, are expected to hold for all four models.

## 3.5 Results

In this section, we present the results of the proposed algorithm through various computer experiments. First, in subsection 3.5.1, a simulated battery model is used to objectively quantify the performance of the ECM identification algorithm. Then, in subsection 3.5.2, a model mismatch analysis is presented based on the same simulated battery model. Finally, in subsection 3.5.4, the proposed ECM identification algorithm is tested using data collected from five different battery cells at eight different temperatures.

### 3.5.1 Objective Performance Analysis

For the analysis in this subsection, typical battery usage data was simulated using the observation model shown in Figure 4.14. First, the current through the battery is simulated to emulate typical battery usage data in a smartphone [4, 6]. Then the voltage across the battery terminal is computed according to the model assumption. For example, for model 1, the measured voltage is computed according to (3.40) — after accounting for the voltage and current measurement noise. This requires one to compute the SOC of the battery so that  $V_o(s(k))$  can be computed. For this purpose, we used the characteristics of a typical smart phone battery for the OCV-SOC parameter and  $C_{\text{batt}} = 1.5 \text{ Ah}$  for battery capacity. The exact equations and in-depth details for such battery data simulation is presented in [5]; in this chapter, we adopt the approach in [5] to simulate battery data for the four different models shown in Figure 4.14. First the analysis is done for Model 1 and then it is repeated for Model 3. For both cases, the true value of the ECM parameters are set at  $R_0 = 0.2246 \Omega$ ,  $R_1 = 1 \Omega$  and  $C_1 = 50 \text{ F}$ . The analysis is repeated for three different values of the measurement errors:  $(\sigma_v = 1\mu\text{V}, \sigma_i = 1\mu\text{V})$ ,  $(\sigma_v = 10\mu\text{V}, \sigma_i = 10\mu\text{V})$ ,



and ( $\sigma_v = 100\mu\text{V}, \sigma_i = 100\mu\text{V}$ ). Hence, with only the value of  $\sigma_v$  is indicated when discussing the results. Figure 3.7(a) shows the resulting voltage across the battery terminals and current through the battery under the Model 1 assumption for ECM.

The Algorithm 3 is used on the voltage and current data to estimate the battery ECM parameters and their performance is analyzed against true values that are used to simulate the data. Throughout this chapter, the batch number at the ECM estimation algorithm is kept at  $L_b = 200$ . At a sampling time of  $\Delta = 0.1$  seconds, this amounts to 20 seconds of data in each batch. For comparison, the time constant of the RC circuit in the simulation is  $R_1 \times C_1 = 1 \times 50 = 50$  seconds.

The average estimation error for parameter identification is obtained by computing 200 *Monte-Carlo* runs and shown in Figure 3.7(b) for three different values of measurement noise,  $\sigma_v = 1\mu\text{V}, 10\mu\text{V}$  and  $100\mu\text{V}$ . The conclusion is that the estimation error is 0.00001% assuming  $\sigma_v = 1\mu\text{V}$  which implies that the parameter estimation performance for model 1 is close to optimal. As expected, the average estimation error slightly increases with the noise. This is further illustrated in Table 3.2 which summarizes the average estimation error over all the blocks and 200 Monte Carlo runs for different values of measurement noise. It shows the expected behavior that the estimation error increases with the noise. Further, one must note the very low error for Model 1 (later we will see the estimation error significantly increasing when estimating the more complicated Model 3 parameters).

Table 3.2: Estimation Error (in %) for Model 1

Parameter	$\sigma_v = 1\mu\text{V}$	$\sigma_v = 10\mu\text{V}$	$\sigma_v = 100\mu\text{V}$
R0	0.000010	0.000095	0.001108

Figure 3.8 shows the average estimation error, from 200 Monte-Carlo runs, for three different values of the standard deviation of the noise, for Model 3. Table 3.3 shows the average estimation error over the entire block for comparison. Comparison of Table 3.2 and Table 3.3 shows that the when the ECM complexity increases from

Model 1 to Model 3, the estimation error also increases very significantly.

Table 3.3: Estimation Error (in %) for Model 3

Parameter	$\sigma_v = 1\mu\text{V}$	$\sigma_v = 10\mu\text{V}$	$\sigma_v = 100\mu\text{V}$
R0	0.8916	0.8916	0.8934
R1	0.9236	0.2208	0.829
C1	0.1508	0.1185	0.1382

### 3.5.2 Model Mismatch Analysis

In subsection 3.5.1, the voltage and current measurement of the battery is generated for the exact same model for estimation error analysis. However, the exact model of a real life battery is not necessarily the same as the one assumed by the ECM system identification algorithm. Hence, it is beneficial to understand the type of error resulting from such a model mismatch. In this section, we present the results of two different model match analysis: first, the battery data was simulated using Model 3 to which the parameter estimation Algorithm 3 was applied assuming Model 1; then the battery data was simulated using Model 4 to which the parameter estimation Algorithm 3 was applied assuming Model 3.

Figure 3.9 and 3.10 shows the average estimation error for the above two cases of model mismatch. Averaged errors over all the batches are also summarized in Table 3.4. These results show that the proposed ECM parameter identification approaches are meaningful even if the assumed battery model at the BMS is not exactly the same as the one in play in the battery.

### 3.5.3 Performance Analysis using Different Temperatures

In this subsection, we demonstrate the performance of the proposed approach for battery parameter estimation using data collected from a Samsung EB575152 battery cell at eight different temperatures ranging from  $-25^\circ\text{C}$  to  $45^\circ\text{C}$  at equal intervals.

Table 3.4: Estimation Error (in %) considering Model Mismatch

standard deviation= $1\mu\text{V}$	Estimation model=1, True model= 3	Estimation model=3, True model= 4
R0	0.4474	0.8992
R1	N/A	4.028
C1	N/A	0.7755

At each temperature, the cell is fully charged and kept at the specified temperature. Then a discharging-charging-discharging current, similar to the one shown in Figure 3.7(a) is applied to the battery and the voltage across the battery terminals is recorded. These voltage-current data is then used by the ECM parameter estimation Algorithm 3 that was set to the battery model to be at Model 3. Figure 3.11 shows the estimated parameters against batch number and Figure 3.12 shows the steady-state estimated parameters against temperature. It is interesting to note that these estimated values, especially  $R_0$ , follows previously known pattern [23] regarding battery behaviour against temperature changes.

### 3.5.4 Performance Analysis Using Multiple Batteries

In this section, we demonstrate the performance of the proposed approach for battery parameter estimation using multiple Li-ion batteries. Figure 3.13 shows the estimated parameter values against batch number for five different batteries: LG LGIP 530B, Nokia BP-4L, Blackberry RIM FS 1, Samsung AB463651, and Samsung EB575152. The objective of this demonstration is to find out whether our proposed approach provides accurate estimation of ECM parameters using real measured voltage data collected from different Li-ion batteries. According to Figure 3.13, all the parameters considering model 3 results into the optimum estimated values for each of the batteries, thus states the proposed approach suitable in expectation of practical scenario.

## 3.6 Conclusion

This chapter presents a novel approach for parameter identification of a Lithium ion battery equivalent circuit model (ECM) based on the recursive least square (RLS) filter. The proposed approach only requires measured voltage across the battery terminals and current through the battery. The proposed parameter estimation algorithm is shown to be generalizable to four different ECM approximations of varying model complexity. Estimation error due to the noise in measured voltage and current is derived based on the standard deviation of these measurement noises.

Proposed ECM identification algorithm is rigorously tested through various means: First, data from a battery simulator is used to test the algorithms. For the simplest ECM, the mean square error (MSE) of estimating the battery resistance is found to be the same as the theoretical error bound derived in the chapter. The MSE increases with model complexity, however, it remained below 1% a common model assumption of ECM complexity (denoted in this chapter as Model 3) for practical values of measurement noise. The worst MSE remained 4.028% when a model mismatch was introduced in the battery simulator. Finally, the proposed ECM identification algorithm is tested on real battery data. First, Model 3 parameters were estimated from the same battery cell at eight different temperatures; estimated parameters conformed to previously understood behaviour against temperature. Then, the algorithm was tested on data collected from five different battery cells at room temperature.

---

**Algorithm 2**  $[\hat{\mathbf{b}}_{\kappa+1}, \mathbf{P}_{\kappa+1}^{-1}] = \text{BattECMID}[\hat{\mathbf{b}}_{\kappa}, \mathbf{P}_{\kappa}^{-1}, \tilde{\mathbf{v}}_{\kappa+1}, \tilde{\mathbf{A}}_{\kappa+1}]$

---

1: Construct the noise covariance matrix:  $\Sigma_{\kappa}$  using (3.110)-(3.113)

(i) *Model 1:*

$$\sigma_{n1}^2 = 2 \left( \sigma_v^2 + \hat{\mathbf{b}}_{\kappa}^2 \sigma_i^2 \right)$$

(ii) *Model 2:*

$$\sigma_{n2}^2 = 2 \left( \sigma_v^2 + \hat{\mathbf{b}}_{\kappa}^2 \sigma_i^2 \right)$$

(iii) *Model 3:*

$$\begin{aligned} \sigma_{n3}^2(0) &= 2(1 + \hat{\mathbf{b}}_{\kappa}^2(1))\sigma_v^2 + 2(\hat{\mathbf{b}}_{\kappa}^2(2) + \hat{\mathbf{b}}_{\kappa}^2(3))\sigma_i^2 \\ \sigma_{n3}^2(1) &= -2\alpha_1\sigma_v^2 - 2\hat{\mathbf{b}}_{\kappa}(2)\hat{\mathbf{b}}_{\kappa}(3)\sigma_i^2 \end{aligned}$$

(iv) *Model 4:*

$$\begin{aligned} \sigma_{n4}^2(0) &= 2(1 + \hat{\mathbf{b}}_{\kappa}^2(1) + \hat{\mathbf{b}}_{\kappa}^2(2))\sigma_v^2 \\ &\quad + 2(\hat{\mathbf{b}}_{\kappa}^2(3) + \hat{\mathbf{b}}_{\kappa}^2(4) + \hat{\mathbf{b}}_{\kappa}^2(5))\sigma_i^2 \\ \sigma_{n4}^2(1) &= -2\hat{\mathbf{b}}_{\kappa}(1)(1 + \hat{\mathbf{b}}_{\kappa}(2))\sigma_v^2 \\ &\quad - 2\hat{\mathbf{b}}_{\kappa}(4)(\hat{\mathbf{b}}_{\kappa}(3) + \hat{\mathbf{b}}_{\kappa}(5))\sigma_i^2 \\ \sigma_{n4}^2(2) &= 2 \left[ \hat{\mathbf{b}}_{\kappa}(2)\sigma_v^2 + \hat{\mathbf{b}}_{\kappa}(3)\hat{\mathbf{b}}_{\kappa}(5)\sigma_i^2 \right] \end{aligned}$$

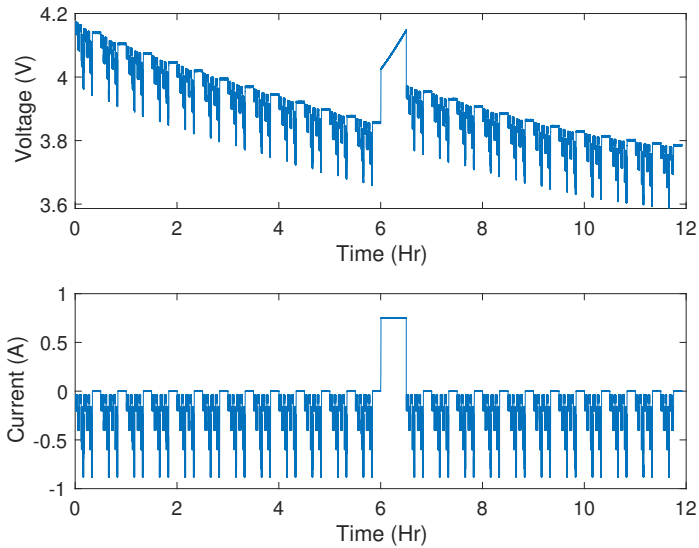
2: Update Error Cov:  $\mathbf{P}_{\kappa+1}^{-1} = \mathbf{P}_{\kappa}^{-1} + \tilde{\mathbf{A}}_{\kappa+1}^T \Sigma^{-1} \tilde{\mathbf{A}}_{\kappa+1}$

3: Update Residual Cov:  $\mathbf{S}_{\kappa+1} = \tilde{\mathbf{A}}_{\kappa+1} \mathbf{P}_{\kappa+1}^{-1} \tilde{\mathbf{A}}_{\kappa+1}^T + \Sigma$

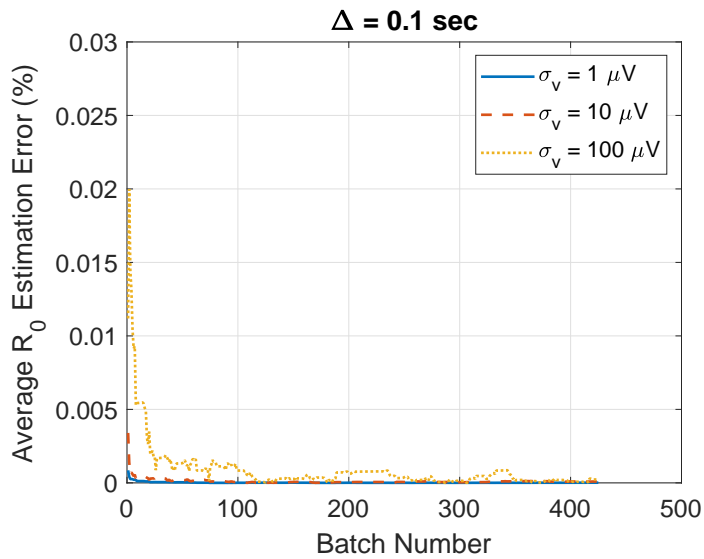
4: Update gain:  $\mathbf{W}_{\kappa+1} = \mathbf{P}_{\kappa+1} \tilde{\mathbf{A}}_{\kappa+1}^T \mathbf{S}_{\kappa+1}^{-1}$

5: Update Parameter:  $\hat{\mathbf{b}}_{\kappa+1} = \hat{\mathbf{b}}_{\kappa} + \mathbf{W}_{\kappa+1}(\tilde{\mathbf{v}}_{\kappa+1} - \tilde{\mathbf{A}}_{\kappa+1} \hat{\mathbf{b}}_{\kappa})$

---



(a) Measured voltage and current



(b) Average over 200 Monte-Carlo runs

Figure 3.7: **Estimation of  $R_0$  in Model 1.** Voltage across the battery terminals and current through the battery is shown in (a); mean square error of estimation over 200 Monte-Carlo runs is shown in (b).

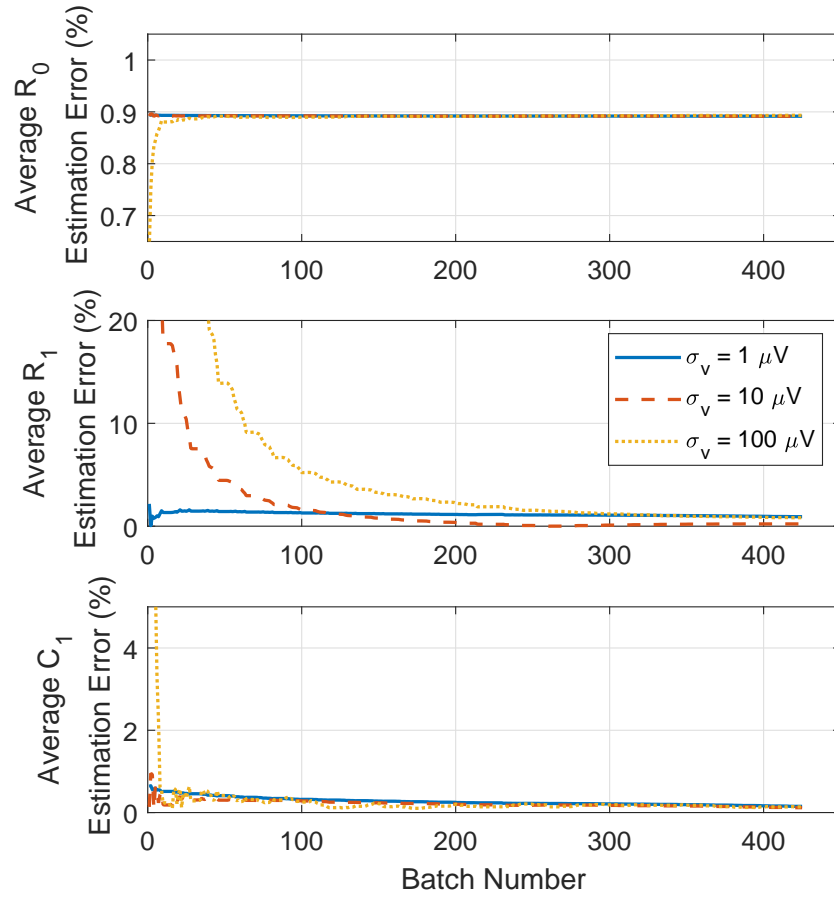


Figure 3.8: **Parameter Estimation for Model 3.** Mean square error of the estimated parameters are plotted for different values of measurement noise.

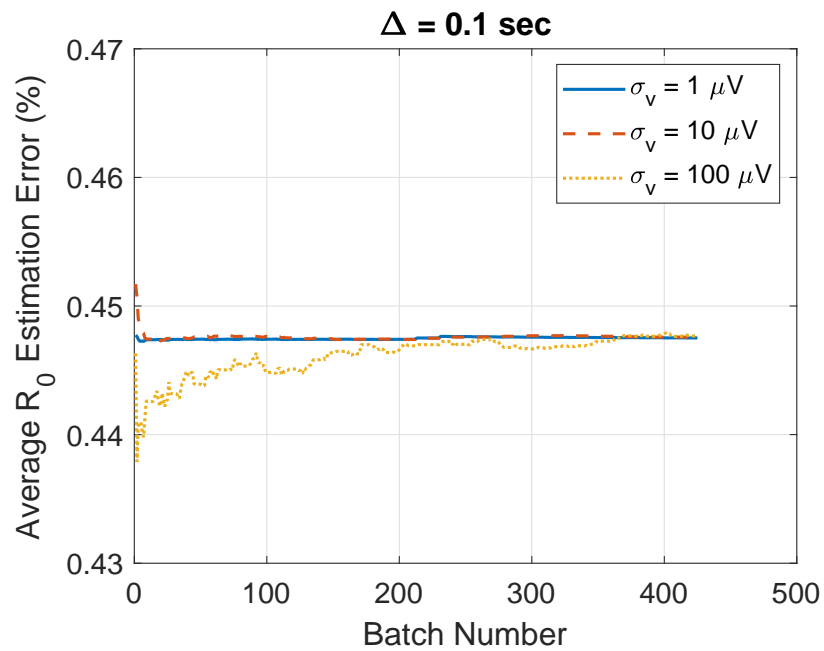


Figure 3.9: **Model mismatch analysis.** The result of estimating Model 1 parameters from data that was simulated using Model 3. Mean square error against batch number is shown for the estimated parameter.



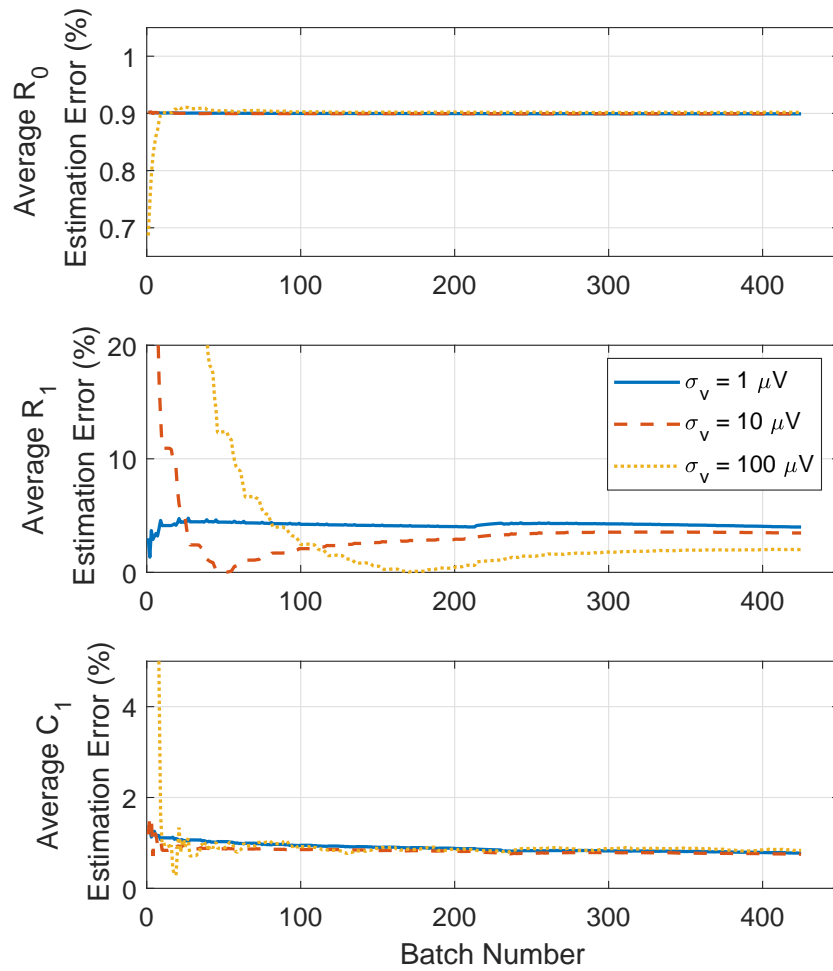


Figure 3.10: **Model mismatch analysis.** The results of estimating Model 3 parameters from data that was simulated using Model 4. Mean square error against batch number is shown for each estimated Model 3 parameter.

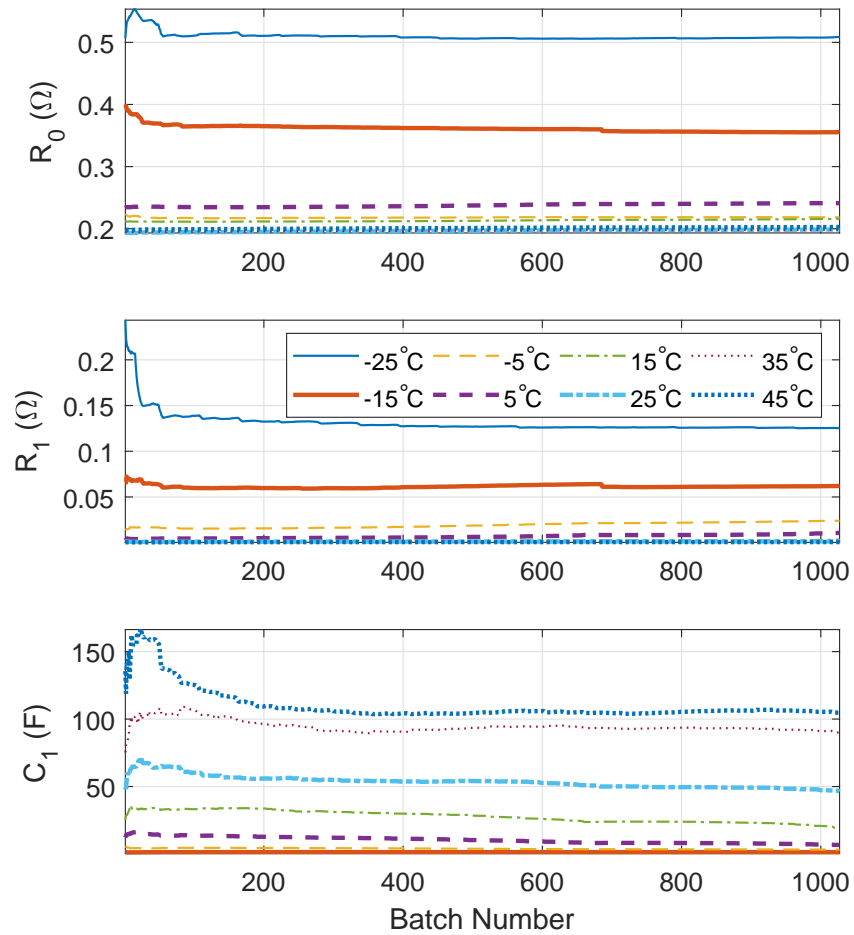


Figure 3.11: **Performance of the ECM identification algorithm at multiple temperatures.** Estimated values of the Model 3 parameters are plotted against batch number for data collected from the same battery cell used in Samsung Galaxy 4 smartphones (Samsung EB 575152) at eight different temperatures.

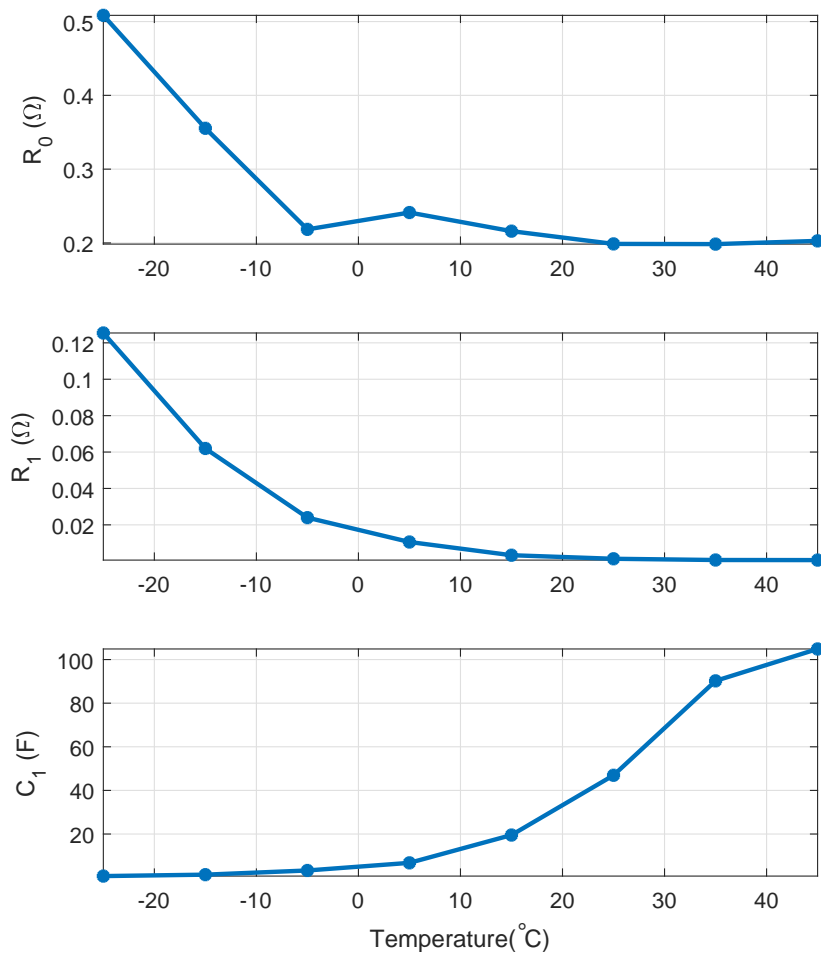


Figure 3.12: **Performance of the ECM identification algorithm on multiple batteries.** Estimated values of the Model 3 parameters are plotted against the temperature in which the battery was kept. Each entry in this plot is obtained by averaging the estimated values for the last 10 batches corresponding to Figure 3.11.

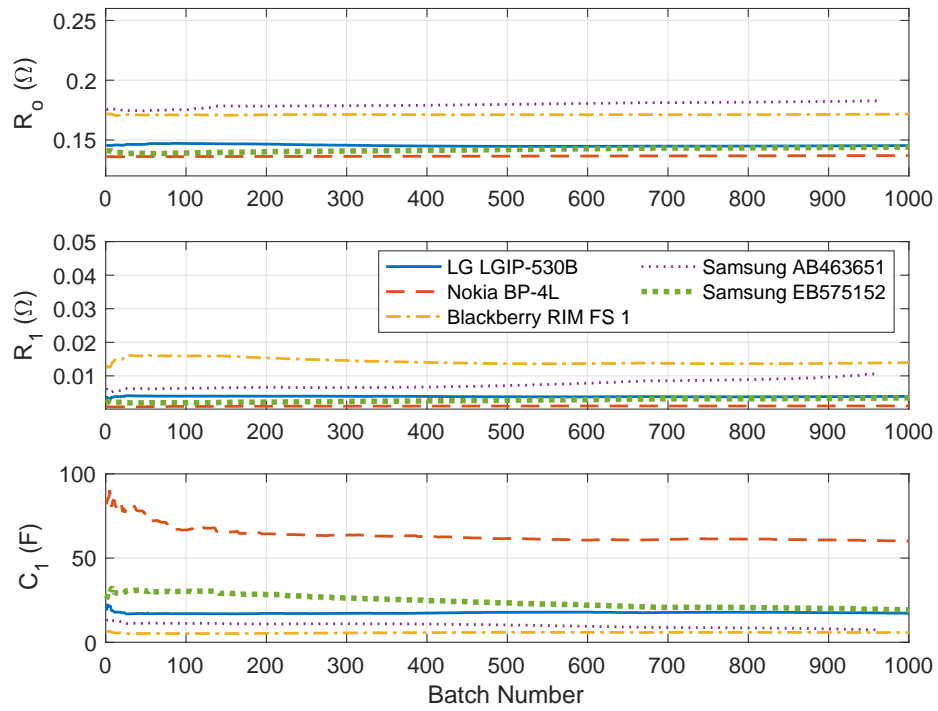


Figure 3.13: **Performance of the ECM identification algorithm on multiple batteries.** Estimated values of the Model 3 parameters are shown against batch number.

## 3.7 Bibliography

- [1] W. Allafi, K. Uddin, C. Zhang, R. M. R. A. Sha, and J. Marco. On-line scheme for parameter estimation of nonlinear lithium ion battery equivalent circuit models using the simplified refined instrumental variable method for a modified wiener continuous-time model. *Applied Energy*, 204:497–508, 2017. pages 6, 29
- [2] R. D. Anderson, Y. Zhao, X. Wang, X. G. Yang, and Y. Li. Real time battery power capability estimation. In *American Control Conference*, pages 592–597, 2012. pages 6, 28
- [3] D. Andre, M. Meiler, K. Steiner, H. Walz, T. Soczka-Guth, and D. Sauer. Characterization of high-power lithium-ion batteries by electrochemical impedance spectroscopy. ii: Modelling. *Journal of Power Sources*, 196(12):5349–5356, 2011. pages 29
- [4] G. Avvari, B. Pattipati, B. Balasingam, K. Pattipati, and Y. Bar-Shalom. Experimental set-up and procedures to test and validate battery fuel gauge algorithms. *Applied energy*, 160:404–418, 2015. pages xiv, 17, 56, 77, 81, 90, 91, 92, 95, 96, 97, 98, 101, 102, 103, 104
- [5] B. Balasingam, G. Avvari, B. Pattipati, K. Pattipati, and Y. Bar-Shalom. A robust approach to battery fuel gauging, part I: Real time model identification. *Journal of Power Sources*, 272:1142–1153, 2014. pages 7, 8, 9, 18, 29, 30, 31, 35, 39, 56, 77, 83
- [6] B. Balasingam, G. Avvari, K. Pattipati, and Y. Bar-Shalom. Performance analysis results of a battery fuel gauge algorithm at multiple temperatures. *Journal of Power Sources*, 273:742–753, 2015. pages xiv, 17, 56, 77, 81, 90, 91, 92, 104

- [7] B. Balasingam and K. Pattipati. Elements of a robust battery-management system: From fast characterization to universality and more. *IEEE Electrification Magazine*, 6(3):34–37, 2018. pages 5, 27
- [8] Y. Bar-Shalom, X. R. Li, and T. Kirubarajan. *Estimation with applications to tracking and navigation: theory algorithms and software*. John Wiley & Sons, 2004. pages 53, 77
- [9] M. Chen, G. A. Rincon-Mora, et al. Accurate electrical battery model capable of predicting runtime and iv performance. *IEEE transactions on energy conversion*, 21(2):504–511, 2006. pages 29, 77
- [10] G. Dong, Z. Chen, J. Wei, C. Zhang, and P. Wang. An online model-based method for state of energy estimation of lithium-ion batteries using dual filters. *Journal of Power Sources*, 301:277–286, 2016. pages 29
- [11] G. Dong, J. Wei, and Z. Chen. Kalman filter for onboard state of charge estimation and peak power capability analysis of lithium-ion batteries. *Journal of Power Sources*, 328:615–626, 2016. pages 29
- [12] A. Farmann and D. U. Sauer. A comprehensive review of on-board state-of-available-power prediction techniques for lithium-ion batteries in electric vehicles. *Journal of Power Sources*, 329:123–137, 2016. pages 29
- [13] A. Farmann, W. Waag, and D. U. Sauer. Adaptive approach for on-board impedance parameters and voltage estimation of lithium-ion batteries in electric vehicles. *Journal of Power Sources*, 299:176–188, 2015. pages 7, 29, 30, 83
- [14] T. Feng, L. Yang, X. Zhao, H. Zhang, and J. Qiang. Online identification of lithium-ion battery parameters based on an improved equivalent-circuit model and its implementation on battery state-of-power prediction. *Journal of Power Sources*, 281:192–203, 2015. pages 6, 29

- [15] C. Fleischer, W. Waag, H.-M. Heyn, and D. U. Sauer. On-line adaptive battery impedance parameter and state estimation considering physical principles in reduced order equivalent circuit battery models: Part 1. requirements, critical review of methods and modeling. *Journal of Power Sources*, 260:276–291, 2014. pages 6, 29
- [16] J. C. Forman, S. J. Moura, J. L. Stein, and H. K. Fathy. Genetic parameter identification of the doyle-fuller-newman model from experimental cycling of a lifepo 4 battery. In *American Control Conference*, pages 362–369, 2011. pages 28
- [17] J. Gomez, R. Nelson, E. E. Kalu, M. H. Weatherspoon, and J. P. Zheng. Equivalent circuit model parameters of a high-power Li-ion battery: Thermal and state of charge effects. *Journal of Power Sources*, 196(10):4826–4831, 2011. pages 7, 30
- [18] X. Hu, F. Sun, Y. Zou, and H. Peng. Online estimation of an electric vehicle lithium-ion battery using recursive least squares with forgetting. In *American Control Conference*, pages 935–940, 2011. pages 28
- [19] Y. Hu and Y.-Y. Wang. Two time-scaled battery model identification with application to battery state estimation. *IEEE Transactions on Control Systems Technology*, 23(3):1180–1188, 2015. pages 28
- [20] S. Jiang. A parameter identification method for a battery equivalent circuit model. Technical report, SAE Technical Paper, 2011. pages 7, 30
- [21] S. Lee, J. Kim, J. Lee, and B. H. Cho. The state and parameter estimation of an Li-ion battery using a new ocv-soc concept. In *Power Electronics Specialists Conference.*, pages 2799–2803, 2007. pages 28

- [22] X. Lin, H. E. Perez, S. Mohan, J. B. Siegel, A. G. Stefanopoulou, Y. Ding, and M. P. Castanier. A lumped-parameter electro-thermal model for cylindrical batteries. *Journal of Power Sources*, 257:1–11, 2014. pages 29
- [23] B. Pattipati, B. Balasingam, G. Avvari, K. R. Pattipati, and Y. Bar-Shalom. Open circuit voltage characterization of lithium-ion batteries. *Journal of Power Sources*, 269:317–333, 2014. pages 7, 20, 30, 59, 82
- [24] G. L. Plett. Extended Kalman filtering for battery management systems of LiPB-based HEV battery packs: Part 1. background. *Journal of Power sources*, 134(2):252–261, 2004. pages 6, 27, 76, 81
- [25] G. L. Plett. Extended kalman filtering for battery management systems of lipb-based HEV battery packs: Part 3. State and parameter estimation. *Journal of Power sources*, 134(2):277–292, 2004. pages 28, 76
- [26] G. L. Plett. Extended kalman filtering for battery management systems of lipb-based hev battery packs: Part 3. state and parameter estimation. *Journal of Power sources*, 134(2):277–292, 2004. pages 29
- [27] G. L. Plett. *Battery Management Systems, Volume I: Battery Modeling*. Artech House Publishers, 2015. pages 6, 28
- [28] G. L. Plett. *Battery Management Systems, Volume II: Equivalent-Circuit Methods*. Artech House Publishers, 2015. pages 6, 27, 28, 81
- [29] A. Seaman, T.-S. Dao, and J. McPhee. A survey of mathematics-based equivalent-circuit and electrochemical battery models for hybrid and electric vehicle simulation. *Journal of Power Sources*, 256:410–423, 2014. pages 7, 28, 30



- [30] F. Sun, R. Xiong, H. He, W. Li, and J. E. E. Aussems. Model-based dynamic multi-parameter method for peak power estimation of lithium-ion batteries. *Applied Energy*, 96:378–386, 2012. pages 29
- [31] P. Vyroubal and T. Kazda. Equivalent circuit model parameters extraction for lithium ion batteries using electrochemical impedance spectroscopy. *Journal of Energy Storage*, 15:23–31, 2018. pages 28, 81
- [32] W. Waag, C. Fleischer, and D. U. Sauer. Adaptive on-line prediction of the available power of lithium-ion batteries. *Journal of Power Sources*, 242:548–559, 2013. pages 6, 28
- [33] W. Waag, C. Fleischer, and D. U. Sauer. On-line estimation of lithium-ion battery impedance parameters using a novel varied-parameters approach. *Journal of Power Sources*, 237:260–269, 2013. pages 6, 7, 29, 30
- [34] W. Waag, C. Fleischer, and D. U. Sauer. Critical review of the methods for monitoring of lithium-ion batteries in electric and hybrid vehicles. *Journal of Power Sources*, 258:321–339, 2014. pages 7, 28, 30
- [35] T. Wang, L. Pei, R. Lu, C. Zhu, and G. Wu. Online parameter identification for lithium-ion cell in battery management system. In *Vehicle Power and Propulsion Conference*, pages 1–6, 2014. pages 6, 28
- [36] A. C. W. Wong, G. Kathiresan, C. K. T. Chan, O. Eljamaly, O. Omeni, D. McDonagh, A. J. Burdett, and C. Toumazou. A 1 v wireless transceiver for an ultra-low-power soc for biotelemetry applications. *IEEE Journal of Solid-State Circuits*, 43(7):1511–1521, 2008. pages 29
- [37] Y. Xing, W. He, M. Pecht, and K. L. Tsui. State of charge estimation of lithium-ion batteries using the open-circuit voltage at various ambient temperatures. *Applied Energy*, 113:106–115, 2014. pages 28

- [38] R. Xiong, H. He, F. Sun, X. Liu, and Z. Liu. Model-based state of charge and peak power capability joint estimation of lithium-ion battery in plug-in hybrid electric vehicles. *Journal of power sources*, 229:159–169, 2013. pages 28
- [39] S. Yuan, H. Wu, and C. Yin. State of charge estimation using the extended kalman filter for battery management systems based on the arx battery model. *Energies*, 6(1):444–470, 2013. pages 28
- [40] C. Zhang, W. Allafi, Q. Dinh, P. Ascencio, and J. Marco. Online estimation of battery equivalent circuit model parameters and state of charge using decoupled least squares technique. *Energy*, 142:678–688, 2018. pages 6, 29
- [41] X. Zhang, J. Lu, S. Yuan, J. Yang, and X. Zhou. A novel method for identification of lithium-ion battery equivalent circuit model parameters considering electrochemical properties. *Journal of Power Sources*, 345:21–29, 2017. pages 29
- [42] X. Zhang, M. Xu, S. Habibi, F. Yan, and R. Ahmed. Offline parameter identification and state-of-charge estimation for healthy and aged electric vehicle batteries based on the combined model. *World Academy of Science, Engineering and Technology, International Journal of Electrical, Computer, Energetic, Electronic and Communication Engineering*, 10(11):1384–1389, 2016. pages 6, 29

# Chapter 4

## Robust Battery Fuel Gauge: Algorithm and Evaluation

### 4.1 Introduction

Li-ion batteries are known for high power density, high capacity and light weight [34]. With the proliferation of portable electronic devices and electric vehicles, Li-ion batteries have become the most common rechargeable batteries. Consequently, it is important to have an accurate estimate of the state of charge (SOC) in order to avoid overcharging or deep discharging conditions in a battery. Further, the knowledge of the SOC of the battery is critical in many applications, such as in electrical vehicles (EV), where the battery replacement is costly and must be planned well in advance to avoid unanticipated breakdowns. The battery fuel gauge (BFG) estimates the SOC, SOH, the time to shut down (TTS) and the remaining useful life (RUL) of the battery. The knowledge of battery capacity has significant impact on the estimation of SOC, SOH, TTS and RUL. The battery capacity fades over time depending on environmental, usage and charging patterns and, as a result, BFG becomes a challenging system identification and state estimation problem.

There has been tremendous interest in the past decade on developing BFG algorithms that involve the solution to a joint state and parameter estimation problem. There have been two significantly different approaches to modeling the internal chemical behavior of the battery: the *electrochemical models* such as [30] and the references therein, and the *electrical equivalent circuit models* that are widespread in the engineering community. The electrical equivalent circuit model based BFG algorithms are based on three important sub-models: the open circuit model (OCV) model, the dynamic equivalent circuit model (ECM), and the battery capacity model. The parameters of the OCV curve (shown to be unchanged over temperature changes and aging, if estimated through the *normalized OCV modeling* approach of [23]) are estimated offline and the ECM parameters (known to vary with temperature, loading [4] and aging) and the battery capacity (known to vary with temperature and aging) are estimated online. In most works, the *combined model* [24, 25] was adopted for modeling the OCV; many other possible OCV models are discussed in [23] as well. In [21, 24–28], different dynamic models, such as a simple (resistance only) model, zero/one state hysteresis model and enhanced self correcting models, are discussed; these works give significant attention to modeling the hysteresis effect in a battery. Combinations of resistance/capacitance models, where the hysteresis effect is either ignored or modeled as an error term, can be found in [6, 8, 10, 12–18].

The existing literature has diverse methods and approaches related to types of ECM, model identification methods, SOC estimation methods and online capacity estimation methods. However, when it comes to validating the SOC estimates, a vast majority of the existing approaches solely depend on the Coulomb counting method. Our objective in this chapter is to show the necessity of having robust BFG validation strategies.

Evaluating a BFG is challenging due to the fact that there are no reliable mathematical models in order to represent the complex features of a Li-ion battery, such as hysteresis and relaxation effects, temperature effects on parameters, aging, power

fade (PF), and capacity fade (CF) with respect to the chemical composition of the battery. To the best of our knowledge, there is little literature focusing on BFG algorithm evaluation under realistic usage conditions; the importance of BFG evaluation is discussed in [31]; in [7], the need to minimize power dissipation and to extend battery run-time for portable devices is discussed; the advantages of hardware-in-the-loop (HIL) testing to validate a battery management system (BMS) under various failure conditions was motivated in [19]; and a HIL test to validate the BFG using a multi-cell battery pack was proposed in [11,33]. Eventually, three *BFG evaluation metrics* were presented and demonstrated in [1,3].

Compared to the previous discussions on this topic [1,3], the contributions of this chapter are listed below:

1. *Rigorous evaluation of BFG evaluation metrics.* In this chapter, we use simulated data to test the validity of the proposed BFG evaluation metrics [1,3]. Using the simulated data (with known battery parameters), we demonstrate the validity of the BFG evaluation metrics. Such practice gives more insights when it comes to using them to validate BFGs.
2. *Stable RLS model for parameter estimation.* In this chapter we present a robust approach to estimate the equivalent circuit model (ECM) parameters of a Li-ion battery based on recursive least square (RLS) estimation method [5].
3. *Comparison of the proposed method with previous BFG.* We use the BFG evaluation metrics [1,3] to show that the proposed RLS implementation outperformed its predecessor presented in [2].

The aforementioned contributions of the chapter are organized as follows: In Section 4.2, we present the detailed attributes of the proposed BFG. The battery equivalent circuit models are presented in 4.2.1. The battery OCV model is summarized in Section 4.2.2. In Section 4.2.3, we present the recursive least square based battery ECM parameter estimation algorithm and analyze the performance on load profile.

Section 4.2.4 presents the new SOC tracking algorithm based on extended Kalman filter. Section 4.2.5 presents the block diagram of the proposed BFG. In Section 4.3, we introduce three validation method of the proposed BFG namely CC metric, OCV metric and TTV metric. In Section 4.4, the performance of the proposed BFG is tested first on simulated data; then the RLS and EKF algorithm is employed on the real data from multiple batteries; finally the three metrics emerge the validity of the proposed BFG. Section 4.5 concludes the chapter.

## List of Notations

$\tilde{\mathbf{a}}(k)^T$  . Oobservation model (4.134)

$\tilde{\mathbf{A}}_\kappa$  . . . . . Observation model in single batch (4.137)

$\mathbf{b}$  . . . . . ECM parameters to be estimated (4.135)

$\mathbf{b}_\kappa$  . . . . . ECM parameters to be estimated at  $\kappa^{th}$  batch(4.137)

$C_1$  . . . . . Battery internal capacitance in Farad (Figure 4.14)

$C_{\text{batt}}$  .. Battery capacity in Ampere-hour (4.147)

$F(k)$  .. State transition matrix(4.154)

$f_{\text{OCV-SOC}}^{-1}$  OCV look up from OCV-SOC characteristics (4.171)

$G(k)$  .. Input gain in EKF (4.154)

$h(k)$  ... Hysteresis at  $k$ (4.169)

$h'(k + 1)$  Linearization of measurement model (4.161)

$i(k)$  ... Current through battery in Ampere (4.147)

$k_{\text{sd}}$  . . . . . Time index at shut down voltage (4.173)

$K_0, \dots, K_7$  OCV-SOC model parameter (4.132)

$m(k+1)$  Innovation variance of Kalman filter (4.163)

$n_i(k)$  .. Process noise at time  $k$  (4.154)

$\tilde{\mathbf{n}}_\kappa$  .. Measurement noise (4.137)

$N_k$  .. Number of time samples to reach  $v_{sd}$  (4.175)

$\mathbf{P}_{\kappa+1}^{-1}$  .. Error covariance(4.142)

$R_0$  .. Battery internal series resistance in  $\Omega$  ( Figure 4.14)

$R_1$  .. Battery internal resistance in  $\Omega$  (Figure 4.14)

$s(k)$  ... SOC using Coulomb counting at time step  $k$  (4.147)

$s'$  .. Scaled SOC (4.148)

$\hat{s}_{sd}$  .. SOC at shut down voltage(4.171)

$\mathbf{S}_{\kappa+1}$  .. Residual covariance(4.142)

$T(k)$  .. Actual TTV in minute (4.173)

$T_{sd}(k)$  . Predicted TTV in minute (4.172)

$T_{ttv}$  ... Total duration of TTV in minute(4.176)

$u(k)$  ... Measured current in EKF in Ampere (4.154)

$\tilde{v}(k)$  ... Measured voltage (V) (4.133)

$\tilde{\mathbf{v}}_\kappa$  .. Measured voltage (V) at  $\kappa^{th}$  batch (4.137)

$v_r$  .. Voltage (V) at rest(4.168)

$v_d$  .. Voltage drop (V)(4.169)

$\hat{v}_{sd}$  . . . . Shut down voltage (V)(4.169)  
 $V_o(s)$  .. Open circuit voltage (V) (OCV) (4.132)  
 $\mathbf{W}_{\kappa+1}$  . Update RLS gain(4.141)  
 $x_s(k)$  .. SOC in EKF (4.153)  
 $W(k+1)$  Gain of Kalman filter (4.164)  
 $x_s(k)$  .. State of the Kalman filter at time  $k$  (4.153)  
 $\hat{x}_s(k|k)$  Estimated state(4.157)  
 $\hat{x}_s(k+1|k)$  State prediction(4.157)eq:stateestimate  
 $\hat{z}(k+1|k)$  Measurement prediction of Kalman filter (4.160)  
 $z_v(k)$  .. Measured terminal voltage (V) at time  $k$  (4.155)  
 $z_i(k)$  .. Measured current(A) at time  $k$  (4.134)  
 $\Delta_k$  . . . . Time interval (seconds) (4.147)  
 $\sigma_v$  . . . . Standard deviation of voltage noise (4.143)  
 $\sigma_i$  . . . . Standard deviation of current noise (4.143)  
 $\sigma_n^2(1)$  .. Noise variance of the measurement model (4.143)  
 $\Sigma$  . . . . Covariance matrix (4.138)  
 $\epsilon$  . . . . . Scaling factor(4.149)  
 $\bar{\epsilon}_{cc}$  . . . . CC metric (%) (4.167)  
 $\bar{\epsilon}_{ocv}$  . . . . OCV metric (%) (4.168)  
 $\epsilon(k)$  . . . . TTV error at  $k^{th}$  time index(4.174)



$\bar{\epsilon}_{ttv}$  .... Mean TTV error in minute(4.175)

$E_{ttv}$  ... TTV metric (%) (4.177)

## 4.2 Details of the New Battery Fuel Gauge

### 4.2.1 Battery Equivalent Circuit Model

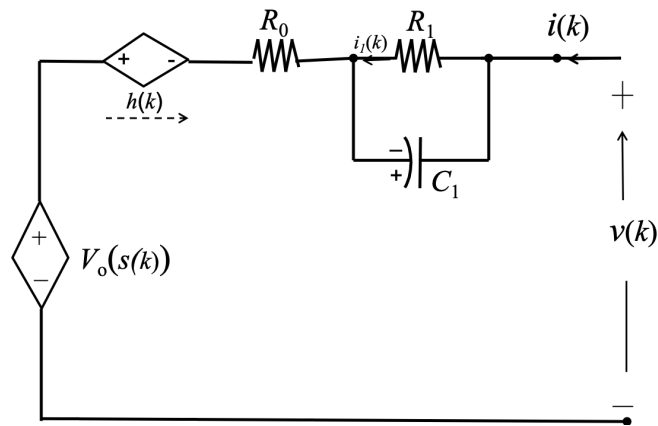


Figure 4.14: **Equivalent circuit models (ECM) of a battery.** Battery equivalent circuit model that is widely used in the literature to represent Li-ion batteries. In this chapter, we use a RLS based approach to estimate the ECM parameter [1, 3] with some improvements.

Battery modeling is important to design and approximate the battery performance. As Li-ion batteries have complex, non-linear characteristics, precise battery modeling is required to define their suitability for different applications and to analyze their dynamic behavior. Two main categories of electrical battery models are namely Thevenin-based electrical models [24, 29] and impedance based electrical models [32]. An equivalent circuit model is widely accepted method for analyzing the dynamic behavior of Li-ion batteries.

We use time domain approach to develop the equivalent circuit model. Figure 4.14 shows the equivalent circuit model that is widely used for parameter identification in

this chapter. In this model,  $v(k)$  represents the measured voltage across the battery terminals and  $i(k)$  represents the current through the battery. Here,  $R_1$  and  $C_1$  represents the resistive and the capacitive elements (RC circuit). Based on [22], the knowledge of the OCV-SOC curve and the SOC of the battery,  $s(k)$ , was used to compute the OCV( $V_0(s(k))$ ) of the battery. Obtaining the OCV-SOC curve is an offline process (the details can be found in [22]). With the knowledge of the OCV-SOC curve, the ECM parameters of the batteries can be estimated based on the battery equivalent circuit model (ECM) – as described later in this chapter. Using these estimated parameters, an online SOC estimation technique, based on the extended Kalman filter, is described to recursively estimate the SOC of the battery. The real time BFG demonstrated in this chapter will estimate the battery ECM parameters in real time simultaneously track the SOC.

## 4.2.2 Battery OCV Model

In this section, we summarize the approach presented in [22] to OCV characterization. The OCV of a Lithium-ion battery varies with its state of charge (SOC) in a non-linear fashion represented as follows<sup>1</sup>:

$$V_o(s) = K_0 + \frac{K_1}{s} + \frac{K_2}{s^2} + \frac{K_3}{s^3} + \frac{K_4}{s^4} + K_5s + K_6 \ln(s) + K_7 \ln(1 - s) \quad (4.132)$$

where  $V_o(s)$  indicates the OCV which is a function of SOC,  $s$ . The set of coefficients  $\{K_0, K_1, K_2, K_3, K_4, K_5, K_6, K_7\}$  are referred to as the *OCV-SOC parameters* or at times simply as *OCV parameters*. These OCV parameters can be estimated offline through a custom experimental data collection process followed by a parameter estimation step (more details can be found in [20, 22]).

---

<sup>1</sup>The OCV-SOC model in (4.132) was introduced as *combined+3 model* in [22].

### 4.2.3 ECM Parameter Estimation

In this section, we summarize a previous approach [2] and discuss some modifications for real-time, linear estimation of dynamic equivalent circuit parameters for batteries. Unlike prior approaches that require SOC, OCV-SOC parameters, temperature, and hysteresis modeling [9], the proposed approach is simplistic in terms of measurement and modeling requirements.

The equivalent circuit models of Li-ion batteries as shown in Figure 4.14 are used to derive the ECM parameters. The proposed ECM identification approach is built around the recursive least square (RLS) filter. As such, it is able to track time-varying parameters, e.g. it can track change in parameters due to temperature, SOC changes and aging. We present the mathematical derivation of the new measurement model that is based only on the measured voltage across the battery and current through the battery.

The voltage drop across the circuit components of the equivalent circuit model can be written in the following form:

$$\tilde{v}(k) = \tilde{\mathbf{a}}(k)^T \mathbf{b} + \tilde{n}(k) \quad (4.133)$$

where

$$\tilde{\mathbf{a}}(k)^T = \left[ \tilde{v}_D(k-1) \quad \tilde{z}_i(k) \quad -\tilde{z}_i(k-1) \right] \quad (4.134)$$

$$\mathbf{b} = \left[ \alpha_1 \quad R_0 \quad \tilde{R}_1 \right]^T \quad (4.135)$$

where

$$\tilde{R}_1 = \alpha_1 R_0 - (1 - \alpha_1) R_1 \quad (4.136)$$



and

$$\begin{aligned}\mathbf{P}_{\kappa+1}^{-1} &= \mathbf{P}_{\kappa}^{-1} + \tilde{\mathbf{A}}_{\kappa+1}^T \Sigma^{-1} \tilde{\mathbf{A}}_{\kappa+1} \\ \mathbf{S}_{\kappa+1} &= \tilde{\mathbf{A}}_{\kappa+1} \mathbf{P}_{\kappa+1}^{-1} \tilde{\mathbf{A}}_{\kappa+1}^T + \Sigma\end{aligned}\tag{4.142}$$

Given the past parameter estimate for the previous batch,  $\hat{\mathbf{b}}_{\kappa}$ , its estimation error covariance  $\mathbf{P}_{\kappa}^{-1}$  (in inverse form), new set of measurements from the current batch  $\tilde{\mathbf{v}}_{\kappa+1}$  and the corresponding model  $\tilde{\mathbf{A}}_{\kappa+1}$ , the Algorithm 3 can be used to obtain the updated estimate  $\hat{\mathbf{b}}_{\kappa+1}$  and the updated estimation error covariance  $\mathbf{P}_{\kappa+1}^{-1}$ . It must be noted that dimension of  $\tilde{\mathbf{b}}_{\kappa}$  and  $\tilde{\mathbf{A}}_{\kappa}$  vary based on the assumed model.

**Remark 7 (Initialization)** *For the very first iteration of Algorithm 3 there is no prior knowledge of  $\hat{\mathbf{b}}_{\kappa}$ , i.e., when  $\kappa = 1$  there is no  $\hat{\mathbf{b}}_0$ . For this case, we will use a least square estimation without assuming any prior information about noise. This will reduce the covariance matrix to be an identity matrix, i.e.,*

$$\Sigma = \mathbf{I}_{L_b}\tag{4.144}$$

where  $\mathbf{I}_{L_b}$  is an  $L_b \times L_b$  identity matrix. As a result, for the first batch, the parameter estimation is carried out using the least square (LS) algorithm as follows

$$\begin{aligned}\hat{\mathbf{b}}_1 &= \left( \tilde{\mathbf{A}}_1^T \tilde{\mathbf{A}}_1 \right)^{-1} \tilde{\mathbf{A}}_1^T \tilde{\mathbf{v}}_1 \\ \mathbf{P}_1 &= \left( \tilde{\mathbf{A}}_1^T \tilde{\mathbf{A}}_1 \right)^{-1}\end{aligned}\tag{4.145}$$

**Remark 8 (Battery parameter recovery)** *At every iteration of Algorithm 3, the parameter  $\hat{\mathbf{b}}_{\kappa}$  has three elements that can be indicated by  $\hat{\mathbf{b}}_{\kappa}(1)$ ,  $\hat{\mathbf{b}}_{\kappa}(2)$  and  $\hat{\mathbf{b}}_{\kappa}(3)$ . The*

parameters of the ECM can be recovered as follows:

$$\begin{aligned}
 R_0 &= \hat{\mathbf{b}}_\kappa(2) \\
 R_1 &= \frac{[\hat{\mathbf{b}}_\kappa(1)\hat{\mathbf{b}}_\kappa(2) - \hat{\mathbf{b}}_\kappa(3)]}{1 - \hat{\mathbf{b}}_\kappa(1)} \\
 C_1 &= -\frac{\Delta}{R_1 \ln(\hat{\mathbf{b}}_\kappa(1))}
 \end{aligned} \tag{4.146}$$

where,  $\Delta$  is the sampling time.

#### 4.2.4 State of Charge Tracking

In order to derive the SOC tracking method, we start with the Coulomb counting equation as follows

$$s(k+1) = s(k) + \frac{\Delta_k i(k)}{3600 C_{\text{batt}}} \tag{4.147}$$

where SOC is denoted by  $s(k) \in [0, 1]$ .

The problems of the offline OCV-SOC model (4.132) is that the OCV is not defined at the SOC values  $s = 0$  and  $s = 1$ . Considering that the OCV-SOC model has ‘ $\log(s)$ ’ and ‘ $1/s$ ’ terms, value of SOC that is closer to “0” and “1” will cause numerical issues. Therefore, a scaling approach is introduced in order to map the range of  $s \in [0, 1]$  to  $s' \in [\epsilon, 1 - \epsilon]$  (more details can be found in [20]). where

$$s' = s(1 - 2\epsilon) + \epsilon \tag{4.148}$$

and

$$\epsilon \in (0, 0.5) \tag{4.149}$$

where  $\epsilon$  is the *scaling factor*. From here on, we use  $s'$  to indicate *scaled SOC* and  $s$  to indicate unscaled (true) SOC. Now  $s'$  will be used instead of  $s$ . Here, it must be noted that  $s'$  does not go to 0 or 1 – it always stays  $\epsilon$  away from these extreme values.

Now, let us re-write (4.147) by replacing  $s(k)$  with the scaled version of SOC  $s'(k)$  that is obtained based on (4.148) as

$$\frac{s'(k+1)}{1-2\epsilon} = \frac{s'(k)}{1-2\epsilon} + \frac{\Delta_k i(k)}{3600C_{\text{batt}}} \quad (4.150)$$

where

$$s'(k) = s(k)(1-2\epsilon) + \epsilon \quad (4.151)$$

The scaled version of the Coulomb counting equation is then

$$s'(k+1) = s'(k) + (1-2\epsilon) \frac{\Delta_k i(k)}{3600C_{\text{batt}}} \quad (4.152)$$

Now, let us denote the scaled SOC,  $s'(k)$  at time  $k$  as

$$x_s(k) \triangleq s'(k) \quad (4.153)$$

considering the process noise  $n_i(k)$ , the state equation can be written by the following form

$$x_s(k+1) = x_s(k) + G(k)u(k) + n_i(k) \quad (4.154)$$

where,

$$\begin{aligned} \text{Input gain, } G(k) &= \frac{\Delta_k}{3600C_{\text{batt}}} \\ \text{Measured current, } u(k) &= z_i(k) \end{aligned}$$

For the battery equivalent circuit model provided in Figure 4.14, the measurement model can be written as

$$z_v(k) = V_o(x_s(k)) + v_d + n_v(k) \quad (4.155)$$

where  $v_d = f(z_i, \hat{R}_0, \hat{R}_1, \hat{C}_1)$  is the voltage drop across the ECM parameter and the noise  $n_v(k)$  is the voltage measurement noise which is assumed to be zero-mean Gaussian with standard deviation  $\sigma_v$ .

The observation model above is non-linear in terms of the SOC, i.e.,

$$\begin{aligned} V_o(x_s(k)) = & K_0 + \frac{K_1}{x_s(k)} + \frac{K_2}{x_s^2(k)} + \frac{K_3}{x_s^3(k)} + \frac{K_4}{x_s^4(k)} \\ & + K_5 x_s(k) + K_6 \ln(x_s(k)) + K_7 \ln(1 - x_s(k)) \end{aligned} \quad (4.156)$$

Now, the *online SOC tracking problem* can be formally stated as follows: Given  $z_v(k)$  and  $z_i(k)$ , the the voltage and current measurements respectively, at time  $k$ , recursively estimate the (scaled) SOC of the battery  $\hat{x}_s(k|k)$  and the associated estimation error covariance  $P_s(k|k)$ . The Algorithm 4 summarizes the extended Kalman filter approach to SOC tracking.

The Algorithm 4 works by taking as an input the previous state  $\hat{x}_s(k|k)$ , previous covariance  $P_s(k|k)$ , current measurement  $z_i(k+1)$  and voltage measurement  $z_v(k+1)$ . It outputs the state  $\hat{x}_s(k+1|k+1)$  and covariance estimate  $P_s(k+1|k+1)$  using (4.165) and (4.166) respectively. In the process, it calculates the state prediction  $\hat{x}_s(k+1|k)$  using (4.157), state prediction variance  $P_s(k+1|k)$  using (4.158) and measurement prediction  $\hat{z}(k+1|k)$  using (4.160). Finally, the innovation variance  $S(k+1|k)$ , innovation  $m(k+1)$  and filter gain  $W(k+1)$  are calculated using (4.162),(4.163) and (4.164) respectively.

The performance of the the SOC tracking is analyzed in Section 4.4. The Coulomb counting method provides a reference SOC because it is computed based on true value of the battery capacity and noiseless current.



## 4.2.5 Block Diagram of the Robust BFG

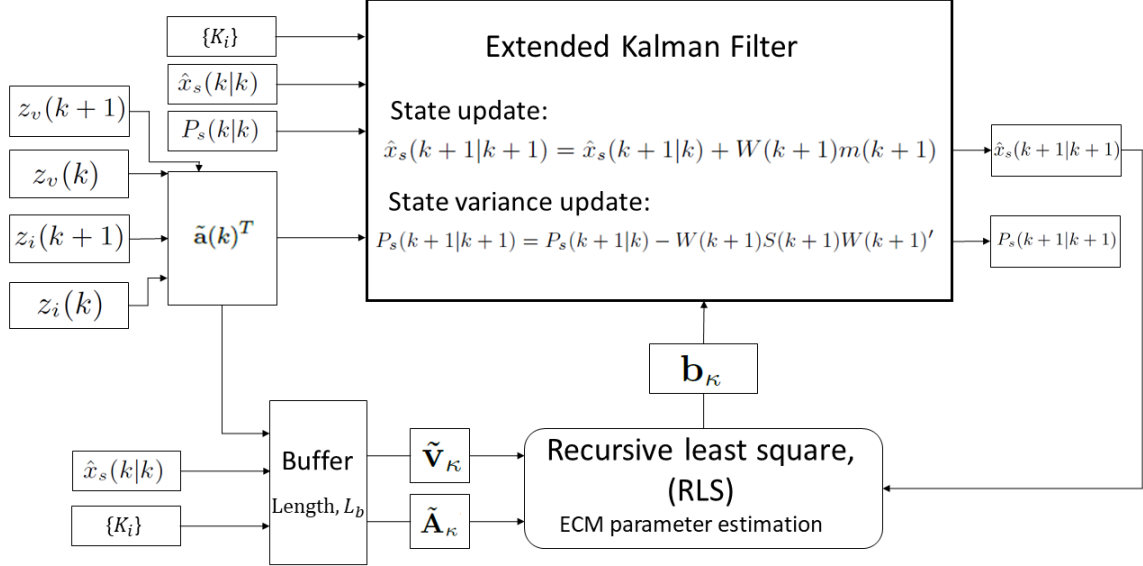


Figure 4.15: **Block diagram of the proposed BFG.** The proposed BFG is designed to estimate ECM parameters as well as the SOC in real time.

Figure 4.15 summarize the block diagram of the BFG algorithm. The recursive least square method is introduced with a view to developing batch-wise ECM parameters estimation and at the same time the extended Kalman filter (EKF) is employed in order to estimate the SOC in real time. First, the observation model,  $\tilde{\mathbf{a}}(k)^T$  is built in terms of measured voltage,  $z_v(k)$  and  $z_i(k)$  using (4.134). This  $\tilde{\mathbf{a}}(k)^T$ , SOC estimate (received from EKF) and the  $K$  parameters (obtained from OCV test) are stored in the buffer and fed into ECM parameter estimation mentioned in Algorithm 3 to launch the proposed BFG. The estimated parameters,  $\mathbf{b}_k$  from the corresponding batch of length,  $L_b$  is further fed into the EKF along with reconsidering the observation model,  $\tilde{\mathbf{a}}(k)^T$  as shown in Figure 4.15 in order to compute the voltage drop  $v_d(k)$  by using (4.159) in order to predict the measurement,  $\hat{z}(k+1|k)$ .

Algorithm 4 is developed based on EKF to predict the state,  $\hat{x}_s(k+1|k+1)$  and the

variance  $\hat{x}_s(k+1|k+1)$  by using (4.165) and (4.166) respectively. The predicted SOC,  $\hat{x}_s(k+1|k+1)$  and the state variance  $P_s(k+1|k+1)$  are accounted as the previous state estimate,  $\hat{x}_s(k|k)$  and previous state variance,  $P_s(k|k)$  in order to employ EKF for the next set of SOC estimation. The online estimation is conducted simultaneously for ECM parameters and the SOC by using recursive least square and extended Kalman filter respectively which upholds the robustness of the proposed BFG presented in Figure 4.15.

## 4.3 Details of the Validation Method

### 4.3.1 Coulomb Counting (CC) Metric

In this section we present a BFG validation metric called Coulomb counting (CC) metric [1, 3]. The CC metric computes average error between the SOC estimated by the BFG and that obtained by the Coulomb counting method; here, the Coulomb counting approach assumes the knowledge of the initial SOC and the accurate knowledge of the battery capacity (the BFG evaluation profile is designed in such a way that both of these information can be obtained in retrospect). The BFG algorithm on the other hand is not supposed to take advantage of these two information that the Coulomb counting method had the access to. Since both of these SOC estimates are in % the unit of the CC metric is also in % — a CC metric of 0% indicates a perfect BFG and a CC metric of 100% indicates completely flawed BFG.

Given the exact knowledge of battery capacity,  $C_{\text{batt}}$ , and the initial SOC,  $s_{\text{cc}}(0)$ , the Coulomb counting based SOC,  $\hat{s}_{\text{cc}}(k)$  can be computed by making use of (4.147). The approach to obtain the SOC estimate by the proposed BFG,  $\hat{x}_s(k|k)$ , is summarized in Section 4.2.4. The BFG error (in %) is then obtained as

$$\bar{\varepsilon}_{\text{cc}} = \left( \sqrt{\frac{1}{T} \sum_{k=1}^T \{s_{\text{cc}}(k) - \hat{x}_s(k|k)\}^2} \right) 100 \quad (4.167)$$

where T is the number of samples on which the validation is performed. Observations and discussions of CC metric based on simulated and real load profile is shown in Section 4.4.1.1 and 4.4.2.2 respectively.

### 4.3.2 OCV Metric

In this section we briefly review the OCV metric [1, 3]. The OCV-SOC characterization is used to obtain a voltage based SOC estimation while battery is resting. A battery is considered resting after experiencing zero current for considerable amount of time, e.g., 1-2 hours. Consequently, the OCV based SOC estimation is not possible while the battery is in use; the OCV metric is computed by defining a BFG evaluation profile that includes a rest period.

In this chapter, the normalized OCV-SOC modeling approach [23] briefed in Section 4.2.2 is used in order to develop OCV look-up based SOC estimation. It must be noted that when the battery is in rest state, there is no voltage drop across the battery ECM parameters. Therefore, the battery terminal voltage at rest can be considered as the OCV of the battery.

In order to develop OCV metric, we compute the SOC related to the battery terminal voltage at rest,  $v_r$  shown in (4.168) and subtract that from the estimated SOC,  $\hat{x}_s(k|k)$  using proposed BFG based on extended Kalman filter. The estimated SOC by the BFG,  $\hat{x}_s(k|k)$ , is taken just after the dynamic part of the load profile, i.e., since the current is zero after that until the point where the rest is achieved. The OCV metric can be written as

$$\bar{\varepsilon}_{ocv} = |\hat{x}_s(k|k) - f_{OCV-SOC}^{-1}(v_r)| \quad (4.168)$$

where, the OCV metric  $\bar{\varepsilon}_{ocv}$  (in %) refers to the (SOC) error of the BFG in terms of the *OCV lookup*. The result of OCV metric applied on simulated and real load profile is visualized and analyzed in 4.4.1.2 and 4.4.2.3 respectively.

### 4.3.3 TTV Metric

The TTV metric [1,3] is the third and comprehensive metric of BFG evaluation that we consider in this chapter. The time to voltage (TTV) interprets the remaining charge of a battery in terms of remaining operational time — when a constant load is applied. When a battery is connected to a system, it is possible to know how much time it takes to reach a certain terminal voltage of the battery from the present states of charge. For example, given that the present states of charge (SOC) of a battery in a cell phone device is 65%, the TTV may notify the users about having 2 hours of browsing time or 4 hours of remaining talking time. Moreover, it is applicable to know the time when we need to shut down the battery while it is discharging in order to secure the safety of the battery.

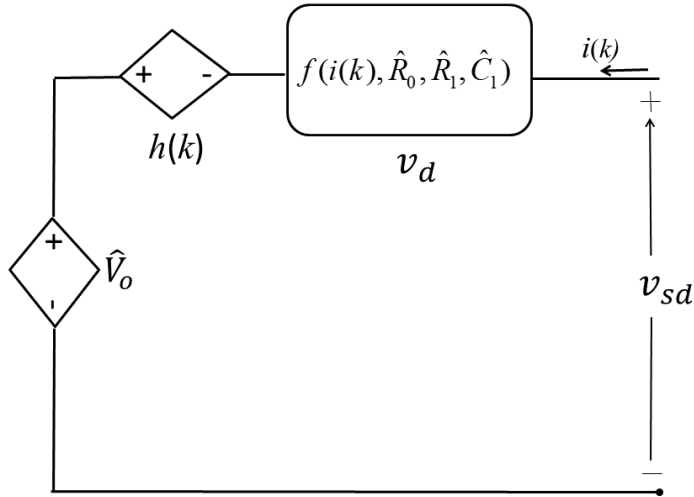


Figure 4.16: **Shut down voltage for TTV metric validation.** Shut down voltage,  $v_{sd}$  for TTV metric is determined by subtracting voltage drop,  $v_d$  and hysteresis,  $h(k)$  from  $v_{sd}$  from the OCV.

The errors in TTV estimate named as TTV metric can be obtained by computing the predicted TTV and the actual TTV. For a given SOC or its corresponding voltage, we calculate the actual time to reach a certain terminal voltage indicating the

actual TTV. Similarly, the predicted time to reach that voltage anticipated from the proposed BFG approach can be introduced as predicted TTV. If  $v_{sd}$  is the voltage in question to be reached as shown in Figure 4.16, then the OCV at that voltage can be written as:

$$\hat{V}_o = \hat{v}_{sd} - v_d - h(k) \quad (4.169)$$

where,  $V_o$  is OCV and  $v_d$  is the voltage drop across the model parameter  $R_0, R_1$  and  $C_1$  as shown in Figure 4.14 which can be computed as:

$$v_d = f(i(k), \hat{R}_0, \hat{R}_1, \hat{C}_1) \quad (4.170)$$

$R_0, R_1$  and  $C_1$  is estimated using the proposed approach based on recursive least square method discussed in Section 4.2.3.

The SOC corresponding to this  $\hat{V}_o$  is obtained from the OCV-SOC characteristics as follows:

$$\hat{s}_{sd} = f_{OCV-SOC}^{-1}(\hat{V}_o) \quad (4.171)$$

where  $\hat{s}_{sd}$  refers to the SOC at the shut down voltage,  $v_{sd}$ . If  $v(k)$  is the present terminal voltage and the present SOC at  $v(k)$  is denoted as  $\hat{x}_s(k|k)$  estimated using the proposed extended kalman filter explained in Section 4.2.4, then the time to reach the voltage  $v_{sd}$  can be computed as

$$T_{sd}(k) = \left( \frac{\hat{s}_{sd} - \hat{x}_s(k|k)}{i(k)} \right) C_{batt}3600 \quad (4.172)$$

where,  $T_{sd}$  refers to the predicted TTV i.e the time to reach the shut sown voltage. It is noted that as the present terminal voltage,  $v(k)$  progresses towards the voltage to be reached  $v_{sd}$  over time, the present SOC,  $\hat{x}_s(k|k)$  in turns progresses towards  $\hat{s}_{sd}$  as well which is the SOC corresponding to the voltage  $v_{sd}$  and thus,  $T_{sd}$  can be obtained for each terminal voltage of the battery.

The actual TTV refers to the actual time required to reach  $v_{sd}$  defined as follows:

$$T(k) = (k_{sd} - k)\Delta \quad (4.173)$$

where  $T$  refers to actual TTV.  $k_{sd}$  is the time sample of the voltage  $v_{sd}$  and  $k$  denotes the time sample of the current voltage,  $v(k)$ .

$\Delta$  = sampling interval

For each time sample  $k$ , the predicted TTV,  $T_{sd}$  and actual TTV,  $T$  are obtained using (4.172) and (4.173) respectively. Subsequently the error in TTV at each time sample  $k$  can be computed as

$$\varepsilon(k) = \frac{1}{60} \sqrt{\{T_{sd}(k) - T(k)\}^2} \quad (4.174)$$

where the value of  $\varepsilon(k)$  is in minute. The validation of TTV metric can be obtained by considering the average of the error as follow:

$$\bar{\varepsilon}_{ttv} = \frac{1}{60} \sqrt{\frac{1}{N_k} \sum_{i=1}^{N_k} \varepsilon(i)} \quad (4.175)$$

where the value of  $\bar{\varepsilon}_{ttv}$  is in minute and  $N_k = k_{sd} - k$  is the number of time samples. The total duration of time in minutes during which the TTV metric is determined

can be written as,

$$T_{\text{ttv}} = \frac{N_k \Delta}{60} \quad (4.176)$$

Now the TTV metric can be defined as ,

$$E_{\text{ttv}} = \frac{\bar{\varepsilon}_{\text{ttv}}}{T_{\text{ttv}}} 100 \quad (4.177)$$

Performance analysis of TTV metric is presented in Section 4.4.1.3 and 4.4.2.4 respectively.

## 4.4 Results

In this section, we test the validity of the proposed BFG by first using simulated data; then by implementing it on real data from multiple batteries. We demonstrate the CC metric , OCV metric and TTV metric for each of the profiles and compare the results with the existing approaches in [1] to verify its robustness.

### 4.4.1 Performance Analysis of Proposed BFG using Simulated Profile

In this section, we validate the proposed BFG by performing the CC metric , OCV metric and TTV metric on the proposed BFG. The simulated load profile as shown in Figure 4.17(a) is used to demonstrate the validation. The reason behind using simulated load profile is that, we assume the true value of the ECM parameters and the SOC as well to be known to us which advice the performance of the proposed BFG in ideal case. 4.17(b) illustrates the estimated SOC using proposed algorithm 4 based on EKF and widely used Coulomb counting performed on the dynamic portion

of the load profile.

#### 4.4.1.1 CC metric using simulated profile

In this section we validate the SOC estimation by comparing Coulomb counting with the proposed approach. First we compute the SOC by Coulomb counting using (4.147) and the proposed BFG tracks the SOC using the approach introduced in Section 4.2.4. Next, in order to validate the BFG, CC metric is computed using (4.167). Figure 4.17(c) shows the CC metric applied on dynamic portion of simulated load profile . CC metric is performed in the dynamic part of the profile shown in Figure 4.17(a) active from 3 hours to 5 hours. For simulated data, the CC metric is  $\bar{\epsilon}_{cc} = 0.060831\%$  also mention in Table 4.5 which establishes the robustness of the proposed BFG algorithm.

Table 4.5: BFG evaluation by CC metric (%)

Data type	Temperature (°C)	CC metric, $\bar{\epsilon}_{cc}$ (%) in proposed BFG	CC metric, $\bar{\epsilon}_{cc}$ (%) from previous BFG in [1]
Simulated	25	0.060831	N/A
LG LGIP	-15	0.134147	0.52
	-10	0.210197	0.90
	-5	0.200909	0.11
	0	0.219882	0.66
Nokia BP 4L	20	0.104948	N/A
	40	0.104272	N/A
Samsung EB555157VA	-15	0.425388	0.86
	-10	0.409190	0.44

#### 4.4.1.2 OCV metric using simulated profile

In this section, we analyze the OCV metric validation on the proposed BFG computed using the simulated and real data from multiple batteries. First, the OCV metric is applied in simulated data shown in Figure 4.17(a). The battery is kept in rest in



order to measure the terminal voltage at rest state,  $v_r$ . After that the OCV-SOC characterization is used to obtain the corresponding SOC which is compared with the estimated SOC based on the proposed BFG. The terminal voltage is collected at time  $t = 5.7$  hours when the battery is resting and the measured voltage,  $v_r$  is 3.8482 V. Figure 4.17(c) shows that the OCV metric is demonstrated on that particular terminal voltage when the battery is in rest state. The OCV-SOC error is calculated using (4.168) and the error is  $\bar{\varepsilon}_{ocv} = 0.001610\%$  mentioned in Table 4.6 which reflects the performance of the proposed BFG algorithm.

Table 4.6: BFG evaluation by OCV metric

Data type	Temperature (°C)	Voltage at rest, $v_r$ (V)	OCV metric, $\bar{\varepsilon}_{ocv}$ (%) in proposed BFG	OCV metric, $\bar{\varepsilon}_{ocv}$ (%) from previous BFG in [1]
Simulated	25	3.8482	0.001610	N/A
LG LGIP	-15	3.8340	0.378342	-0.06
	-10	3.8164	0.303083	2.40
	-5	3.8205	0.251305	0.38
	0	3.8244	0.254673	0.61
Nokia BP 4L	20	3.7588	0.220708	0.23
	40	3.7756	0.184159	1.12
Samsung EB555157VA	-15	3.8196	0.028815	1.22
	-10	3.8086	0.059137	0.38

#### 4.4.1.3 TTV metric using simulated profile

In this section we evaluate the proposed BFG algorithm based on the TTV metric discussed in Section 4.3.3 by showing the results obtained from both simulated and real data. Figure 4.18 illustrates the TTV analysis using the constant part of the current profile shown in Figure 4.17(a). The duration of time during which the TTV metric is computed is assumed to be  $T_{ttv} = 60$  minutes from the beginning of the current profile. Therefore, we calculate the corresponding shut down voltage  $v_s = 3.6471V$  after 60 minutes as mentioned in Table 4.7. The TTV evaluation starts

from the present voltage of the battery,  $v(k)$ . In order to obtain the corresponding SOC ( by (4.171)), we compute the OCV using (4.169). It is noted that the voltage drop is calculated using (4.170) after we determine the model parameter from the BFG algorithm applied in the dynamic part of the load profile shown in Figure 4.17(a).

Table 4.7: BFG evaluation by TTV metric (%)

Data type	Temp, (°C)	$v_{sd}(V)$	$T_{ttv}$ (min)	$\bar{\epsilon}_{ttv}$ (min)	$E_{ttv}$ (%), in proposed BFG	$E_{ttv}$ (%) in [1]
Simulated	25	3.6471	60	0.20543	0.205432	N/A
LG LGIP	-15	3.2043	60	0.29265	0.487760	0.7
	-10	3.3134	60	0.244462	0.407437	3.8
	-5	3.3999	60	0.37555	0.625927	3.8
	0	3.4840	60	0.200690	0.334484	3.0
Nokia BP 4L	20	3.5864	60	0.521901	0.869835	4.6
	40	3.6889	60	0.085889	0.143149	4.5
Samsung EB555157VA	-15	3.2013	60	1.815107	3.025179	17.7
	-10	3.4079	60	1.342440	2.23740	1.9

Next we determine the predicted time to reach the desired shut down voltage (Predicted TTV). Also the actual TTV is calculated based on the time sample from the data. Figure 4.18(a) shows the predicted and actual Time to reach  $v_{sd}$  plotted against the time. It clear that the predicted TTV line is following the True TTV line throught the duration of time during which the TTV is computed. The effectiveness of the proposed algorithm can be further realized from Figure 4.17(c) which illustartes the error in TTV computed at each voltage by using (4.174). As we use the discharging load profile , the present terminal voltage  $v(k)$  will decrease and move toward the shut down voltage,  $v_{sd}$ . For each of the value of the voltage, the predicted TTV and actual TTV are calculated by using (4.172) and (4.173) respectively illustrated in Figure 4.18(b). The mean error in TTV is found to be 0.20543 minutes. The TTV metric for the simulated data is 0.205432 % mentioned in Table 4.7.

## 4.4.2 Performance Analysis of Proposed BFG using Real Load Profile

In this section, the proposed EKF algorithm is performed on the real data from multiple batteries recorded at different temperature. The load profile from LG LGIP, Nokia BP 4L and Samsung EB555157VA batteries as shown in Figure 4.19 are used to employ the SOC tracking algorithm based on EKF. We test Algorithm 3 and Algorithm 4 on these profile to estimate the SOC and compare the results with Coulomb counting approach. It must be noted that, the Coulomb counting approach requires the knowledge of initial SOC and true capacity. Therefore, we assume the SOC computed using Coulomb counting to be true SOC (reference SOC) and correlate with the SOC estimated from the EKF.

Figure 4.20(a) shows the true SOC using Coulomb counting and the estimated SOC using the proposed EKF on load profile of LG LGIP shown in Figure 4.19(a). The initial SOC is different among all the load profile recorded at different temperature as shown in Figure 4.20(a) depending on how much charge is remaining when the proposed algorithm starts. Figure 4.20(b) and Figure 4.20(c) illustrate the true SOC using Coulomb counting and the estimated SOC using the proposed EKF on load profile of Nokia BP 4L and Samsung EB555157VA respectively shown in Figure 4.19(b) and Figure 4.19(c). It is clear that, The estimated SOC is following the true SOC, thus, establishing the effectiveness of the proposed BFG.

### 4.4.2.1 ECM parameter estimation using real load profile

Proposed ECM identification algorithm is precisely tested on real battery data collected from three different batteries namely LG LGIP, Nokia BP 4L and Samsung EB555157VA shown in Figure 4.19. The load profile from LG LGIP battery is recorded at  $-15^{\circ}C$ ,  $-10^{\circ}C$ ,  $-5^{\circ}C$  and  $-0^{\circ}C$ . The load profile from Nokia BP 4L battery is recorded at  $20^{\circ}C$  and  $40^{\circ}C$  whereas the load profile from Samsung

EB555157VA battery is recorded at  $-15^{\circ}C$  and  $-10^{\circ}C$ . ECM parameters are estimated for each of the battery cell as illustrated in Figure 4.21.

At each temperature, the cell is fully charged and kept at the specified temperature. Then a discharging-charging-discharging current shown in Figure 4.19 is applied to the corresponding battery and the voltage across the battery terminals is recorded. These voltage-current data is then used by the ECM parameter estimation Algorithm 3. The estimated ECM parameter  $R_0$  based on the proposed model for multiple batteries are plotted against time in Figure 4.21(a). The ECM parameter estimation is performed in the dynamic portion of the load profile for each of the battery cells. The dynamic portion of LG LGIP battery ranges from 2 to 4 hours shown in Figure 4.19(a), thus the ECM parameters  $R_0$ ,  $R_1$  and  $C_1$  for LG LGIP battery are estimated during that time period as shown in 4.21. Further, The dynamic portion of Nokia BP 4L and Samsung EB555157VA batteries range from 3 to 4 hours shown in Figure 4.19(b) and Figure 4.19(c), thus the ECM parameters  $R_0$ ,  $R_1$  and  $C_1$  for Nokia BP 4L and Samsung EB555157VA battery are estimated during that time period as shown in 4.21. It must be noted that the  $R_0$  values for all three batteries maintain the impedance properties against the temperature shown in 4.21(a). The estimated ECM parameter  $R_1$  and  $C_1$  based on proposed model for multiple batteries are also plotted against time in Figure 4.21(b) and Figure 4.21(b) respectively. According to Figure 4.21, all the parameters considering model 3 results into the optimum estimated values for each of the batteries, thus states the proposed approach suitable in expectation of practical scenario.

#### 4.4.2.2 CC metric using real load profile

In order to verify the effectiveness of the BFG, we further perform the CC metric on the real data recorded from multiple batteries. and Figure 4.22 shows the CC metric validation. The dynamic part of the load profile of LG LGIP batteries is from 2 hours to 3.929 hours at different temperature ranging from  $-15^{\circ}C$  to  $0^{\circ}C$  illustrated

in Figure 4.19(a) where we perform the CC metric using (4.167) and Figure 4.22(a) shows the error in the proposed technique. The CC metric for all the load profile of LG LGIP at different temperature ranging from  $-15^{\circ}C$  to  $0^{\circ}C$  are 0.134147%, 0.210197%, 0.200909% and 0.219882% respectively mentioned in Table 4.5.

Next, CC metric validation is demonstrated on the real data from Nokia BP 4L and Samsung EB555157VA batteries. The dynamic part of the load profile of Nokia BP 4L is from 3.012 hours to 4.932 hours at  $20^{\circ}C$  and  $40^{\circ}C$  illustrated in Figure 4.19(b) where we perform the CC metric using (4.167) and Figure 4.22(b) shows the error in the proposed technique. The CC metric for all the load profile of Nokia BP 4L batteries at  $20^{\circ}C$  and  $40^{\circ}C$  are 0.104948% and 0.104272% respectively. The dynamic part of the load profile of Samsung EB555157VA batteries is from 3.012 hours to 5.05 hours at  $-15^{\circ}C$  and  $-10^{\circ}C$  illustrated in Figure 4.19(c) the CC metric is performed using (4.167) and Figure 4.22(c) indicates the error in the proposed technique. The CC metric for all the load profile of Samsung EB555157VA batteries at  $-15^{\circ}C$  and  $-10^{\circ}C$  are 0.425388% and 0.409190% respectively based on the proposed approach. Using the same load profiles as shown in Figure 4.19, [1] proposed a BFG and the results of the CC metric validation of that BFG is collected from [1] and mentioned in Table 4.5. This comparison proves the nobility of the proposed BFG over the existing BFG.

#### 4.4.2.3 OCV metric using real load profile

The OCV metric is further performed in validating the proposed BFG using the real data from multiple batteries. The terminal voltages of the battery at rest are measured using the load profile collected from LG LGIP batteries shown in Figure 4.19(a). The OCV metric is tested at different temperature ( $-15^{\circ}C$ ,  $-10^{\circ}C$ ,  $-5^{\circ}C$ ,  $-0^{\circ}C$ ) mentioned in Table 4.6. It also shows the OCV metric validation employed on Nokia BP 4L and Samsung EB555157VA batteries. The OCV metric,  $\bar{\varepsilon}_{ocv}$  for the data using Nokia BP 4L batteries recorded at  $20^{\circ}C$  and  $40^{\circ}C$  are 0.220708% and 0.184159%.

Finally, we compute the OCV metric using the data from Samsung EB555157VA shown in Figure 4.19(c) and the error is 0.028815% and 0.059137%. Therefore, the observation of OCV metric validation presented in Table 4.6 implies that the proposed BFG performs as a "look-up" for OCV-SOC characterization. Using the same load profiles as shown in Figure 4.19, [1] proposed a BFG and the results of the OCV metric validation of that BFG is collected from [1] and mentioned in Table 4.6. It is clear from the comparison that the proposed BFG certainly establish the robustness over the existing BFG.

#### 4.4.2.4 TTV metric using real load profile

The proposed BFG algorithm to estimate SOC is further validated by the TTV metric on real data recorded at different temperature coming from LG LGIP, Nokia BP 4L and Samsung EB555157VA shown in Figure 4.19. The predicted and actual TTV at each time within the duration of the TTV computed using these real data is illustrated in Figure 4.23. The zoomed version of 4.23(a) is shown in Figure 4.23(b) coming from LG LGIP which indicates that, at the end of the TTV operation, the present voltage  $v(k)$  catches up the desired shut down voltage  $v_{sd}$ . Therefore, The actual time to reach  $v_{sd}$  at that particular time sample seems to be 0 minute as expected. However, when we calculate the predicted TTV based obtained from the proposed BFG, it shows that the predicted TTV approaches very close to 0 minute which satisfies the expectation. This minor error in TTV remains in the predicted TTV throughout the time during which TTV is computed. Figure 4.23(c) and Figure 4.23(d) shows us the predicted TTV calculated using Nokia BP 4L and Samsung EB555157VA. Similar observations can also be noticed in Figure 4.24.

For all the real data, the total duration of TTV analysis is assumed to be 60 min. As the voltage drop across the model parameter changes depending on the impedances of the ECM model due to the variation of the temperature in the real data, the terminal voltages profile at each temperature differs accordingly. Therefore,

the desired shut down voltage is different for each of the load profiles illustrated in Figure 4.24. Figure 4.24(b) which is a zoomed version of 4.24(a) indicates that the predicted TTV looks very close to zero when the desired shut down voltage is reached justifying the robustness of the proposed BFG.

TTV metric (error in %) is calculated using (4.177) for both simulated data and real data presented in Table 4.7. For simulated data, the error in TTV,  $E_{ttv}$  is 0.205432% shown in Figure 4.17(c). Furthermore, we compute TTV metric for the load profile of aforementioned batteries. As the duration of TTV is assumed  $T_{ttv} = 60$  minutes, the averaged TTV error (in minute) for LG LGIP batteries is computed by using the data recorded at different temperature ranging from  $-15^{\circ}C$  to  $0^{\circ}C$  and the TTV metric are 0.487760%, 0.407437%, 0.625927% and 0.334484% respectively. Figure 4.25(a) shows the TTV metric validation for load profile of LG LGIP batteries.

The averaged TTV error for Nokia BP 4L batteries is computed by using the data recorded at  $20^{\circ}C$  and  $40^{\circ}C$  and the TTV metric are 0.869835% and 0.143149% respectively whereas TTV metric for Samsung EB555157VA are 3.025179% and 2.23740%. The performance of the proposed BFG based on TTV metric validation can be further realized from the Figure 4.25(b) and Figure 4.25(c) which illustrate the error in TTV measured at each time sample of the individual load profile. Using the same load profiles as shown in Figure 4.19, [1] proposed a BFG and the results of the TTV metric validation of that BFG is collected from [1] and mentioned in Table 4.7. It is evident from the observation that the proposed BFG indeed has more accuracy in estimation than the existing BFG.

## 4.5 Conclusion

Battery system identification, performed by the battery fuel gauge (BFG), is crucial to the safety, efficiency and reliability of a battery storage system. Evaluating a BFG is a challenging problem and recently an approach and procedure is presented for

BFG evaluation [1, 3]. The BFG evaluation scheme consisted of a BFG evaluation profile and three BFG evaluation metrics: the Coulomb counting metric *CC metric*, the open circuit voltage metric *OCV metric*, and the time to voltage metric *TTV metric*. These three metrics are designed in a way that each of their values vary between 0% and 100% indicating the error in the BFG algorithm.

In this chapter, first, we rigorously tested the applicability/suitability of the BFG evaluation metrics using simulated battery data where the true system parameters are known a priori. This procedure resulted in close to 0% error for all three BFG evaluation metrics, reconfirming the suitability of BFG evaluation metrics. Then, a supposedly improved BFG algorithm was tested using the BFG evaluation scheme. The BFG evaluation metrics produced objective numbers indicating the improvement made in the new BFG algorithm.



---

**Algorithm 3**  $[\hat{\mathbf{b}}_{\kappa+1}, \mathbf{P}_{\kappa+1}^{-1}] = \text{BattECMID}[\hat{\mathbf{b}}_{\kappa}, \mathbf{P}_{\kappa}^{-1}, \tilde{\mathbf{v}}_{\kappa+1}, \tilde{\mathbf{A}}_{\kappa+1}]$

---

- 1: Construct the noise covariance matrix:  $\Sigma_{\kappa}$  using (4.138)

$$\begin{aligned}\sigma_n^2(0) &= 2(1 + \hat{\mathbf{b}}_{\kappa}^2(1))\sigma_v^2 + 2(\hat{\mathbf{b}}_{\kappa}^2(2) + \hat{\mathbf{b}}_{\kappa}^2(3))\sigma_i^2 \\ \sigma_n^2(1) &= -2\alpha_1\sigma_v^2 - 2\hat{\mathbf{b}}_{\kappa}(2)\hat{\mathbf{b}}_{\kappa}(3)\sigma_i^2\end{aligned}\tag{4.143}$$

- 2: Update Error Cov:  $\mathbf{P}_{\kappa+1}^{-1} = \mathbf{P}_{\kappa}^{-1} + \tilde{\mathbf{A}}_{\kappa+1}^T \Sigma^{-1} \tilde{\mathbf{A}}_{\kappa+1}$   
3: Update Residual Cov:  $\mathbf{S}_{\kappa+1} = \tilde{\mathbf{A}}_{\kappa+1} \mathbf{P}_{\kappa+1}^{-1} \tilde{\mathbf{A}}_{\kappa+1}^T + \Sigma$   
4: Update gain:  $\mathbf{W}_{\kappa+1} = \mathbf{P}_{\kappa+1} \tilde{\mathbf{A}}_{\kappa+1}^T \mathbf{S}_{\kappa+1}^{-1}$   
5: Update Parameter:  $\hat{\mathbf{b}}_{\kappa+1} = \hat{\mathbf{b}}_{\kappa} + \mathbf{W}_{\kappa+1} (\tilde{\mathbf{v}}_{\kappa+1} - \tilde{\mathbf{A}}_{\kappa+1} \hat{\mathbf{b}}_{\kappa})$
-

---

**Algorithm 4**

$$[\hat{x}_s(k+1|k+1), P_s(k+1|k+1)] =$$

$$\text{EKF-SOC}(\hat{x}_s(k|k), P_s(k|k), z_i(k+1), z_v(k+1), \tilde{\mathbf{A}}_\kappa, \mathbf{b}_\kappa)$$

---

1: State prediction:

$$\hat{x}_s(k+1|k) = \hat{x}_s(k|k) + G(k)u(k) \quad (4.157)$$

2: State prediction variance:

$$P_s(k+1|k) = P_s(k|k) + \sigma_s^2 \quad (4.158)$$

3: Voltage drop update:

$$v_d(k) = \tilde{\mathbf{A}}_\kappa \mathbf{b}_\kappa \quad (4.159)$$

4: Measurement prediction:

$$\hat{z}(k+1|k) = V_o(\hat{x}_s(k+1|k)) + v_d(k) \quad (4.160)$$

5: Linearization of observation model:

$$\begin{aligned} h'(k+1) = & -\frac{K_1}{\hat{x}_s^2(k+1|k)} - \frac{2K_2}{\hat{x}_s^3(k+1|k)} - \frac{3K_3}{\hat{x}_s^4(k+1|k)} \\ & -\frac{4K_4}{\hat{x}_s^5(k+1|k)} + K_5 + \frac{K_6}{\hat{x}_s(k+1|k)} \\ & -\frac{K_7}{1 - \hat{x}_s(k+1|k)} \end{aligned} \quad (4.161)$$

6: Innovation variance:

$$S(k+1|k) = \sigma_v^2 + h'(k+1)P(k+1|k)h'(k+1)' \quad (4.162)$$

7: Innovation:

$$m(k+1) = z_v(k+1) - \hat{z}(k+1|k) \quad (4.163)$$

8: Filter gain:

$$W(k+1) = P(k+1|k)h'(k+1)'S(k+1)^{-1} \quad (4.164)$$

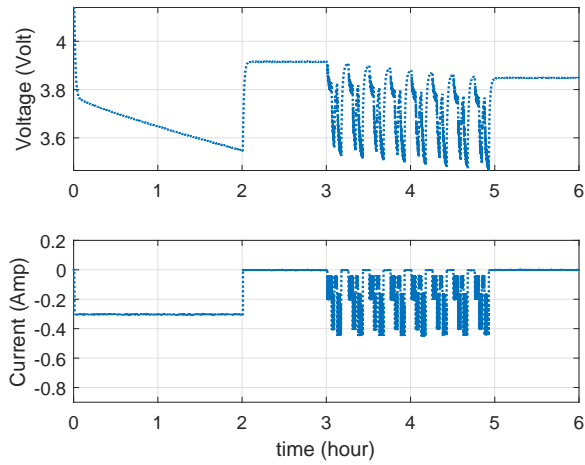
9: State estimate:

$$\hat{x}_s(k+1|k+1) = \hat{x}_s(k+1|k) + W(k+1)m(k+1) \quad (4.165)$$

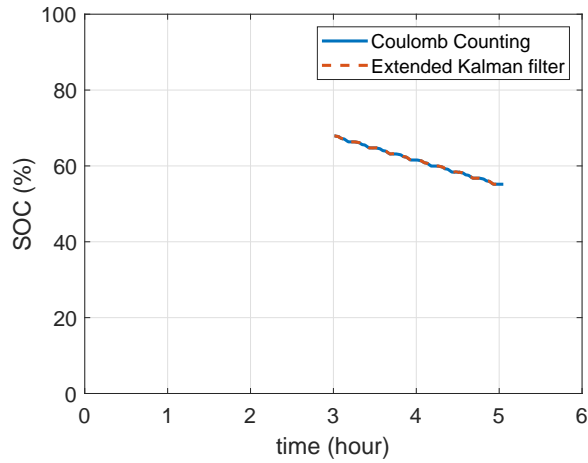
10: State estimate variance:

$$P_s(k+1|k+1) = P_s(k+1|k) - W(k+1)S(k+1)W(k+1)' \quad (4.166)$$

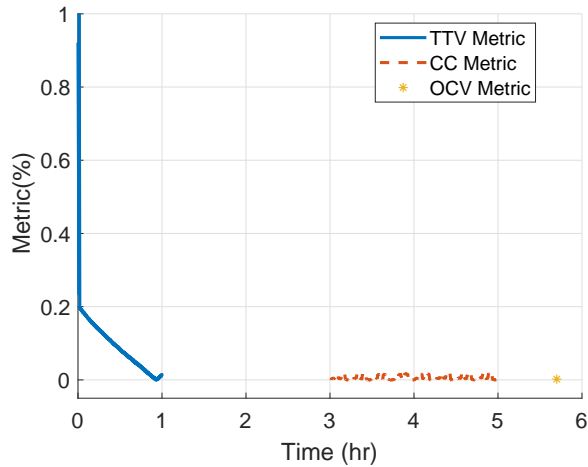
---



(a) Load profile

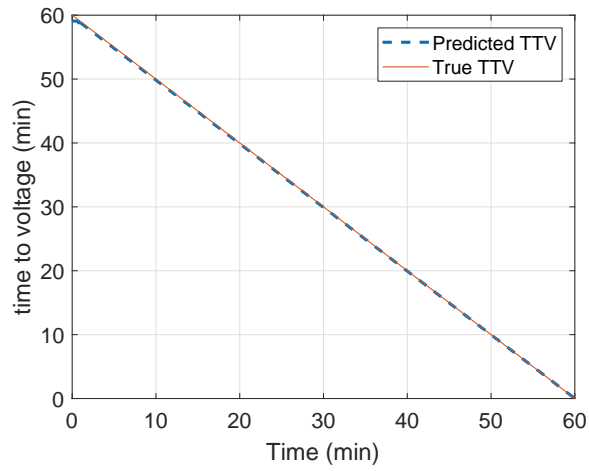


(b) SOC estimation

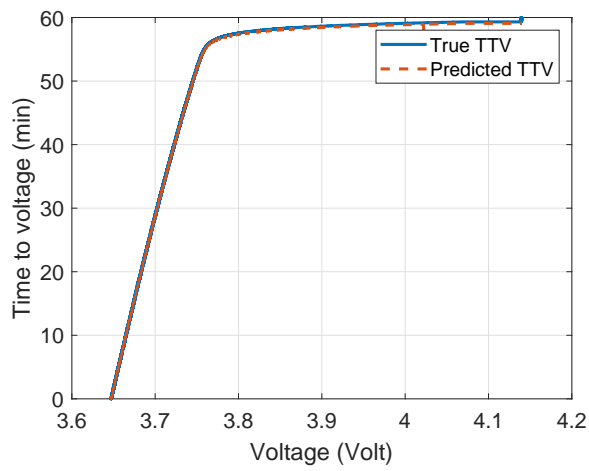


(c) All three BFG evaluation metrics

Figure 4.17: **BFG evaluation using simulated load profile.** Simulated voltage and current are shown in (a); Estimated SOC is presented in (b); finally the validation of the proposed BFG is illustrated in (c).

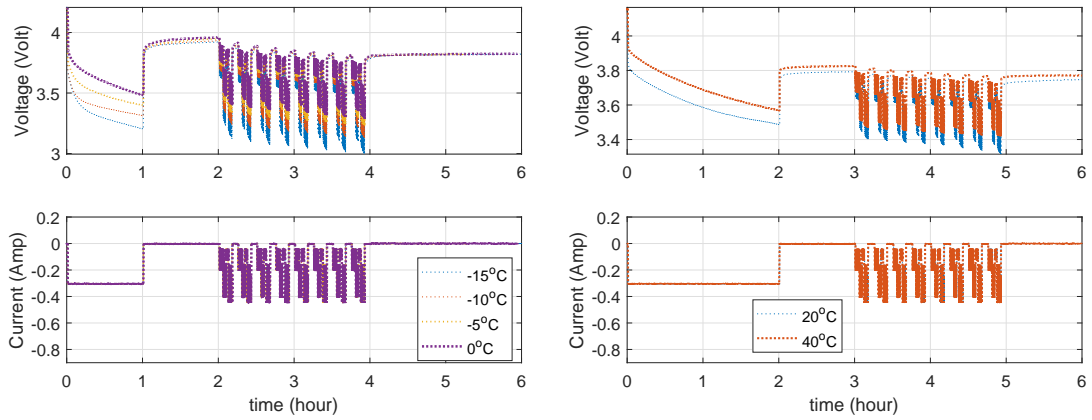


(a) **TTV vs. time**

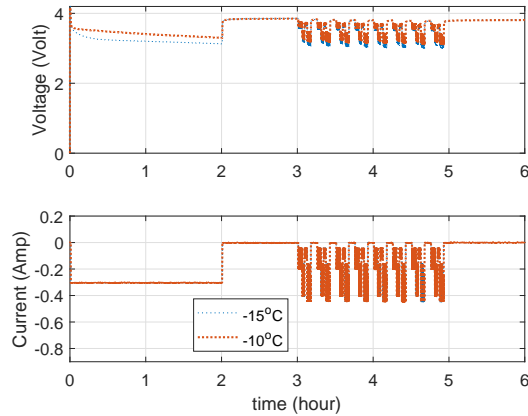


(b) **TTV vs. voltage**

Figure 4.18: **Visualization of TTV error in minutes.** A close up visualization of TTV metric using simulated data

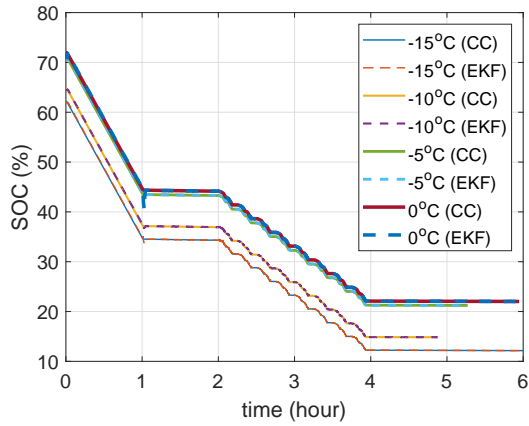


(a) Voltage and current profile of LG LGIP (b) Voltage and current profile of Nokia BP 4L

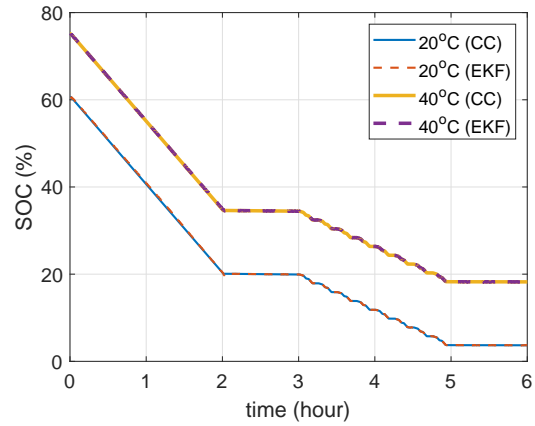


(c) Voltage and current profile of Samsung EB555157VA

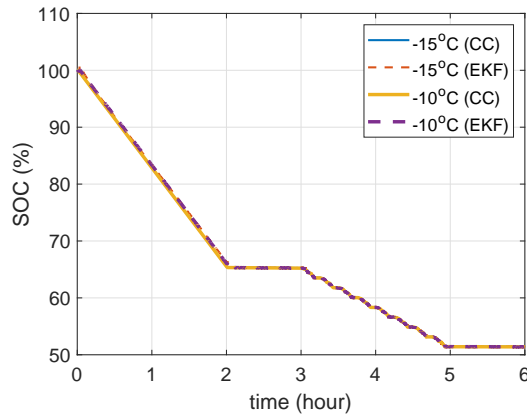
Figure 4.19: **Real voltage and current data from multiple batteries.** The effectiveness of the proposed BFG algorithm is verified by implementing it in three different batteries which are LG LGIP, Nokia BP 4L and Samsung EB555157VA measured at different temperature as indicated in the plots.



(a) SOC estimation of LG LGIP

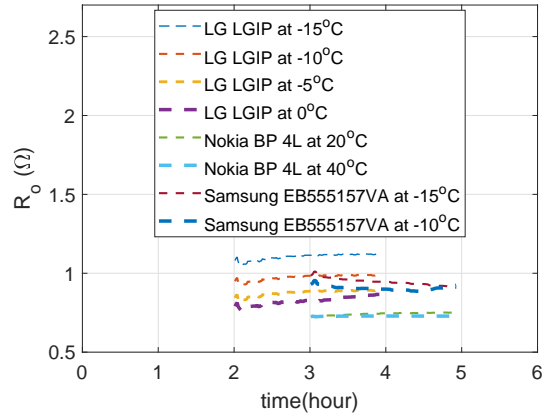


(b) SOC estimation of Nokia BP 4L

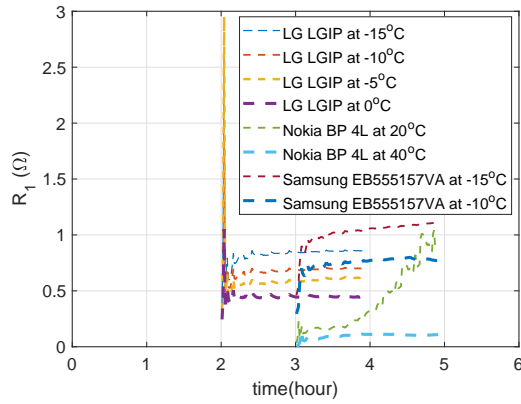


(c) SOC estimation of Samsung EB555157VA

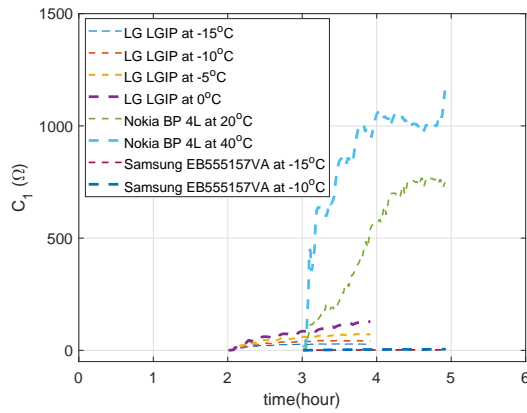
Figure 4.20: **SOC estimation using proposed BFG.** The SOC is estimated on-line using the proposed BFG and compared with the widely-used Coulomb counting approach in order to verify the robustness. The Coulomb counting approach uses battery capacity that was estimated prior to the experiment.



(a)  $R_0$  estimation of LG LGIP

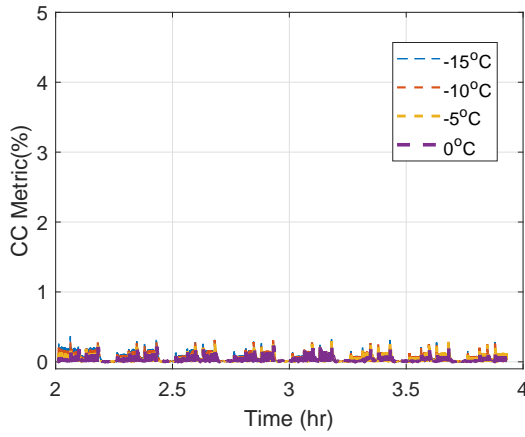


(b)  $R_1$  estimation of Nokia BP 4L

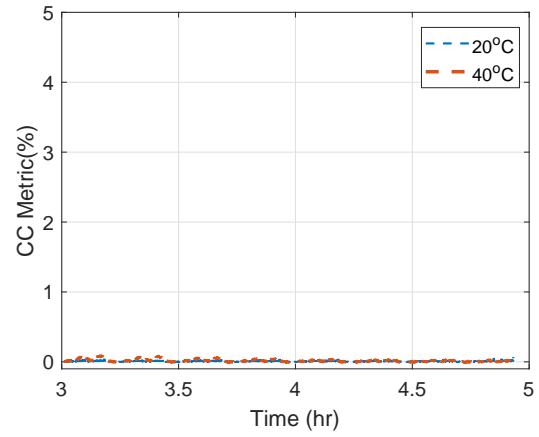


(c)  $C_1$  estimation of Samsung EB555157VA

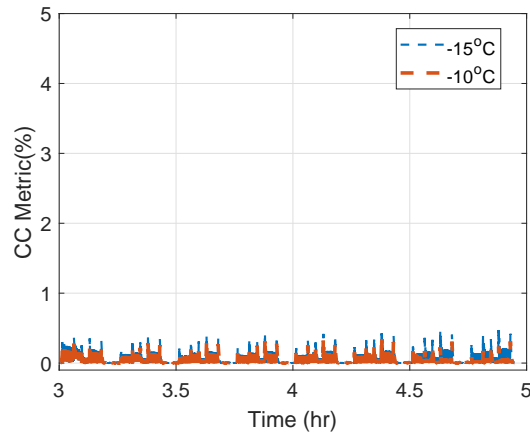
Figure 4.21: **ECM parameter estimation using the real load profile.** ECM parameter estimation is performed using the battery model shown in Figure 4.14. The  $R_0$ ,  $R_1$  and  $C_1$  estimations is illustrated in (a), (b) and (c) respectively for multiple batteries.



(a) CC metric for LG LGIP



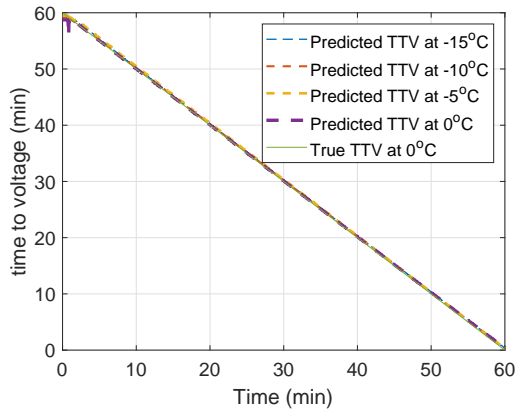
(b) CC metric for Nokia BP 4L



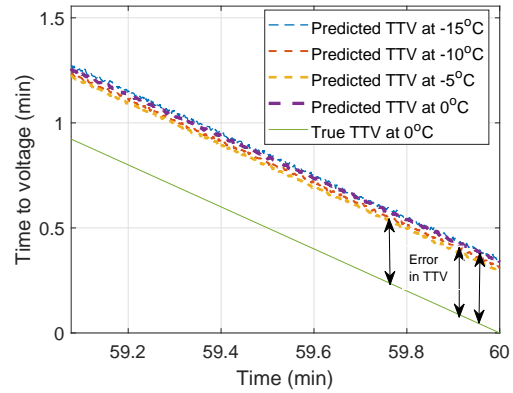
(c) CC metric For Samsung EB555157VA

Figure 4.22: **BFG** evaluation based on **CC** metric using multiple batteries. New **CC** metric is developed in order to validate the proposed algorithm to estimate **SOC** based on extended Kalman filter discussed in Section 4.2.4

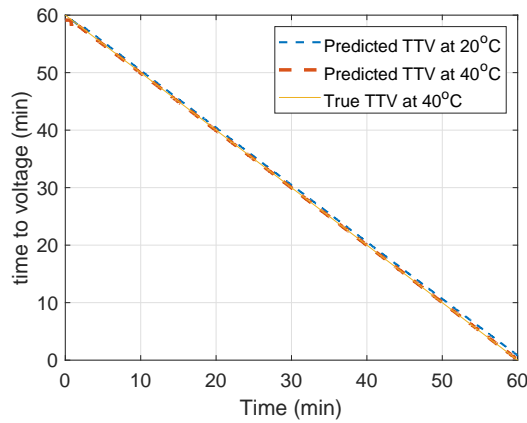




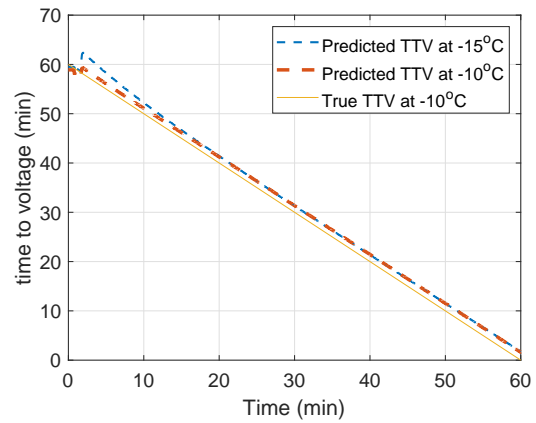
(a) TTV for LG LGIP



(b) Zoomed version of Fig (a) from 59 to 60 minutes

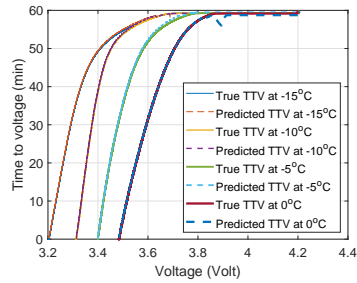


(c) TTV for Nokia BP 4L

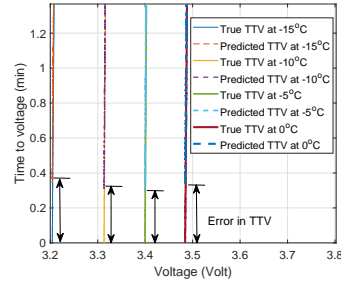


(d) TTV for Samsung EB555157VA

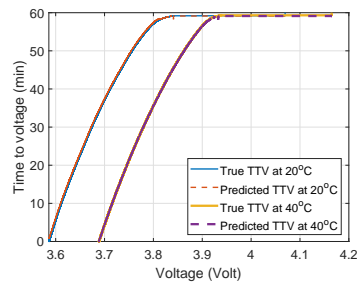
Figure 4.23: **Predicted time to reach shut down voltage vs. actual TTV.** The real data from multiple batteries are used to calculate and compare the predicted time to reach certain shut down voltages. The zoomed version of Figure (a) is shown in Figure (b) illustrating the true TTV calculated using the data from LG LGIP at different temperature and the expected TTV. Figure (c) and (d) shows the results of predicted and actual TTV using the data from Nokia BP 4L and Samsung EB555157VA.



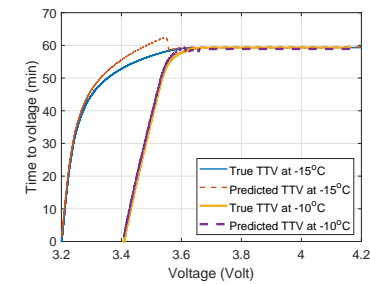
(a) TTV vs. voltage for LG LGIP



(b) Zoomed version of Fig (a) from 3.2V to 3.6V

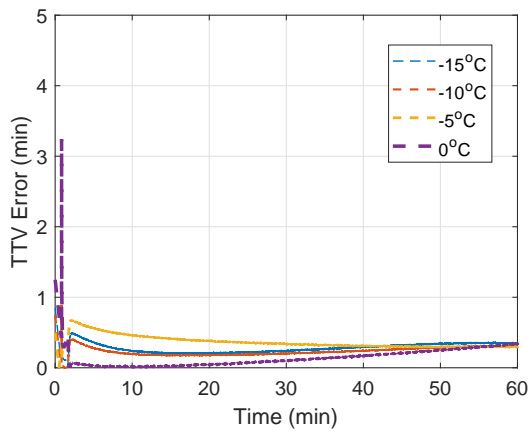


(c) TTV vs. voltage for Nokia BP 4L

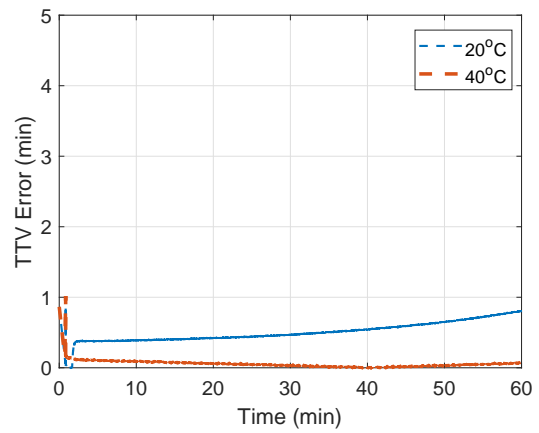


(d) TTV vs. voltage for Samsung EB555157VA

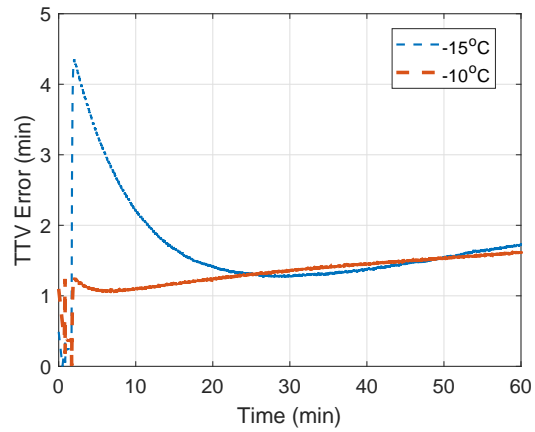
Figure 4.24: **Predicted time to reach shut down voltage vs. actual terminal voltage.** The real data from multiple batteries are used to calculate and compare the predicted time to reach certain shut down voltages. The zoomed version of Figure (a) is shown in Figure (b) illustrating the true TTV calculated using the data from LG LGIP at different temperature and the expected TTV. Figure (c) and (d) shows the results of predicted and actual TTV plotted against the voltage using the data from Nokia BP 4L and Samsung EB555157VA.



(a) TTV metric for LG LGIP



(b) TTV metric for Nokia BP 4L



(c) TTV metric For Samsung EB555157VA

Figure 4.25: **BFG evaluation based on TTV metric** The proposed BFG is evaluated based on TTV errors (in minute) for each time index.

## 4.6 Bibliography

- [1] G. Avvari, B. Pattipati, B. Balasingam, K. Pattipati, and Y. Bar-Shalom. Experimental set-up and procedures to test and validate battery fuel gauge algorithms. *Applied energy*, 160:404–418, 2015. pages xiv, 17, 56, 77, 81, 90, 91, 92, 95, 96, 97, 98, 101, 102, 103, 104
- [2] B. Balasingam, G. Avvari, B. Pattipati, K. Pattipati, and Y. Bar-Shalom. A robust approach to battery fuel gauging, part I: Real time model identification. *Journal of Power Sources*, 272:1142–1153, 2014. pages 7, 8, 9, 18, 29, 30, 31, 35, 39, 56, 77, 83
- [3] B. Balasingam, G. Avvari, K. Pattipati, and Y. Bar-Shalom. Performance analysis results of a battery fuel gauge algorithm at multiple temperatures. *Journal of Power Sources*, 273:742–753, 2015. pages xiv, 17, 56, 77, 81, 90, 91, 92, 104
- [4] B. Balasingam, G. V. Avvari, B. Pattipati, K. R. Pattipati, and Y. Bar-Shalom. A robust approach to battery fuel gauging, part II: Real time capacity estimation. *Journal of Power Sources*, 269:949–961, Dec 2014. pages 76
- [5] Y. Bar-Shalom, X. R. Li, and T. Kirubarajan. *Estimation with applications to tracking and navigation: theory algorithms and software*. John Wiley & Sons, 2004. pages 53, 77
- [6] B. Bhangu, P. Bentley, D. Stone, and C. Bingham. Nonlinear observers for predicting state-of-charge and state-of-health of lead-acid batteries for hybrid-electric vehicles. *Vehicular Technology, IEEE Transactions on*, 54(3):783–794, 2005. pages 76
- [7] M. Chen, G. A. Rincon-Mora, et al. Accurate electrical battery model capable of predicting runtime and iv performance. *IEEE transactions on energy conversion*, 21(2):504–511, 2006. pages 29, 77

- [8] S. Chen, Y. Fu, and C. Mi. State of charge estimation of lithium ion batteries in electric drive vehicles using extended kalman filtering. 2013. pages 76
- [9] A. Farmann, W. Waag, and D. U. Sauer. Adaptive approach for on-board impedance parameters and voltage estimation of lithium-ion batteries in electric vehicles. *Journal of Power Sources*, 299:176–188, 2015. pages 7, 29, 30, 83
- [10] H. He, R. Xiong, X. Zhang, F. Sun, and J. Fan. State-of-charge estimation of the lithium-ion battery using an adaptive extended kalman filter based on an improved thevenin model. *Vehicular Technology, IEEE Transactions on*, 60(4):1461–1469, 2011. pages 76
- [11] Y. He, W. Liu, and B. J. Koch. Battery algorithm verification and development using hardware-in-the-loop testing. *Journal of Power Sources*, 195:2969–2974, 2010. pages 77
- [12] C. Hu, B. D. Youn, and J. Chung. A multiscale framework with extended kalman filter for lithium-ion battery soc and capacity estimation. *Applied Energy*, 92:694–704, 2012. pages 76
- [13] X. Hu, F. Sun, and Y. Zou. Estimation of state of charge of a lithium-ion battery pack for electric vehicles using an adaptive luenberger observer. *Energies*, 3(9):1586–1603, 2010. pages 76
- [14] I.-S. Kim. The novel state of charge estimation method for lithium battery using sliding mode observer. *Journal of Power Sources*, 163(1):584–590, 2006. pages 76
- [15] J. Kim and B.-H. Cho. State-of-charge estimation and state-of-health prediction of a li-ion degraded battery based on an ekf combined with a per-unit system. *Vehicular Technology, IEEE Transactions on*, 60(9):4249–4260, 2011. pages 76

- [16] J. Kim, S. Lee, and B. Cho. Discrimination of Li-ion batteries based on hamming network using discharging–charging voltage pattern recognition for improved state-of-charge estimation. *Journal of Power Sources*, 196(4):2227–2240, 2011. pages 76
- [17] J. Lee, O. Nam, and B. Cho. Li-ion battery SOC estimation method based on the reduced order extended kalman filtering. *Journal of Power Sources*, 174(1):9–15, 2007. pages 76
- [18] S. Lee, J. Kim, J. Lee, and B. Cho. State-of-charge and capacity estimation of lithium-ion battery using a new open-circuit voltage versus state-of-charge. *Journal of Power Sources*, 185(2):1367–1373, 2008. pages 76
- [19] Y. Li, Z. Sun, and J. Wang. Design for battery management system hardware-in-loop test platform. In *Electronic Measurement & Instruments, 2009. ICEMI'09. 9th International Conference on*, pages 3–399. IEEE, 2009. pages 77
- [20] B. B. M. S. Ahmed, S. A. Raihan. A scaling approach for improved state-of-charge representation in li-ion batteries (submitted, july). *Journal of Power Sources*, 2019. pages 82, 86
- [21] M. Mastali, J. Vazquez-Arenas, R. Fraser, M. Fowler, S. Afshar, and M. Stevens. Battery state of the charge estimation using Kalman filtering. *Journal of Power Sources*, 239:294–307, 2013. pages 76
- [22] B. Pattipati, B. Balasingam, G. Avvari, K. R. Pattipati, and Y. Bar-Shalom. Open circuit voltage characterization of lithium-ion batteries. *Journal of Power Sources*, 269:317–333, 2014. pages 7, 20, 30, 59, 82
- [23] B. Pattipati, B. Balasingam, G. V. Avvari, K. Pattipati, and Y. Bar-Shalom. Open circuit voltage characterization of lithium-ion batteries. *Journal of Power Sources*, 269:317–333, Dec. 2014. pages 76, 91

- [24] G. L. Plett. Extended Kalman filtering for battery management systems of LiPB-based HEV battery packs: Part 1. background. *Journal of Power sources*, 134(2):252–261, 2004. pages 6, 27, 76, 81
- [25] G. L. Plett. Extended Kalman filtering for battery management systems of lipb-based HEV battery packs: Part 2. Modeling and identification. *Journal of power sources*, 134(2):262–276, 2004. pages 76
- [26] G. L. Plett. Extended kalman filtering for battery management systems of lipb-based HEV battery packs: Part 3. State and parameter estimation. *Journal of Power sources*, 134(2):277–292, 2004. pages 28, 76
- [27] G. L. Plett. Sigma-point kalman filtering for battery management systems of lipb-based hev battery packs: Part 1: Introduction and state estimation. *Journal of Power Sources*, 161(2):1356–1368, 2006. pages 76
- [28] G. L. Plett. Sigma-point kalman filtering for battery management systems of lipb-based hev battery packs: Part 2: Simultaneous state and parameter estimation. *Journal of Power Sources*, 161(2):1369–1384, 2006. pages 76
- [29] G. L. Plett. *Battery Management Systems, Volume II: Equivalent-Circuit Methods*. Artech House Publishers, 2015. pages 6, 27, 28, 81
- [30] S. Santhanagopalan and R. E. White. Online estimation of the state of charge of a lithium ion cell. *Journal of Power Sources*, 161(2):1346–1355, 2006. pages 76
- [31] D. Stolitzka. An electronic fuel gauge accuracy study. In *Battery Conference on Applications and Advances, 1997., Twelfth Annual*, pages 211–213. IEEE, 1997. pages 77

- [32] P. Vyroubal and T. Kazda. Equivalent circuit model parameters extraction for lithium ion batteries using electrochemical impedance spectroscopy. *Journal of Energy Storage*, 15:23–31, 2018. pages 28, 81
- [33] H. Wu. Hardware-in-loop verification of battery management system. In *Power Electronics Systems and Applications (PESA), 2011 4th International Conference on*, pages 1–3. IEEE, 2011. pages 77
- [34] M. Yoshio, R. J. Brodd, and A. Kozawa. *Lithium-Ion Batteries*. Springer, 2009. pages 75



# Chapter 5

## Conclusion and Future Work

In this thesis, author has aimed at the system identification of a battery management system. First, we present a novel approach for parameter identification of a Lithium ion battery equivalent circuit model (ECM) based on the recursive least square (RLS) filter. The proposed approach only requires measured voltage across the battery terminals and current through the battery. Estimation error due to the noise in measured voltage and current is derived based on the standard deviation of these measurement noises.

The MSE increases with model complexity, however, it remained 1% for battery equivalent circuit model under the assumption of the practical values of measurement noise. The worst MSE remained 4.028% when a model mismatch was introduced in the battery simulator. Finally, the proposed ECM identification algorithm is tested on real battery data. First, Model 3 parameters were estimated from the same battery cell at eight different temperatures; estimated parameters conformed to previously understood behaviour against temperature. Then, the algorithm was tested on data collected from five different battery cells at room temperature.

We describe the mathematical derivation of the new measurement model that is based only on the measured voltage across the battery and current through the

battery. Then the proposed algorithm has been summarized for ECM parameter estimation using this measurement model. The theoretical performance analysis has been discussed regarding the proposed ECM parameter estimation approach which shows that the more the number of samples in one batch of data, the less the estimation error. It tells that the estimation error can be reduced by increasing the time between two adjacent samples.

Finally, author has validated the improved BFG using the BFG evaluation scheme termed as “BFG evaluation metrics”. An objective performance analysis has been conducted first using the simulated data where the true value is assumed to be known. The CC metric has been applied on dynamic portion of simulated load profile and the error is 0.060831%. The OCV metric for simulated data is found to be 0.001610% considering that the battery is in rest state. The TTV metric for the simulated data is 0.205432% performed in the constant portion of the current profile. The BFG evaluation metrics produced objective numbers indicating the improvement made in the new BFG algorithm.

# Vita Auctoris

NAME: Sheikh Arif Raihan

PLACE OF BIRTH: Meherpur, Bangladesh

YEAR OF BIRTH: 1993

EDUCATION: BCSIR High School, Dhaka, Bangladesh  
2009

Dhaka College, Dhaka, Bangladesh  
2011

Bangladesh University of Engineering and Technology,  
Dhaka, Bangladesh  
2017, Bachelor of Science  
Electrical and Electronic Engineering

University of Windsor, Windsor, Ontario  
2019, Master of Applied Science  
Electrical Engineering